NTNU

Norwegian University of
Science and Technology

Nonlinear Identification of Ship Autopilot Models

Vidar Ødegård

Master of Science in Engineering Cybernetics
Submission date: June 2009
Supervisor: Thor Inge Fossen, ITK

Norwegian University of Science and Technology
Department of Engineering Cybernetics

Problem Description

The purpose of the thesis is to develop methods for identification of nonlinear models to be used in ship autopilots.

The following elements must be considered:
1. Literature study on nonlinear identification methods. Give a presentation of different autopilot models and identification methods found in the literature. Also include a discussion on stability and parameter convergence.
2. Specify a sequence of ship maneuvers that can be used for identification.
3. Estimate the parameters of the model using simulated and experimental data. Discuss the results and presents results for parameter estimation/convergence. Also show which maneuvers that have best convergence properties.
4. Simulate the system with a model-based autopilot in closed loop.
5. Present your findings and theoretical results in the report.

Assignment given: 12. January 2009
Supervisor: Thor Inge Fossen, ITK

Abstract

The purpose of this thesis has been to develop methods for identification of nonlinear models to be used in ship autopilots. An accurate model is essential when developing autopilot systems. Although a number of identification methods are available, only a few ship maneuvers are described in the literature.

During this report a literary study on nonlinear identification methods has been carried out and an overview over several methods is presented. A new maneuvering model derived by Andrew Ross is simulated to generate measurement data. Based on the measurements during several predefined maneuvers, an iterative prediction error method is applied to identify the parameters of two different autopilot models.

Secondly, a new ship maneuver is suggested for identification of ship steering dynamics. Compared to the classic turning circle and zig-zag maneuver the new maneuver shows better convergence properties and perform good adaptation of the dynamics.

At last the identified autopilot models are verified by simulating the ship in closed-loop using a model-based autopilot controller.

Acknowledgments

"As far as the laws of mathematics refer to reality, they are not certain; and as far as they are certain, they do not refer to reality."

Albert Einstein, January 27, 1921

This thesis finish my last year studying engineering cybernetics at the Norwegian University of Science and Technology. Two incredible year has gone since I started on the two-year master program in engineering cybernetics, and I can hardly believe I have made it. After finishing my bachelor degree at Aalesund University College I was looking for greater challenges. This wish has undoubtedly come true. During this one and a half year I have learned much more than I had imagined and I have definitively reached another level in engineering.

Working on this thesis has been interesting and at times challenging. First of all, the literary study on system identification was much more challenging than expected. Although a number of methods and techniques are described, it was hard to form a good overview of the field. Secondly, reading the doctoral thesis of Andrew Ross and implementing the model was time consuming. Although the system identification toolbox provide a graphical interface, it could not be used since the data was not uniformly sampled and the model structure had to be defined explicitly. The creativity was also tested during the development of the new ship maneuver.

I would like to thank my supervisor Thor I. Fossen for giving me this project and for his support and guidance. Further I will thank Andrew Ross for deriving the new maneuvering model used in this project and for giving me experimental data. I would also express thanks to Jann Peter Strand and Rolls Royce Marine for giving me the opportunity to learn more about autopilot design during the summer of 2008. At last I would like to thank the two-year master students in engineering cybernetics for an invaluable co-operation the first year at NTNU.

Trondheim, Norway, June 2009

Vidar Ødegård

Contents

List of Figures

List of Tables

Chapter 1

Introduction

Throughout the history of automatic control it has been known that mathematical models and their environment seldom is known a priori. Although a number of autopilot models are derived by means of first principles, most of the parameters are unknown. To determine the ship steering equations predefined steering experiments, such as turning circles and zig-zag maneuvers have been utilized. The parameters are subsequently obtained using several identification techniques.

In this thesis a new ship maneuver is developed. The maneuver is developed by trying to make maximum informative signals, when the slowly ship dynamics are taken into consideration. By reviewing the most acknowledge methods in the field of system identification, two different autopilot models are identified using an iterative prediction error technique.

The simulated vessel used in this thesis is based on a maneuvering model derived by Andrew Ross. In addition, a model of the rudder motion and dynamics is added. To emphasize the nonlinear characteristics the vessels rudder effect is strongly increased.

1.1 Background and Motivation

Identification of dynamic systems are well known in the literature. A number of identification methods have been developed, such as Kalman filtering, maximum likelihood estimation and prediction error methods. Identification of parametric autopilot models require data from open- or closed-loop experiments. To obtain the steering characteristics from scaled or full-scale experiments a few maneuvers have been utilized, such as the turning circle, zig-zag maneuvers, spiral maneuvers and pull-out tests.

The motivation behind this thesis is to make the most of already derived nonlinear autopilot models. An accurate model is essential in feedback control and although good identification techniques exist, few predefined ship maneuvers are suitable for the purpose of system identification.

1.2 Contribution

The main contribution of this thesis is a new developed ship maneuver designed to excite the nonlinear steering characteristics for stable ships. The new maneuver is during the thesis simulated and compared to other maneuvers. Subsequently, the autopilot models are identified using an iterative prediction error estimation technique to compare the convergence properties.

1.3 Outline of the Thesis

This thesis is organized into eight chapters, in which the first is an introduction and the two last chapters are the conclusion and further research.

Chapter 2 - Mathematical Modelling

In this chapter the basic kinematics and kinetics for a marine vessel are presented. A new maneuvering model utilized in this thesis is briefly described in section three.

Chapter 3 - Identification of Maneuvering Characteristics

In this chapter several identification methods applied on ship autopilot models are reviewed. The first section provide an introduction to different types of identification. In section two the different autopilot models used in this thesis are derived. Section three gives an overview over the most known ship maneuvers in addition to a new suggested ship maneuver. The last section briefly describes the most acknowledged identification methods used for identification of ship steering dynamics in the literature, followed by an introduction to parameter convergence.

Chapter 4 - Identification Results

In this chapter the identification results are presented. The simulation of the predefined maneuvers is shown i section one. In section two the identification results based on data from the single experiments are reviewed. The last section shows the identification results based on several experiments of the ship maneuvers. For each of the maneuvers both the first order Nomoto model and the autopilot model derived by Ross are identified.

Chapter 5 - Autopilot Design

In this chapter the identified models are verified using a model-based autopilot controller. The first section gives a historical overview over autopilot controllers, while the model-based controllers are derived in the following section. Further is the simulation environment described in section three and the final simulation results are presented in section four.

Chapter 6 - Discussion

In this chapter the different choices taken during the thesis are discussed. The two autopilot models are reviewed in the first section. In section two the suggested maneuver is compared to its competitors. Identification results and convergence properties are discussed in section three, followed by a discussion on the utilized autopilot controller in section four.

Chapter 2

Mathematical Modelling

In this chapter the basic dynamics of a marine vessel is presented. The study of dynamics can be divided into two parts: kinematics and kinetics, which is also discussed separately in the following sub chapters. Further the final maneuvering model will be presented. In this document kinematic and kinetic models are given in the vectorial setting [16] using standard SNAME [53] notation.

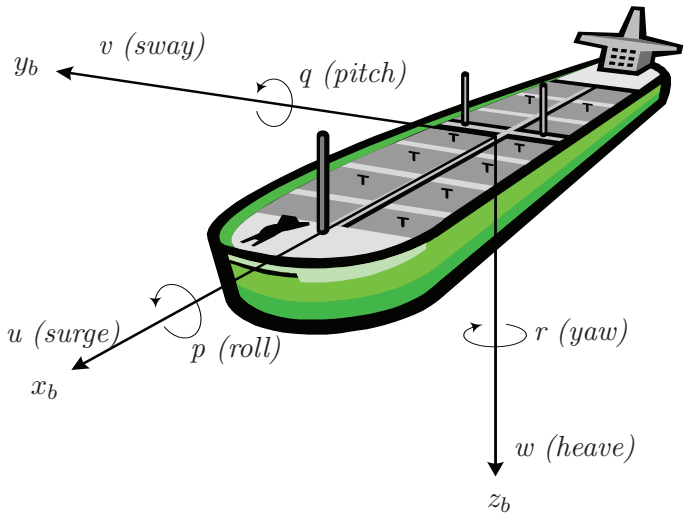

Figure 2.1: Motion variables for a marine vessel [53].

2.1 Kinematics

Kinematics treat only the geometrical aspects of motion without regard for their causes. In the kinematic model the linear and angular velocity are specified by a set of motion variables, which represent the vessels *degree of freedom* (DOF). To deal with kinematics, the motion variable must be given relative to a specified reference frame.

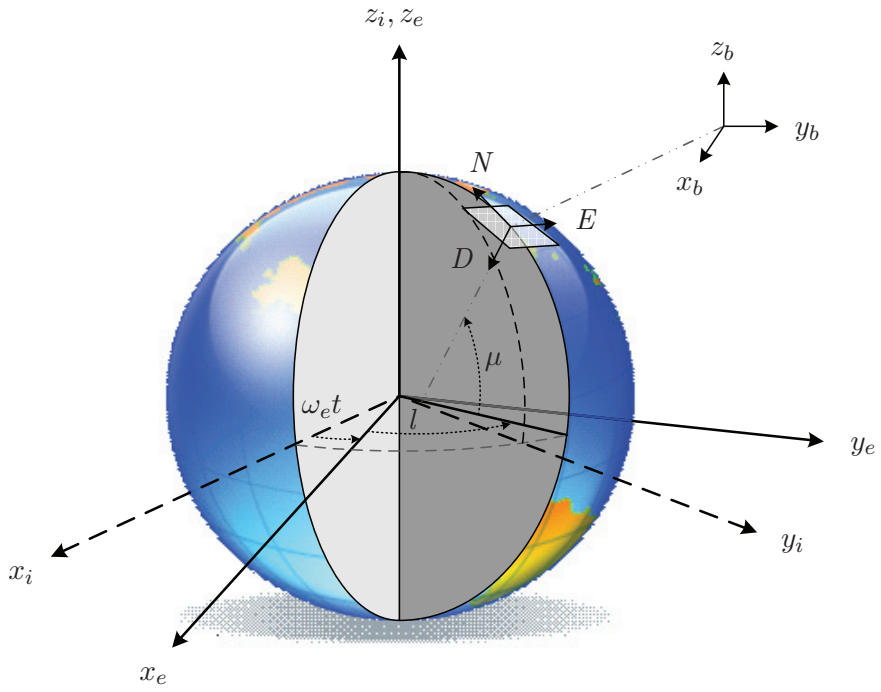

Figure 2.2: Illustration of the ECI, ECEF, NED and BODY reference frames.

2.1.1 Reference Frames

Reference frames may be divided into two groups whereas the origin is placed. In Earth centered reference frame the origin is placed at the Earth's center, while it in geographic reference frame is placed either on a specific body or at an other reference on Earth.

Earth Centered Inertial The *Earth Centered Inertial* (ECI) reference frame has its origin in the center as shown i Figure 2.2. Its axes does not rotate with the Earth and is assumed to be a non accelerating reference frame in which Newtons's laws of motion apply.

Earth Centered Earth Fixed The *Earth Centered Earth Fixed* (ECEF) reference frame has its origin, similar to ECI, fixed to the center of the Earth. Its axes rotate relative to ECI which is fixed in space. This causes any ECEF location on the Earth's surface to be time-invariant. The angular rate of rotation is $\omega_e = 7.2921 \cdot 10^{-5}$ as illustrated on Figure 2.2.

North-East-Down The *North-East-Down* (NED) reference frame is defined relative to the Earth's reference ellipsoid [68] with the coordinates N, E, D as shown in Figure 2.2. Further, the NED-frame is defined relatively to the ECEF-frame by using two angles l and μ denoting the longitude and latitude, respectively.

For marine vessels operating in a local area the rotational effect can be neglected by assuming the NED-frame as inertial.

Body-fixed The body-fixed reference frame is defined fixed to a useful point on a specified body as illustrated on Figure 2.2. The position and orientation are described relative to an inertial reference frame while the linear and angular velocities are described relative to the body-frame.

State Vectors

When assuming the NED-frame as sufficient inertial, the generalized position and orientation vector $\boldsymbol{\eta}$ and the linear and angular velocity vector $\boldsymbol{\nu}$ can be stated as:

$$\boldsymbol{\eta} \triangleq \left[n, e, d, \phi, \theta, \psi\right]^\top \tag{2.1}$$

$$\boldsymbol{\nu} \triangleq \left[u, v, w, p, q, r,\right]^\top \tag{2.2}$$

where $(n, e, d, \phi, \theta, \psi)$ are the positions north, east, down and angels roll, pitch and yaw respectively. The components (u, v, w, p, q, r) signifies the velocity in surge, sway, heave, roll, pitch and yaw respectively.

2.1.2 Transformation between BODY and NED

The state vector $\boldsymbol{\eta}$ describes the position in NED-frame while the vector $\boldsymbol{\nu}$ describes the velocity in BODY-frame. To avoid complex equations of motion it is conventional to transform vectors between different reference system. When analyzing the transformation properties it is advantageous to split up the state vectors in linear and angular velocity parts according to [16] which yields:

$$\boldsymbol{\eta} = \begin{bmatrix} \mathbf{p}^n \\ \boldsymbol{\Theta} \end{bmatrix}, \ \boldsymbol{\nu} = \begin{bmatrix} \mathbf{v}_o^b \\ \boldsymbol{\omega}_{nb}^b \end{bmatrix}, \tag{2.3}$$

where $\mathbf{p}^n = [n, e, d]^\top$ is the position vector decomposed in NED and $\boldsymbol{\Theta} = [\phi, \theta, \psi]^\top$ is a vector of Euler angles, while $\mathbf{v}_o^b = [u, v, w]^\top$ denotes the linear velocity vector and $\boldsymbol{\omega}_{nb}^b = [p, q, r]^\top$ denotes the angular velocity vector, both decomposed in the body-fixed frame.

Linear Velocity Transformation

The body-fixed linear velocity vector $\mathbf{v}_o^b$ and the NED velocity vector $\dot{\mathbf{p}}^n$ are related through the transformation matrix $\mathbf{R}_b^n$ according to:

$$\dot{\mathbf{p}}^n = \mathbf{R}_b^n(\boldsymbol{\Theta})\mathbf{v}_o^b. \tag{2.4}$$

In marine control the most commonly used transformation is called *zyx*-convention [18]. Although the convention generally is not accepted in mathematics and physics due to singularities, it is widely used in aerospace and marine

engineering. The transformation can be written:

$$\mathbf{R}_b^n(\mathbf{\Theta}) = \mathbf{R}_z(\psi)\mathbf{R}_y(\theta)\mathbf{R}_x(\phi), \tag{2.5}$$

where $\mathbf{R}_z(\psi)$, $\mathbf{R}_y(\theta)$ and $\mathbf{R}_x(\phi)$ are the tree principal rotation matrices defined in [18]. When expanding 2.5 the final linear velocity transformation matrix yields:

$$\mathbf{R}_b^n(\mathbf{\Theta}) = \begin{bmatrix} c\psi c\theta & -s\psi c\phi + c\psi s\theta s\phi & s\psi s\phi + c\psi c\phi s\theta \\ s\psi c\theta & c\psi c\phi + s\phi s\theta s\psi & -c\psi s\phi + s\theta s\psi c\phi \\ -s\theta & c\theta s\phi & c\theta c\phi \end{bmatrix}, \tag{2.6}$$

where $s\cdot \triangleq \sin(\cdot)$ and $c\cdot \triangleq \cos(\cdot)$.

Angular Velocity Transformation

The body-fixed angular velocity vector $\boldsymbol{\omega}_{nb}^b = [p, q, r]^\top$ and the Euler rate vector $\dot{\mathbf{\Theta}} = [\dot{\phi}, \dot{\theta}, \dot{\psi}]^\top$ are related through the transformation matrix $\mathbf{T}_\Theta(\mathbf{\Theta})$ according to:

$$\dot{\mathbf{\Theta}} = \mathbf{T}_\Theta(\mathbf{\Theta})\boldsymbol{\omega}_{nb}^b, \tag{2.7}$$

where the transformation matrix $\mathbf{T}_\Theta(\mathbf{\Theta})$ is given by:

$$\mathbf{T}_\Theta(\mathbf{\Theta}) = \begin{bmatrix} 1 & s\phi t\theta & c\phi t\theta \\ 0 & s\phi & -s\phi \\ 0 & s\phi/c\theta & c\phi/c\theta \end{bmatrix}, \tag{2.8}$$

where $s\cdot \triangleq \sin(\cdot)$, $c\cdot \triangleq \cos(\cdot)$ and $t\cdot \triangleq \tan(\cdot)$.

Complete Transformation

Finally, the 6 DOF kinematic equations can be expressed in vector form [16] as:

$$\dot{\boldsymbol{\eta}} = \mathbf{J}(\mathbf{\Theta})\boldsymbol{\nu} \tag{2.9}$$

$$\Updownarrow$$

$$\begin{bmatrix} \mathbf{p}^n \\ \mathbf{\Theta} \end{bmatrix} = \begin{bmatrix} \mathbf{R}_b^n(\mathbf{\Theta}) & 0_{3\times 3} \\ 0_{3\times 3} & \mathbf{T}_\theta(\mathbf{\Theta}) \end{bmatrix} \begin{bmatrix} \mathbf{v}_o^b \\ \boldsymbol{\omega}_{nb}^b \end{bmatrix}, \tag{2.10}$$

where $\mathbf{R}_b^n(\mathbf{\Theta})$ is the rotation matrix from body-fixed to NED reference frame and $\mathbf{T}_\theta(\mathbf{\Theta})$ is the angular velocity transformation matrix.

2.2 Kinetics

Kinetics deal with the forces and moments acting on objects, and explain the accelerations caused by these. In this section a superficial presentation of the different methods will be given and the equations will only be presented without further derivations, which are done in [58].

Figure 2.3: Illustration of a moving vessel (UT 731 CD). Courtesy to Farstad Shipping.

2.2.1 Rigid Body Equation of Motion

The rigid body equation of motion can be expressed in a vectorial setting as [16]:

$$\mathbf{M}_{RB}\dot{\boldsymbol{\nu}} + \mathbf{C}_{RB}(\boldsymbol{\nu})\boldsymbol{\nu} = \boldsymbol{\tau}_{RB}, \tag{2.11}$$

where $\mathbf{M}_{RB}$ is the mass matrix, $\mathbf{C}_{RB}$ is the coriolis centripetal matrix and $\boldsymbol{\tau}_{RB}$ is a generalized vector of external forces and moments.

2.2.2 Hydrodynamic Forces and Moments

The equations given by (2.9) and (2.11) are sufficient to model a body moving through water, but do not take the kinetic energy imparted to the fluid (added mass) or friction into account. In addition a complete model also should include hydrodynamic damping and restoring forces. These forces are only briefly presented in this subsection. Further explanation is found in [18] and [58].

Added Mass

Added (virtual) mass is pressure-induced forces and moments due to the inertia of the surrounding fluid. The surrounding fluid has to move while the vessel is propagating through the water. These forces act in proportion to the vessel's acceleration.

Hydrodynamic Damping

Hydrodynamic damping describes the damping effect caused by the fluid's inertia. The effect is mainly caused by potential damping, skin friction, wave drift damping and damping due to vortex shedding.

Restoring forces and moments

These forces arise from gravity and buoyancy, which are a result of the displacement of water around the vessel. The gravitational force will act on the center of gravity while the buoyancy will act through the center of buoyancy.

2.3 Complete Model

The maneuvering model used in this thesis is suggested by [58] to be used on calm waters. It is derived in 4 DOF containing the linear velocity in surge and sway in addition to the angular velocity in yaw and roll. According to [58] the model can be expressed:

$$\dot{\boldsymbol{\eta}} = \mathbf{J}(\boldsymbol{\theta})\boldsymbol{\nu} \tag{2.12}$$

$$\mathbf{M}\dot{\boldsymbol{\nu}} + \mathbf{C}(\boldsymbol{\nu})\boldsymbol{\nu} + \mathbf{D}(\boldsymbol{\nu})\boldsymbol{\nu} + \mathbf{g}(\boldsymbol{\eta}) = \boldsymbol{\tau}, \tag{2.13}$$

where $\mathbf{M} \triangleq \mathbf{M}_{RB} + \bar{\mathbf{M}}_A$ and $\mathbf{C}(\boldsymbol{\nu}) \triangleq \mathbf{C}_{RB}(\boldsymbol{\nu}) + \mathbf{C}_A^0(\boldsymbol{\nu})$. Notice that the model is assuming the NED-frame as inertial and does not compensate for external disturbances as wind, waves and current.

The rigid body matrix mass $\mathbf{M}_{RB}$ and the added mass $\bar{\mathbf{M}}_A$ are given by:

$$\mathbf{M}_{RB} = \begin{bmatrix} m & 0 & 0 & 0 \\ 0 & m & 0 & 0 \\ 0 & 0 & I_x & I_{xz} \\ 0 & 0 & I_{xz} & I_z \end{bmatrix} \tag{2.14}$$

$$\bar{\mathbf{M}}_A = \frac{1}{2}\left(\mathbf{M}_A + \mathbf{M}_A^\top\right). \tag{2.15}$$

where $\mathbf{M}_A$ is given by:

$$\mathbf{M}_A = -\begin{bmatrix} X_{\dot{u}}^0 & 0 & 0 & 0 \\ 0 & Y_{\dot{v}}^0 & Y_{\dot{p}}^0 & Y_{\dot{r}}^0 \\ 0 & K_{\dot{v}}^0 & K_{\dot{p}}^0 & K_{\dot{r}}^0 \\ 0 & N_{\dot{v}}^0 & N_{\dot{p}}^0 & N_{\dot{r}}^0 \end{bmatrix}. \tag{2.16}$$

Further can the Coriolis-centripetal matrix $\mathbf{C}_{RB}(\boldsymbol{\nu})$ and the added mass Coriolis-

centripetal matrix $\mathbf{C}_A^0(\boldsymbol{\nu})$ in 4 DOF be written as:

$$\mathbf{C}_{RB}(\boldsymbol{\nu}) = \begin{bmatrix} 0 & 0 & 0 & -mv \\ 0 & 0 & -mw & mu \\ 0 & mw & 0 & -I_y q \\ mv & -mu & I_y q & 0 \end{bmatrix} \tag{2.17}$$

$$\mathbf{C}_A^0(\boldsymbol{\nu}) = \begin{bmatrix} 0 & 0 & 0 & Y_{\dot{v}}^0 v + \frac{1}{2}\left(N_{\dot{v}}^0 + Y_{\dot{r}}^0\right) r \\ & & & +\frac{1}{2}\left(Y_{\dot{p}}^0 + K_{\dot{v}}^0\right) p \\ 0 & 0 & 0 & -X_{\dot{u}}^0 u \\ 0 & 0 & 0 & 0 \\ -Y_{\dot{v}}^0 v - \frac{1}{2}\left(N_{\dot{v}}^0 + Y_{\dot{r}}^0\right) r & X_{\dot{u}}^0 u & 0 & 0 \\ -\frac{1}{2}\left(Y_{\dot{p}}^0 + K_{\dot{v}}^0\right) p & & & \end{bmatrix}. \tag{2.18}$$

A simplified formulation of the restoring matrix $\mathbf{g}(\boldsymbol{\eta})$ when assuming small angles can be formulated:

$$\mathbf{g}(\boldsymbol{\eta}) = \begin{bmatrix} 0 & 0 & \rho g \nabla \overline{GM_t} \sin\phi & 0 \end{bmatrix}^\top. \tag{2.19}$$

At last the damping matrix $\mathbf{D}(\boldsymbol{\nu})$ describing hydrodynamic forces and moments can be written on matrix formulation as:

$$\mathbf{D}(\boldsymbol{\nu}) = \begin{bmatrix} -X_{uu}^L u - X_{uuu}^L u^2 - X_{rvu}^L rv & -X_{vv}^L v - X_{rv}^L r - X_{uvv}^L uv \\ & -X_{vv\phi\phi}^L v\phi^2 - X_{vr\phi\phi}^L r\phi \\ -Y_{uv\phi\phi}^L v\phi^2 - Y_{ur\phi\phi}^L r\phi^2 & -Y_{uv}^L u - Y_{uuv}^L u^2 - Y_{vvv}^L v^2 \\ & -Y_{rrv}^L r^2 - Y_{|v|v}|v| - Y_{|r|v}|r| \\ -K_{uv\phi\phi}^L v\phi^2 - K_{ur\phi\phi}^L r\phi^2 & -K_{uv}^L u - K_{uuv}^L u^2 - K_{vvv}^L v^2 \\ & -K_{rrv}^L r^2 - K_{|v|v}|v| - K_{|r|v}|r| \\ -N_{uv\phi\phi}^L v\phi^2 - N_{ur\phi\phi}^L r\phi^2 & -N_{uv}^L u - N_{uuv}^L u^2 - N_{vvv}^L v^2 \\ & -N_{rrv}^L r^2 - N_{|v|v}|v| - N_{|r|v}|r| \end{bmatrix}$$

$$\begin{bmatrix} 0 & -X_{rr}^L r - X_{urr}^L ur - X_{rr\phi\phi}^L r\phi\ 2 \\ 0 & -Y_{ur}^L u - Y_{uur}^L u^2 - Y_{rrr}^L r^2 \\ & -Y_{vvr}^L v^2 - Y_{|v|r}|v| - Y_{|r|r}|r| \\ -K_p - K_{ppp} p^2 & -K_{ur}^L u - K_{uur}^L u^2 - K_{rrr}^L r^2 \\ & -K_{vvr}^L v^2 - K_{|v|r}|v| - K_{|r|r}|r| \\ 0 & -N_{ur}^L u - N_{uur}^L u^2 - N_{rrr}^L r^2 \\ & -N_{vvr}^L v^2 - N_{|v|r}|v| - N_{|r|r}|r| \end{bmatrix}. \tag{2.20}$$

Chapter 3

Identification of Maneuvering Characteristics

This chapter starts with an introduction to system identification followed by a presentation of the autopilot models utilized in this thesis. In section three an overview over the most utilized ship maneuvers is carried out in addition to a new suggested ship maneuver. The last section briefly describes the most acknowledged identification methods used for identification of ship steering dynamics in the literature.

3.1 System Identification

The field of system identification is far too broad to be completely covered, so this thesis has focused on identification techniques applied to determine ship steering dynamics. Although, a briefly introduction to the subject is given in the following subsection. More theory on system identification can for instance be found in [14], [35] and [64], and more theoretical background on parametric estimation and curve fitting can be found in [22], [24] and [75].

3.1.1 Introduction

System identification is a subject area where the goal is to determine the behavior of a dynamic system. A more precise definition is given in [24]:

> *"In its most general form system identification is the process of properly mathematically modeling the behavior of a given system."*

Further is the following formulation of the identification problem given by [78]:

> *"Identification is the determination, on the basis of input and output, of a system within a specified class of systems, to which the system under test is equivalent."*

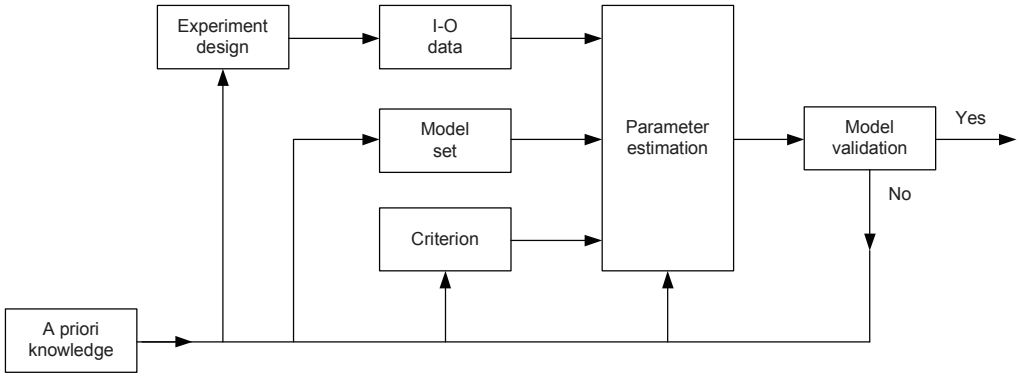

Figure 3.1: A flow diagram of system identification [28].

A natural logical flow of the system identification procedure is described in Figure 3.1. As seen in the figure a priori knowledge about the system is used in all parts of the identification procedure. The main objective with experiment design is to make the data maximally informative. However, the most important and difficult choice is to find a suitable model structure. Constructing a model from data basically involves three entities:

- a data set,
- a model structure,
- a rule to assess the quality of the models.

When standard models are employed without reference to the physical background, it is called *black-box modeling*. Further when physical insight is available, but still with unknown adjustable parameters, it is called *grey-box modeling*. At last when deeper physical insight and prior knowledge is known it is called *white-box modeling*. In any cases the models could be either linear or nonlinear. Although almost all physical systems are nonlinear, linear models can usually be applied in a bounded operation point.

Since the steering dynamics of a marine vessel can be modeled by means of Newtonian mechanics, this thesis has focused on grey-box modeling. Compared to black-box modeling, grey-box modeling has the following advantages:

- known constraints can be imposed, such as parameters and noise variance,
- potentially fewer parameters to estimate,
- couplings between parameters can be specified,
- in the nonlinear case, the dynamic equations can be specified explicitly.

3.2 Autopilot Models

The steering dynamics of surface vessels have been derived by several researchers based on first principles using Newton's laws of motion such as [1], [13] and [51]. In this thesis only the linear model of Nomoto and the nonlinear autopilot model of Ross are considered.

3.2.1 The Nomoto Model

The widely used Nomoto model derived in [49], is obtained by eliminating the sway velocity from an earlier model derived by [13]. This results in the second order model:

$$\frac{r}{\delta}(s) = \frac{K(1+T_3 s)}{(1+T_1 s)(1+T_2 s)}, \tag{3.1}$$

where T_1, T_2 and T_3 are time constants and K is the gain constant.

The first order Nomoto model is obtained by defining the effective time constant $T = T_1 + T_2 - T_3$, in such a way that the transfer function between r and δ can be written:

$$\frac{r}{\delta}(s) = \frac{K}{(1+Ts)}, \tag{3.2}$$

where T and K are the Nomoto time and gain constants, respectively. When neglecting the roll and pitch modes such that $\dot{\psi} = r$, the model can be written in the time domain as:

$$T\ddot{\psi} + \dot{\psi} = K\delta. \tag{3.3}$$

A nonlinear extension of the first order model can be done according to [50], by adding static nonlinearities. Then, the model can be stated:

$$T\dot{r} + H_N(r) = K\delta \tag{3.4}$$

$$H_N(r) = n_3 r^3 + n_2 r^2 + n_1 r + n_0, \tag{3.5}$$

where $H_N(r)$ is a nonlinear function describing the nonlinear maneuvering characteristics.

3.2.2 Autopilot Model of Ross

The second autopilot model considered in this thesis is derived by [58], based on longstanding analyses in low aspect-ratio aerodynamics. Ross suggests this model for heading autopilot design:

$$\begin{aligned}
(I_z - N_{\dot{r}})\dot{r} - N^L_{uv\phi\phi}uv\phi^2 - N^L_{uv}uv - N^L_{uuv}u^2 v - N^L_{vvv}v^3 \\
-N^L_{rrv}r^2 v - N_{|v|v}|v|v - N_{|r|v}|r|v - N^L_{ur}ur - N^L_{uur}u^2 r \\
-N^L_{rrr}r^3 - N^L_{vvr}v^2 r - N_{|v|r}\ |v|r - N_{|r|r}|r|r + (X^0_{\dot{u}} - Y^0_{\dot{v}})uv \\
-\frac{1}{2}(N^0_{\dot{v}} + Y^0_{\dot{r}})ru - \frac{1}{2}(Y^0_{\dot{p}} + K^0_{\dot{v}})p &= N \qquad (3.6) \\
\dot{\phi} &= r. \qquad (3.7)
\end{aligned}$$

This model is nonlinear and time-varying, and should not be directly compared to the linear Nomoto model which only contain two parameters. In contrast the autopilot model of Ross contains 20 parameters. In addition is this model also capable of dealing with varying surge and sway velocities, which is essential for an accurate autopilot model. The model also contain the roll motion, but that is not covered in this research.

3.3 Ship Maneuvers

A few ship maneuvers (experimental designs) have been proposed for testing the maneuverability and identification of maneuvering characteristics, such as [29], [49] and [48]. In this section the most utilized ship maneuvers is presented. In addition is a new maneuver proposed for identification of stable ship steering dynamics.

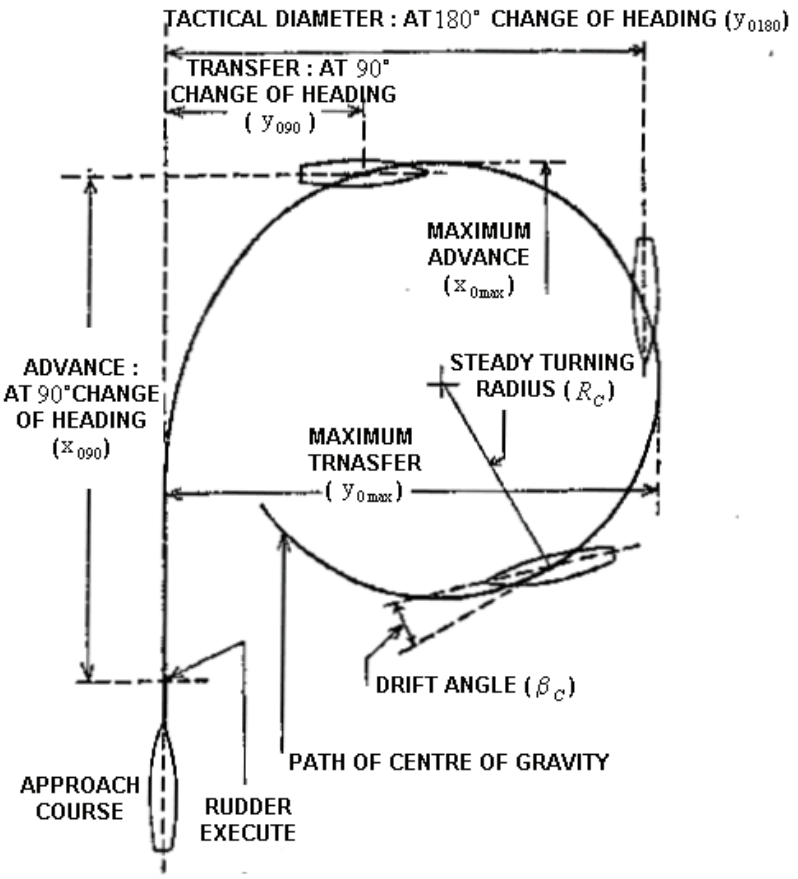

Figure 3.2: Turning circle definition. Courtesy to [26].

3.3.1 Standard Ship Maneuvers

A maneuvering characteristic can be obtained by doing predefined maneuvers. The International Towing Tank Conference (ITTC) have proposed the following standard ship maneuvers [26].

Turning Circle

The turning circle is simply to apply a rudder angle at an initial speed. It is necessary to do a turning circle of at least 540 degrees to determine the main parameters of this trial which are: tactical diameter, advance, transfer, loss of speed on steady turn, time to change heading 90 degrees and time to change heading 180 degrees.

Zig-zag Maneuver

The zig-zag maneuver is performed by reversing the rudder alternately by a rudder angle to either side. The rudder angle is held constant until the heading is changed to 20 degrees, then the rudder is reversed. This is done until a total of 5 rudder steps have been completed. Common values for the rudder angle is 20/20 and 10/10. However, other combinations can be applied. For larger ships a rudder angle of 10 degrees are recommended to reduce the time and waterspace required. As seen in Figure 3.3, the results of a zig-zag test are: initial turning rate, execute heading angle, time to check yaw, heading, reach, time of a complete cycle, angular speed and unit time. Further definitions are explained in [26]. The zig-zag maneuver was first proposed by Kempf [29]. Hence, the name Kempf's zig-zag maneuver also is used in the literature.

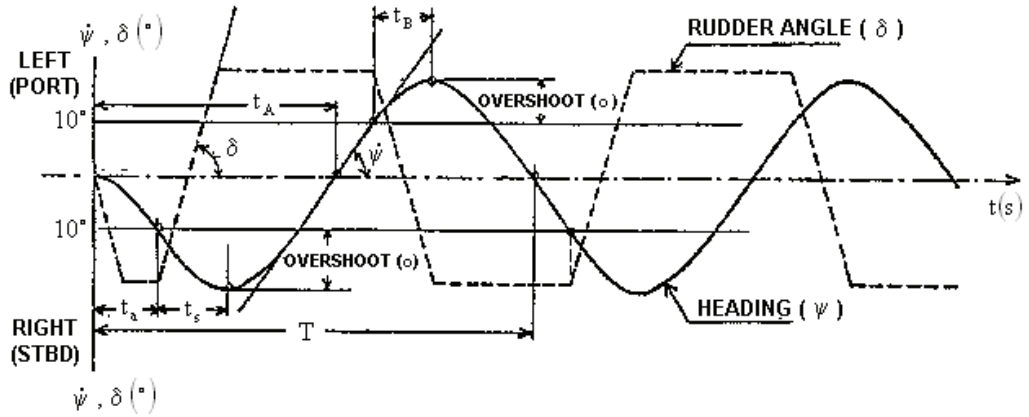

Figure 3.3: Time trace of zig-zag maneuver parameters. Courtesy to [26].

Spiral Maneuvers

Spiral maneuvers are applied to assess the course stability. For stable ships, both the direct (Dieudonné's) spiral maneuver and the reverse (Bech's) spiral maneuver can be used. The direct spiral maneuver starts with an initial straight course, followed by a rudder input of about 25 degrees to starboard held until constant rate of turn is obtained. Then the rudder angle is decreased by 5 degrees and held until steady conditions have been achieved. This procedure is repeated until the rudder has covered the range to 25 degrees port and back again. During this test the steady rate of turn is registered for each rudder angle.

For unstable ships the reverse spiral maneuver is recommended within the limits indicated by the pull-out test, described in the following subsection. In contrast to the direct spiral maneuver the rate of turn is now held constant, while the mean rudder angle required to produce this rate of turn is measured. Although an autopilot is recommended it is not required. The necessary equipment is a rate gyro and an accurate rudder angle indicator. In addition, the reverse spiral maneuver is less time-consuming than the direct spiral maneuver, and has been quite popular because of the simplicity and reliability of the method [18].

Pull-Out Test

The pullout maneuver is a simple test to check whether the vessel is straight-line stable or not. A rudder angle of approximately 20 degrees is applied until the ship achieves a steady rate of turn. Then the rudder angle returns to zero and it can be determined whether the vessel is straight-line stable. If the ship is straight-line stable the rate of turn will decay to zero for both port and starboard turn. Contrary, if the ship is unstable, the steady rate of turn will reduce to some residual yaw rate.

Stopping Test

Stopping tests or crash-stops trials can be used to determine the vessel's maneuverability during emergency situations. The most common stopping trials starts from full ahead speed, and then full astern power is given when the approach conditions are satisfied.

3.3.2 Suggested Ship Maneuver

Although several of the maneuvers described above can be used for the purpose of identification, improvements can be done in sense of *informative* signals defined by [35] in the following definitions, theorem and corollary:

Definition 13.1 *A quasi-stationary signal u(t), with spectrum $\Phi_u(\omega)$, is said to be persistently exciting of order n if, for all filters of the form*

$$M_n(q) = m_1 q^{-1} + ... + m_n q^{-n} \tag{3.8}$$

the relation

$$|M_n(e^{i\omega})|^2 \equiv 0 \quad \text{implies that} \quad M_n(e^{i\omega}) \equiv 0 \tag{3.9}$$

Definition 13.2 *A quasi-stationary signal u(t) with spectrum $\Phi_u(\omega)$, is said to be persistently exciting if*

$$\Phi_u(\omega) > 0, \qquad \text{for almost all } \omega \tag{3.10}$$

Theorem 13.1 *Consider a set $\mathcal{M}^*$ of SISO models given by (3.9) such that the transfer functions $G(z,\theta)$ are rational functions:*

$$G(q,\theta) = \frac{B(q,\theta)}{F(q,\theta)} = \frac{q^{n_k}(b_1 + b_2 q^{-1} + ... + b_{n_b} q^{-n_b+1})}{1 + f_1 q^{-1} + ... + f_{n_f} q^{-n_f}} \tag{3.11}$$

Then an open-loop experiment with an input that is persistently exciting of order $n_b + n_f$ is sufficiently informative with respect to $\mathcal{M}^*$.

Corollary *An open-loop experiment is informative if the input is persistently exciting.*

In elucidation of Theorem 13.1 which define persistence excitation, this thesis suggests a new ship maneuver to be used for system identification of stable ship steering dynamics. Although the proposed maneuver has something in common with both the turning circle, zig-zag maneuver and the direct spiral maneuver, it excite the steering system better and give more informative signals. In addition the suggested maneuver described below also utilize all range of rudder deflection in one maneuver.

Rudder steps	5, 10, 20, 40 and 45 (deg)
Thrust levels	200 and 500 (rpm)
Relative period to hold the rudder deflection	2 seconds x deflection
Linear decrease of rudder deflection	0,3 deg/s

Table 3.1: Suggested adjustments employed to the proposed maneuver.

The proposed maneuver starts at an initial course with a constant thrust level. The rudder angle is then reversed alternately by predefined steps to either side. But as distinct from the zig-zag maneuver, the rudder deflection is held a predefined period relative to the angle before it decrease to zero with a linear constant. This procedure continues for all predefined rudder steps at either sides as shown in Figure 3.4. At last the rudder deflection is held to zero to ensure that identified model will be stable. Suggested adjustments which are also used in this thesis are shown in Table 3.1.

This maneuver should be repeated using several thrust levels to excite the nonlinear rudder effect. The maneuver parameters should also be adjusted for ships with rather fast or slow turning capabilities. For unstable ships the reverse spiral maneuver is still necessary to identify the nonlinear characteristics around zero rudder deflection.

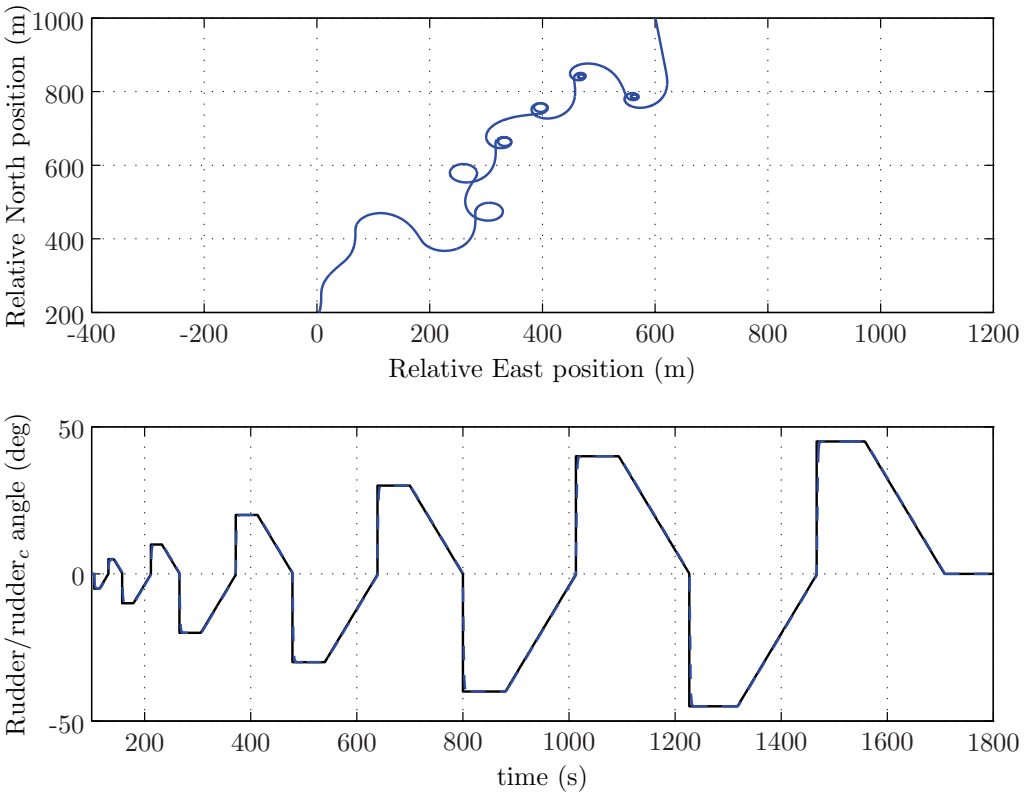

Figure 3.4: North-East plot and rudder input during the proposed maneuver.

3.4 Identification Methods

System identification techniques applied to determine ship steering dynamics have been under research for ages. The techniques varies from simple determination to more sophisticated algorithms. Although a diversity of identification methods is described in the literature, a number of methods are based on more or less the same principles. In the paragraphs below, three general procedures reviewed in [35] are introduced.

This section also presents some of the reported methods utilized for identification of ship steering dynamics. The last subsection describes a few methods utilized for validation of models and parameter convergence.

Prediction-Error Identification Approach (PEM) This approach contains well-known procedures, such as the least-square method and the maximum likelihood method. It is also closely related to the Bayesian maximum a posteriori estimation. The method is according to [35] defined by:

$$\hat{\theta}_N = \underset{\theta \in D_{\mathcal{M}}}{\arg\min}\, V_N(\theta, Z^N) \tag{3.12}$$

$$V_N(\theta, Z^N) = \frac{1}{N}\sum_{t=1}^{N} \ell(\epsilon(t,\theta), \theta, t). \tag{3.13}$$

Subspace Approach to Identifying State-Space Models Subspace methods avoid the problem connected to parametrization. In general the approach consists of three steps: (1) estimating ahead predictors using a least-square algorithm, and (2) selecting the state vector, and (3) estimate the state-space matrices using the least-square method.

Correlation Approach Another approach is to utilize the correlation between regression variables and the chosen instruments. The approach contains the instrumental-variable technique, as well as several methods for rational transfer function models and is defined by:

$$\epsilon_F(t,\theta) = L(q)\epsilon(t,\theta) \tag{3.14}$$

$$\hat{\theta}_N = \underset{\theta \in D_{\mathcal{M}}}{\text{sol}}\, [f_N(\theta, Z^N) = 0] \tag{3.15}$$

$$f_N(\theta, Z^N) = \frac{1}{N}\sum_{t=1}^{N} \zeta(t,\theta)\alpha(\epsilon_F(t,\theta). \tag{3.16}$$

3.4.1 Simple Curve Fitting of Turning Circles

One simple method to identify the Nomoto time and gain constant is presented in [18]. By considering the results from the turning circle the ordinary differential

equation (3.3) can be written explicitly. For a constant step input δ_0 the rate of change $r(t)$ can be written as:

$$r(t) = \exp(-t/T)r(0) + (1 - \exp(-t/T))K\delta_0, \tag{3.17}$$

where $r(0)$ is the initial value, T is the Nomoto time constant and K is the Nomoto gain. Using nonlinear least square curve fitting T and K can be estimated.

3.4.2 Classic Determination from Zig-zag Trials

A widely used technique is to determine the parameters in the Nomoto model from the zig-zag maneuver using an index estimator published in [48]. Further has Journée [27] developed a method to deal with overshoot and transient effects caused by rudder delay and limitations. Using Nomoto's first order model, a large number of zig-zag maneuvers have been calculated at a practical range of K and T values. These data have been analyzed and the relation between the zig-zag maneuvering characteristics and the Nomoto parameters have been reflected in graphs.

Further work in the field of identification from zig-zag trials has been accomplished by [50] and [73]. The steering dynamics has also been estimated by simple integration of the measurements during planar motion mechanism tests as in [12] and [67].

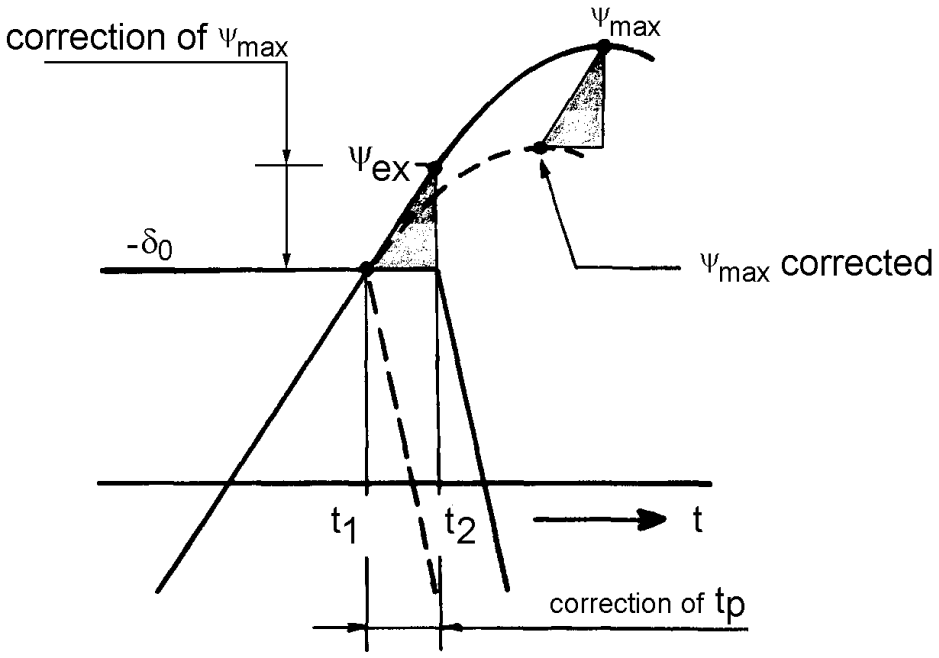

Figure 3.5: Graph describing Journée's method. Courtesy to [27].

3.4.3 Closed Loop/Adaptive Identification

Identification of parameters can also be done in closed-loop. A survey on closed-loop identification is given in [23]. Several papers, such as [11], [34] and [45], have reported great results. Adaptive steering of ships have for instance been utilized in [21], [44] and [61]. In general there is some basic issues associated with closed loop identification:

- a closed loop experiment is less informative,
- an accurate noise model is necessary to apply direct methods,
- for indirect methods, the exact regulator mechanisms have to be known.

3.4.4 Maximum Likelihood Estimation

The parameters of a second-order model has been successfully determined in [63], [65] and [66] using the maximum likelihood method. The identification is done by manual generation of test signals with a full scale freighter. As many other techniques, the method minimizes a loss function.

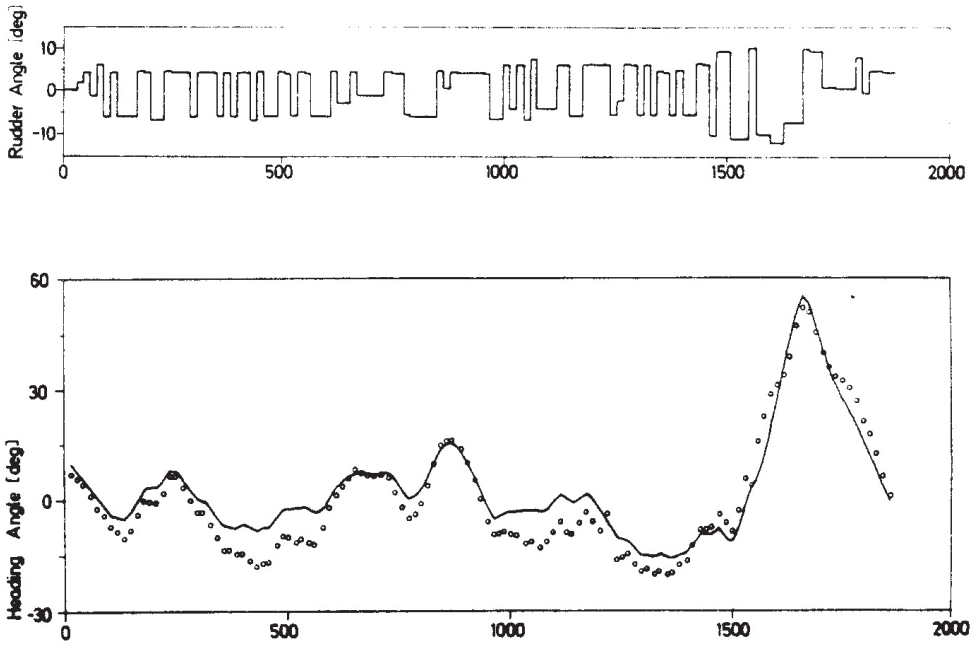

Figure 3.6: Results of identification of a second-order model using maximum likelihood estimation. Courtesy to [66].

3.4.5 Extended Kalman filter Estimation

Several researchers have reported great results using identification techniques based on the extended Kalman filter such as [2], [9], [10], [25] and [39]. In contrast to other estimators this approach treats the parameters as additional state variables, which must be constant in time. Further work based on the extended Kalman filter in the field of system identification is accomplished by [42] and [77]. The Kalman filtering technique is also widely used in dynamic positioning of ships, which for instance is described in [5] and [20].

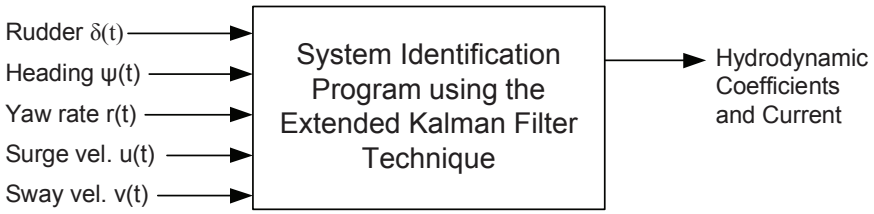

Figure 3.7: Illustration of the extended Kalman filtering technique used in the purpose of system identification [2].

3.4.6 Frequency Domain Methods

Another method applied to ship maneuvering is a frequency domain method reported in [8], [7] and [59]. The method has its origin in the work of [56] and further work is accomplished by [6]. This is a non-iterative, spectral method performing the nonlinear operations in the time domain and the linear operations in the frequency domain.

3.4.7 Prediction Error Identification Methods

In [31] several identification methods are considered such as output error, maximum likelihood and more general prediction error methods. The recursive (iterative) prediction error method is closely related to the extended Kalman filtering technique. In contrast, the nonlinear prediction error method treat the Kalman gain as elements of the parameter vector to be estimated, which is also known as Ljung's innovations filter model. Hence, this identification method is less critical to the a priori knowledge about the noise covariance. The family of prediction error methods also have a close kinship with the maximum likelihood estimation. The method is based on the theory of Ljung [36][37] and is also thorough described and utilized in [79].

3.4.8 Other Methods

In addition several other identification techniques are applied to this identification problem. For instance is a neural network approach considered in [55]. Another approach is based on Lyapunov identification which in the work of [70] is compared to classic least-square techniques.

3.4.9 Parameter Convergence

Validating the model and identification algorithm is an important step in system identification. Although visual inspection of the results can be valuable, it is often preferable to use numerically calculations. In [35] several ways of comparing models is presented, such as the variance:

$$J_k(m) = \frac{1}{N}\sum_{t=1}^{N} |y(t) - \hat{y}_k(t|m)|^2, \tag{3.18}$$

sum of residuals:

$$J_k(m) = \sum_{t=1}^{N} |y(t) - \hat{y}_k(t|m)|, \tag{3.19}$$

standard deviation:

$$J_k(m) = \sqrt{\frac{1}{N}\sum_{t=1}^{N} |y(t) - \hat{y}_k(t|m)|^2} \tag{3.20}$$

and Akaike's *final prediction-error* (FPE) criterion [3]:

$$\bar{J}_p(\mathcal{M}) \approx \frac{1 + (d_{\mathcal{M}}/N)}{1 - (d_{\mathcal{M}}/N)} V_N(\hat{\theta}_N, Z^N) \tag{3.21}$$

$$= \frac{1 + (d_{\mathcal{M}}/N)}{1 - (d_{\mathcal{M}}/N)} \frac{1}{N}\sum_{t=1}^{N} \epsilon^2(t, \hat{\theta}_N). \tag{3.22}$$

In addition to several methods of cross-validation, [41] introduces the fit-function. This method describes the percentage of the measured output that was explained by the model. The function is defined by:

$$fit = 100/(1 - norm(y - \hat{y})/norm(y - mean(y))). \tag{3.23}$$

Chapter 4

Identification Results

In this thesis the autopilot models are estimated using the iterative prediction error minimization method provided by the System Identification Toolbox [41] in Matlab. This method is comparable to the prediction error method reviewed in subsection 3.4.7. Each iteration involves the approximate solution of a large linear system using the method of preconditioned conjugate gradients. The Trust Region Reflective Newton search method of nonlinear least-squares (lsqnonlin), provided by the Optimization Toolbox [40] is chosen because it handles bounds better than line search methods.

This chapter describes the simulation environment and the identification results. In the first section the experiment design is simulated. The predefined maneuvers: turning circle and zig-zag maneuver are compared to the maneuver suggested in subsection 3.3.2. All of the maneuvers are simulated with different initial velocities and rudder deflections. The turning circle is carried out at 5, 10, 20 and 40 degrees, while the same deflections and headings are used in the zig-zag maneuvers, namely 5-5, 10-10, 20-20 and 40-40 degrees. In contrast is only one suggested maneuver necessary to excite the various rudder deflections. Subsequently are all maneuvers executed in both 200 rpm and 500 rpm.

In section two and three the identification results are presented. Estimation of the model parameters is first carried out on single experiments at a constant revolution for all of the maneuvers. Subsequently, the same identification procedures are carried out for the merged data including simulations in both 200 rpm and 500 rpm for each of the three maneuvers. In addition is the identification procedure executed for both the linear Nomoto model and the nonlinear autopilot model of Ross.

4.1 Simulation of the Experimental Designs

The maneuvering model and the suggested maneuver is implemented in Matlab as an m-function and imported to Simulink. An overview over the simulation environment is shown in Figure 4.1.

The model parameters used in this report are identified by Ross [58] from a

Length between perpendiculars	Lpp	4.002 m
Maximum beam at the waterline	Bwl	0.538 m
Vertical distance from bottom of hull to waterline	T	0.172 m
Displacement	$Disp$	0.188 m^3
Yaw Inertia	I_z	0.295*Lpp
Roll Inertia	I_x	0.37*Bwl
Maximum rudder rate	rr	15.0 deg/s

Table 4.1: The vessel's main particulars [69].

scaled model. Unfortunately, the roll data was not included so the simulation is done in 3 DOF namely surge, sway and yaw. The vessel's main particulars are published on Simman [69] and are partly presented in Table 4.1.

Compared to [69] the maximum rudder rate is decreased to emphasize the saturation effect on the maneuvering model. In addition to the vessel model presented in (2.13), a highly nonlinear rudder effect on the yaw motion is included as shown in Figure B.15. The simulated ship has an approximately maximum speed of 3.5 knots (1.8 m/s) and is able to turn as much as 10 radians per second using the maximum rudder deflection of 45 degrees.

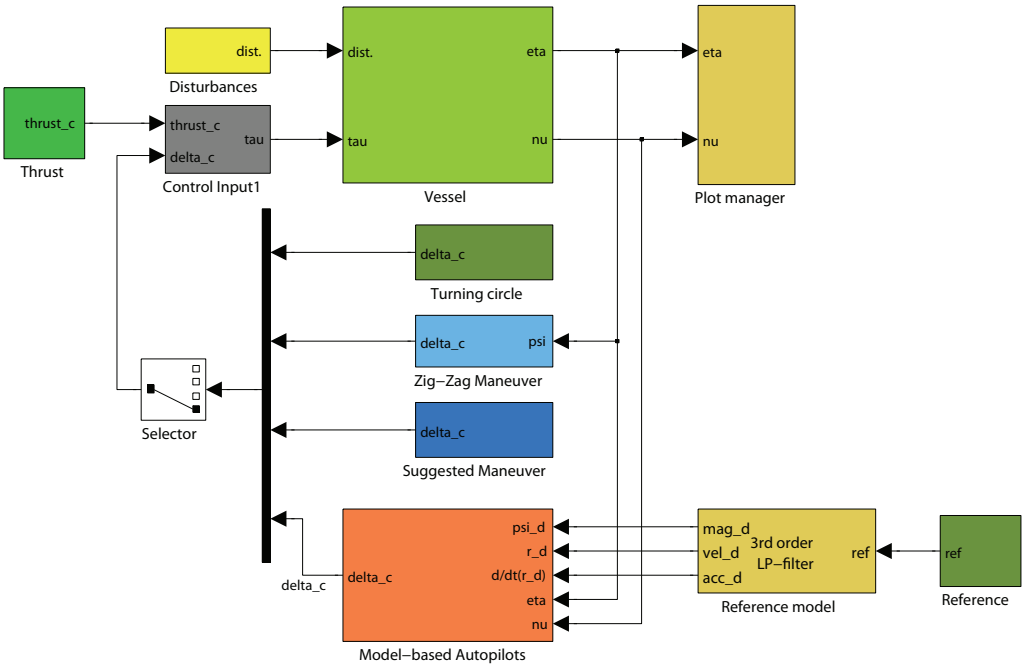

Figure 4.1: Overview over the simulation environment.

4.1.1 Turning Circle

Figure 4.2 and 4.3 shows the results of the 40 degree turning circle in 500 rpm. Results of the other turning circle experiments are presented in section A.1.

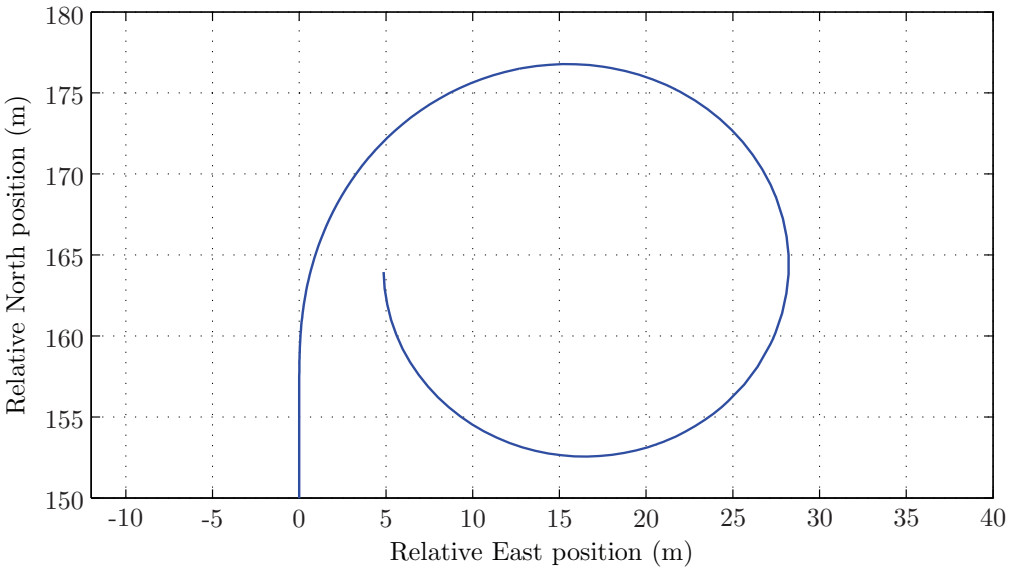

Figure 4.2: North-East plot of the 40 degree turning circle (500 rpm).

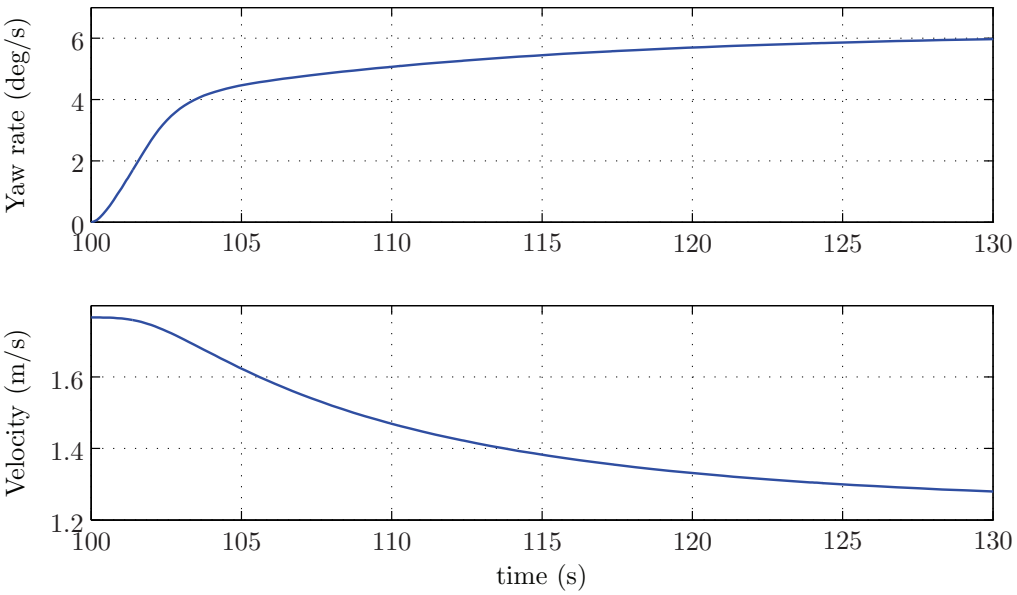

Figure 4.3: Yaw rate and velocity during the 40 degree turning circle (500 rpm).

4.1.2 Zig-zag Maneuver

The 40-40 zig-zag maneuver in 500 rpm in shown in Figure 4.4 and 4.5. The other zig-zag maneuvers are available in section A.2.

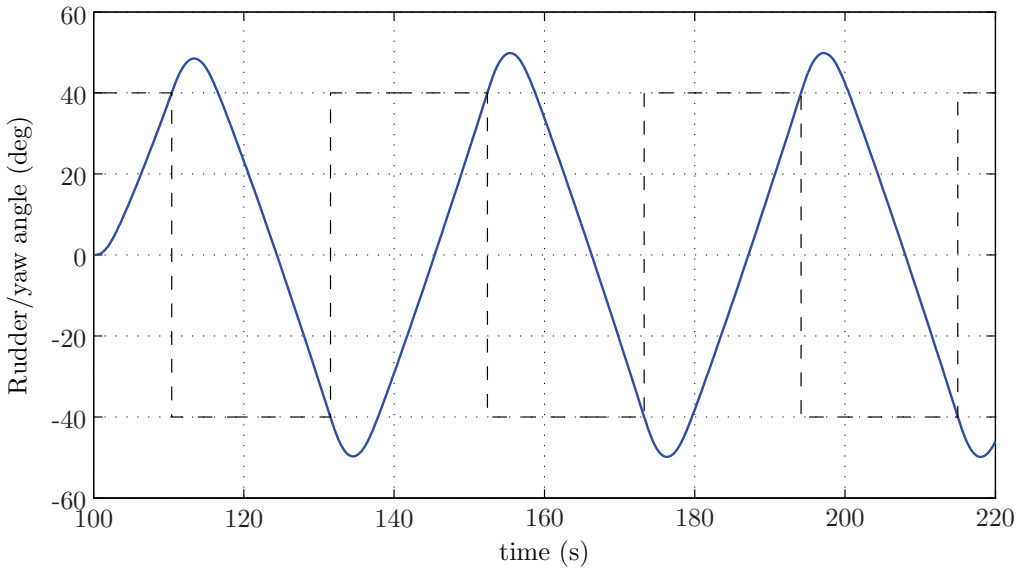

Figure 4.4: Rudder/yaw plot of the 40-40 zig-zag maneuver (500 rpm).

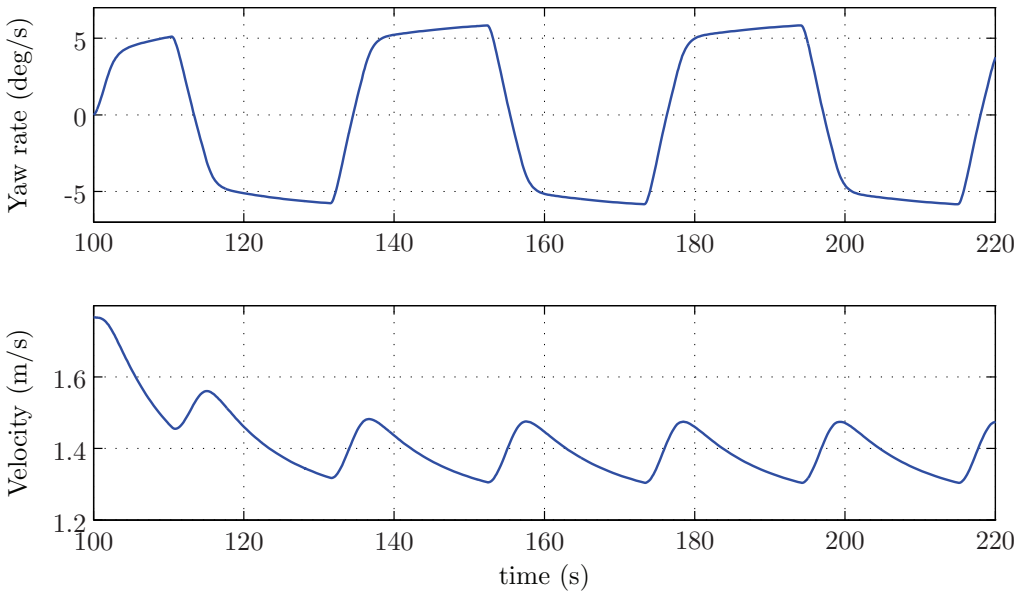

Figure 4.5: Yaw rate and velocity during the 40-40 zig-zag maneuver (500 rpm).

4.1.3 The Suggested Maneuver

Below, in Figure 4.6 and 4.7 the results during the suggested maneuver in 500 rpm is presented. The other experiment during 200 rpm is shown in section A.3.

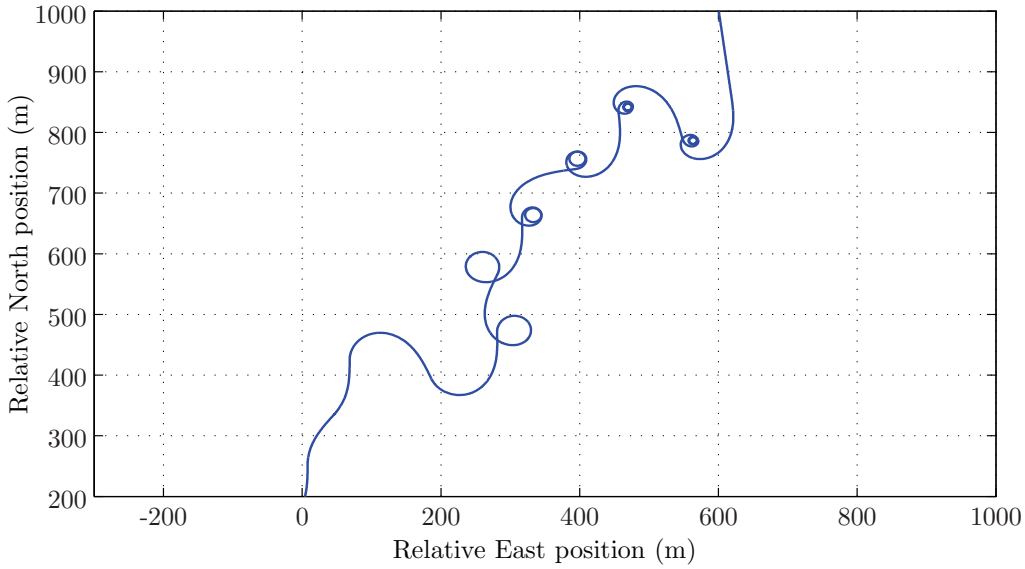

Figure 4.6: North-East plot of the suggested maneuver (500 rpm).

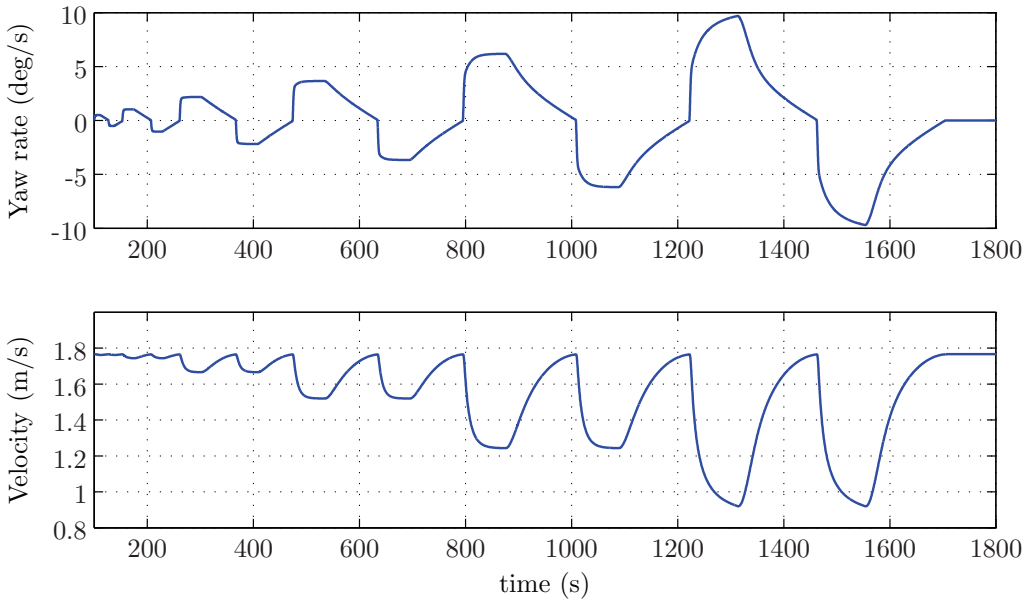

Figure 4.7: Yaw rate and velocity during the suggested maneuver (500 rpm).

4.2 Identification based on Single Experiments

4.2.1 Data from the Turning Circle

Now the two autopilot models are identified using measured data from the 40 degree turning circle. The measured behavior is not linear, as seen in Figure 4.8. But as expected, the autopilot model of Ross is able to adapt the maneuver very well in Figure 4.10.

The Nomoto Model

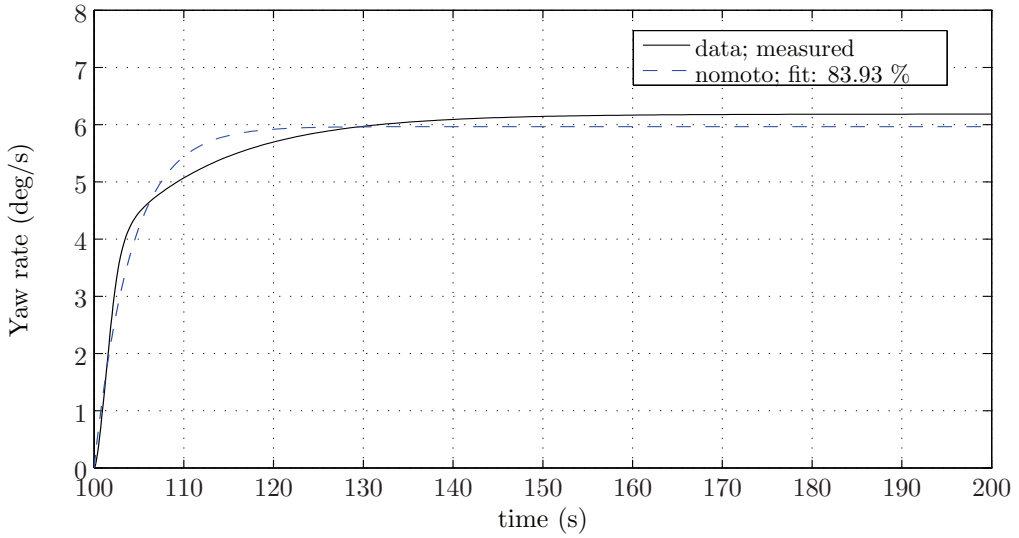

Figure 4.8: The estimated Nomoto model compared to measured data from a single turning circle.

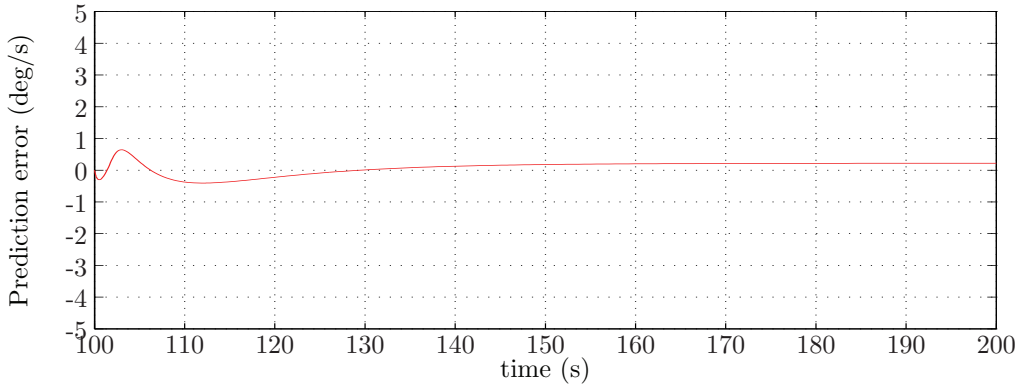

Figure 4.9: Prediction error for yaw rate.

Autopilot Model derived by Ross

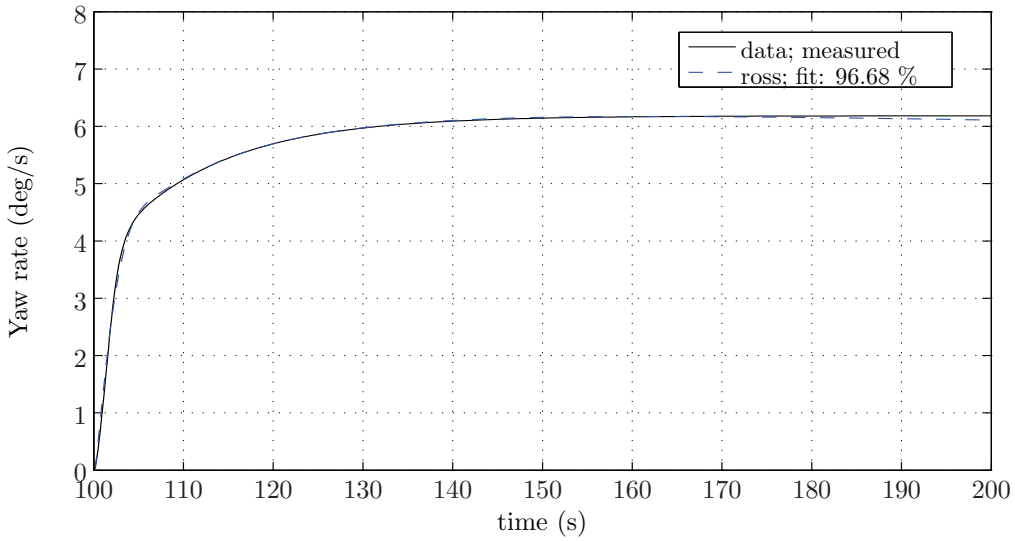

Figure 4.10: The estimated autopilot model of Ross compared to measured data from a single turning circle.

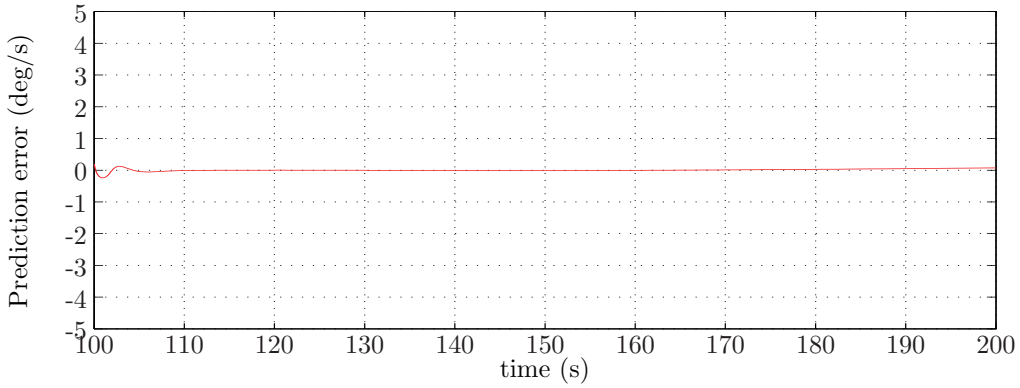

Figure 4.11: Prediction error for yaw rate.

The results above indicates the huge difference between the linear Nomoto model and the nonlinear autopilot model of Ross. The reason why the Nomoto model does not converge to the steady-state yaw rate is the relative short simulation time. The identified Nomoto model's loss function is 0.061179 and Akaike's FPE is 0.0620058. Contrary, the identified model of Ross has the loss function 0.00289805 and the Akaike's FPE 0.00325052.

4.2.2 Data from the Zig-zag Maneuver

Identification of the parameters based on the 40-40 zig-zag maneuver is presented in Figure 4.12 and 4.14. The identified Nomoto model shows a fair capability to adapt the chosen zig-zag maneuver, while the autopilot model of Ross not surprisingly is able to adapt very well.

The Nomoto Model

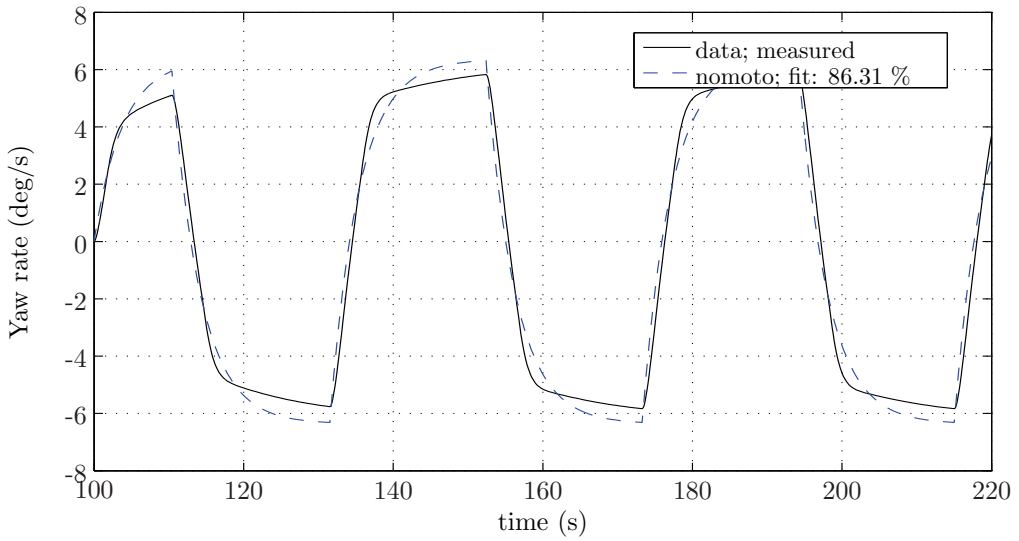

Figure 4.12: The estimated Nomoto model compared to measured data from a single zig-zag maneuver.

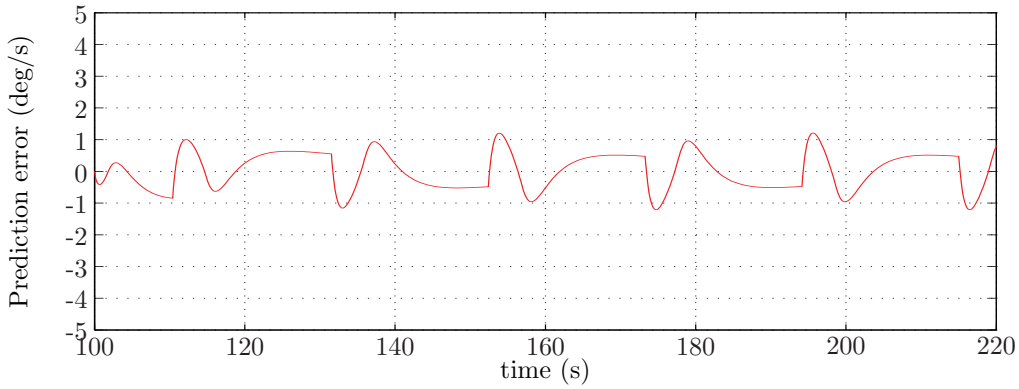

Figure 4.13: Prediction error for yaw rate.

Autopilot Model derived by Ross

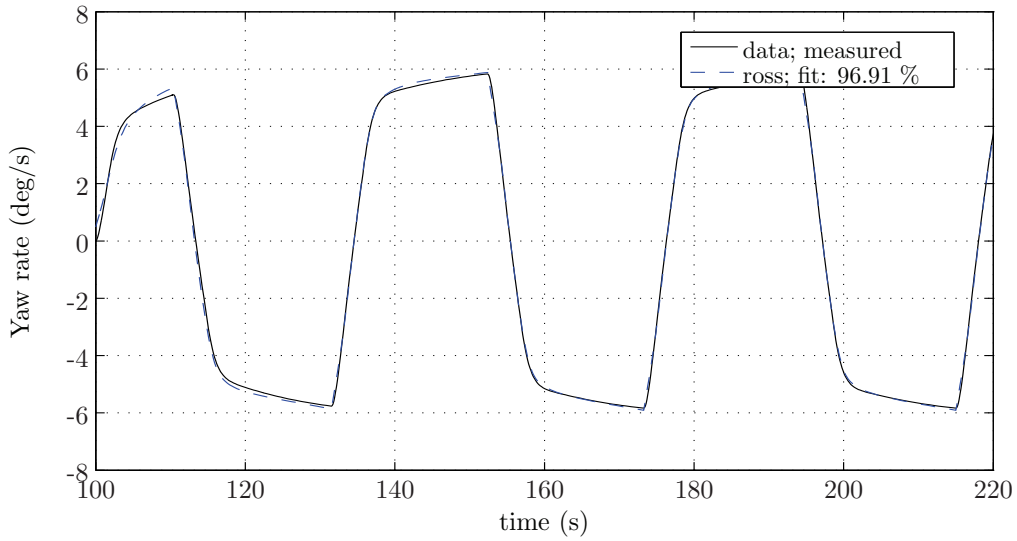

Figure 4.14: The estimated autopilot model of Ross compared to measured data from a single zig-zag maneuver.

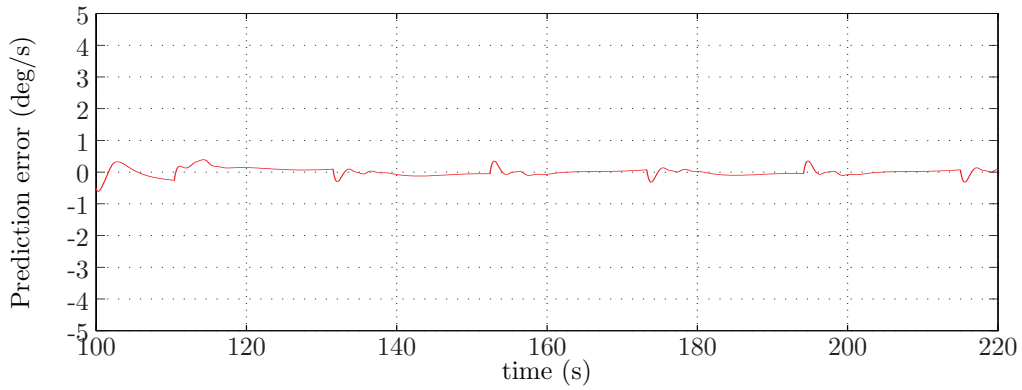

Figure 4.15: Prediction error for yaw rate.

The Nomoto model has a loss function of 0.399596 and Akaike's FPE of 0.40137. On the other hand has the autopilot model of Ross a loss function of 0.0203783 and Akaike's FPE of 0.0211926 which is substantially higher than during the turning circle.

4.2.3 Data from the Suggested Maneuver

Finally the models are identified using the suggested maneuver at 500 rpm. As imagined the Nomoto model is neither able to adapt the nonlinearities nor the various rudder deflections. In contrast the Ross model easily adapted this maneuver at 500 rpm.

The Nomoto Model

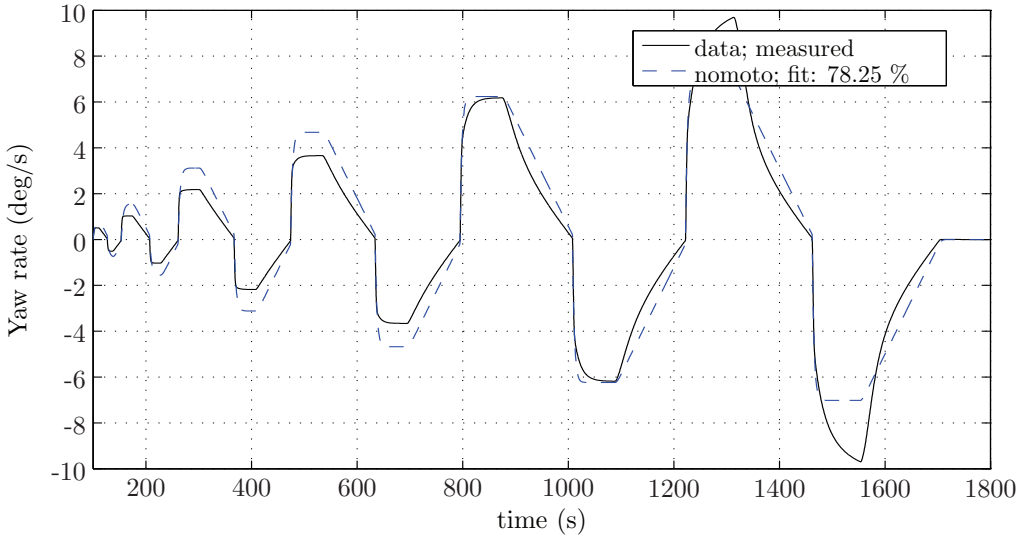

Figure 4.16: The estimated Nomoto model compared to measured data from a single suggested maneuver.

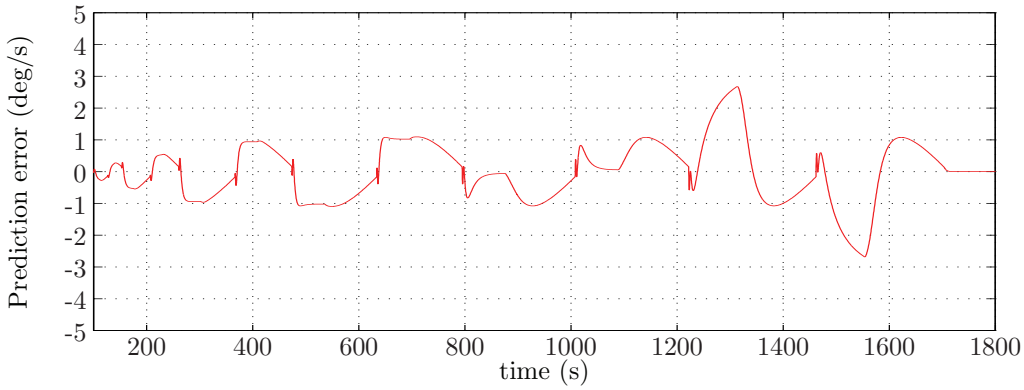

Figure 4.17: Prediction error for yaw rate.

Autopilot Model derived by Ross

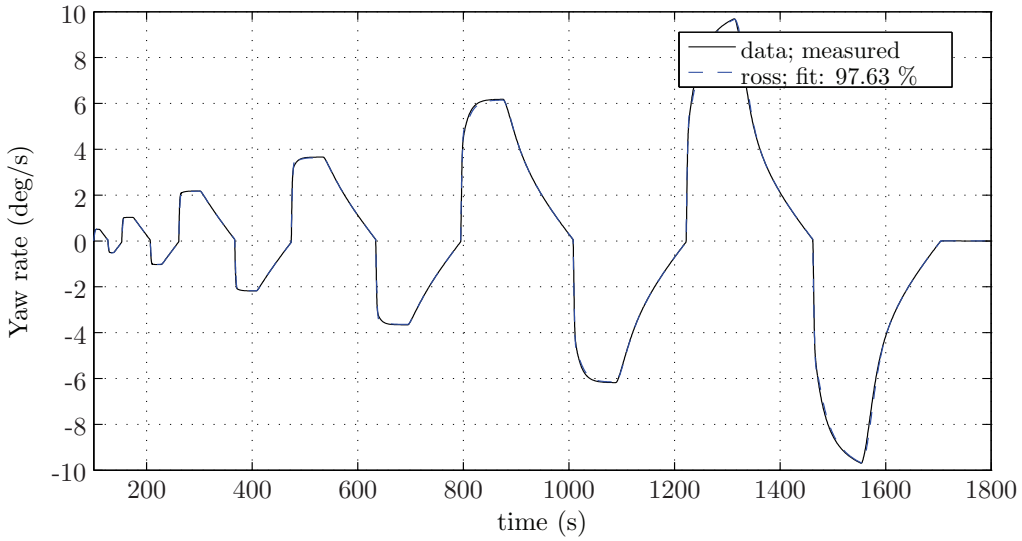

Figure 4.18: The estimated autopilot model of Ross compared to measured data from a single suggested maneuver.

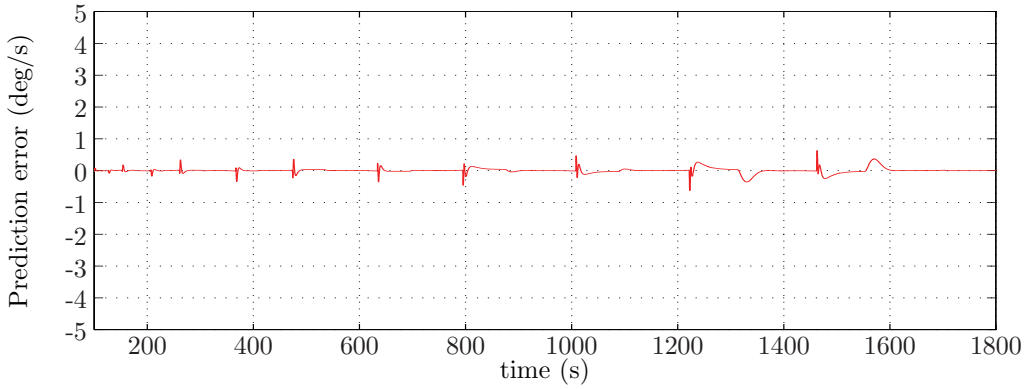

Figure 4.19: Prediction error for yaw rate.

Identification of the Nomoto model gave the loss function 0.730669 and the Akaike's FPE 0.731346. The estimated model of Ross yields the loss function 0.00867066 and Akaike's FPE 0.00874294. This is nearly as low as the turning circle even though the simulation time is nine times longer. One of the reasons the suggested maneuver has a substantially lower loss function compared to the zig-zag maneuver is because of the change in velocity during the first rudder deflection during the zig-zag maneuver.

4.3 Identification based on Merged Experiments

4.3.1 Data from the Turning Circles

In this section identification is carried out using measured data from several experiments. However, the plots are only displaying the measurements from the 40 degree step in 500 rpm. Thus, the figures itself has to be considered accordingly. Figures 4.20 and 4.22 shows the results of the Nomoto model and model of Ross, respectively.

The Nomoto Model

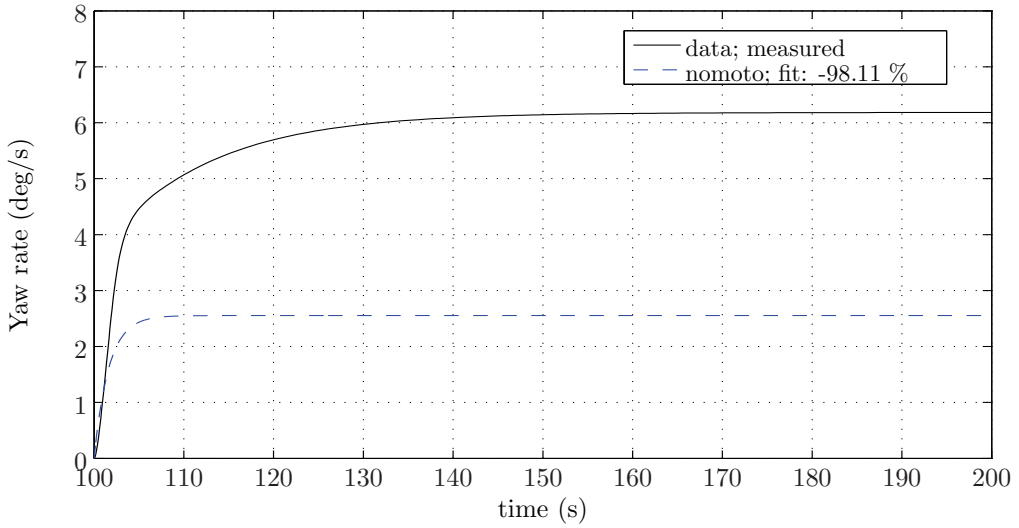

Figure 4.20: The estimated Nomoto model compared to measured data from several turning circles.

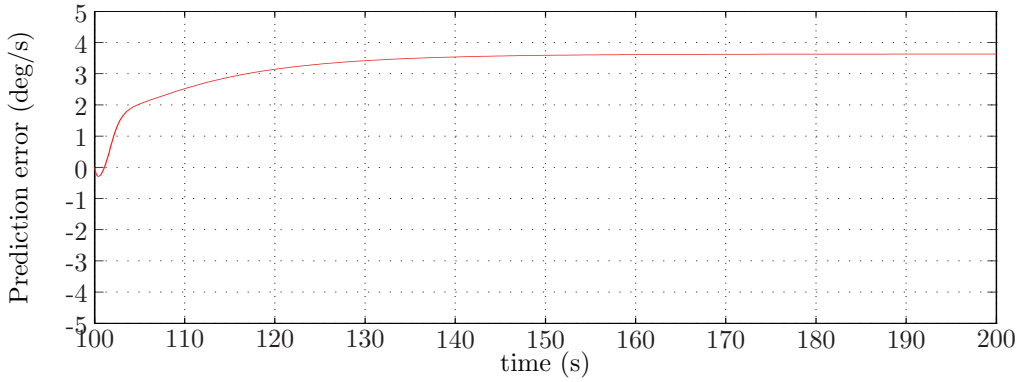

Figure 4.21: Prediction error for yaw rate.

Autopilot Model derived by Ross

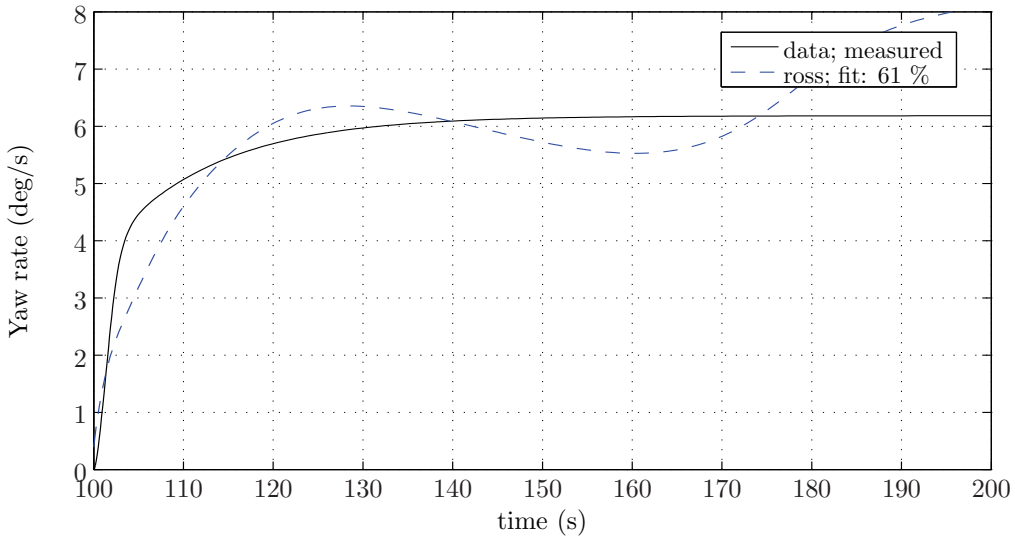

Figure 4.22: The estimated autopilot model of Ross compared to measured data from several turning circles.

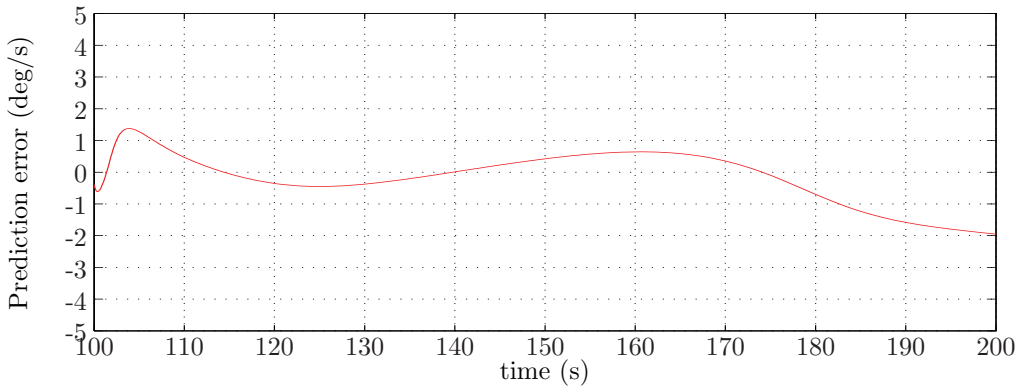

Figure 4.23: Prediction error for yaw rate.

The result of the identified Nomoto model is as expected rather poor. More surprisingly is the identified autopilot model of Ross. The rather strange response is probably caused by too short steady-state simulation data. The Nomoto model's loss function become 1.25724 and Akaike's FPE 1.25859 during all experiments. The loss function and Akaike's FPE of the identified Ross model yields 0.109565 and 0.110618, respectively.

4.3.2 Data from the Zig-zag Maneuvers

The models are now estimated using zig-zag measurements from all of the executed zig-zag maneuver including both 200 and 500 rpm. But only the measurements of the 40-40 zig-zag maneuver in 500 rpm is compared to the estimated models. Figures 4.24 and 4.26 shows the results of the Nomoto model and model of Ross, respectively.

The Nomoto Model

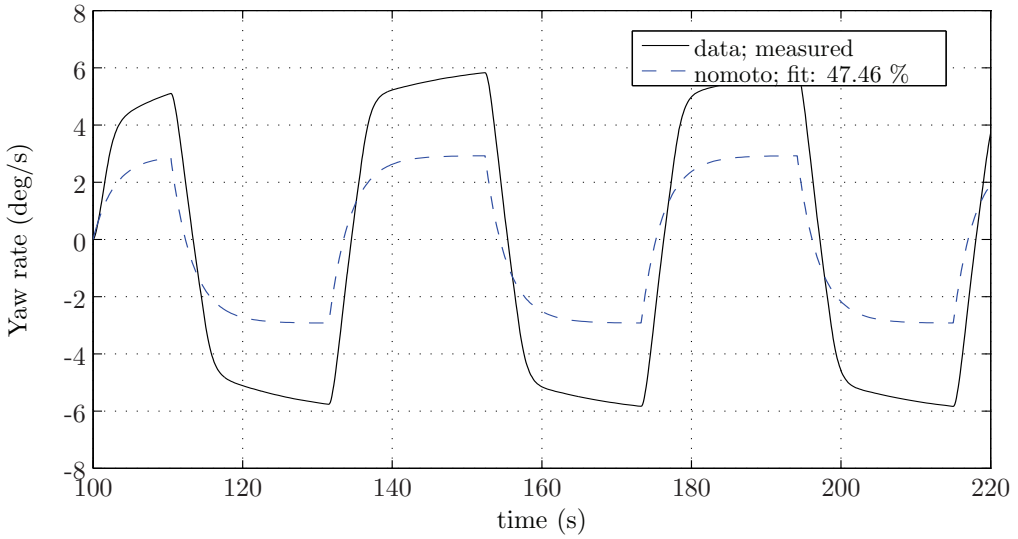

Figure 4.24: The estimated Nomoto model compared to measured data from several zig-zag maneuvers.

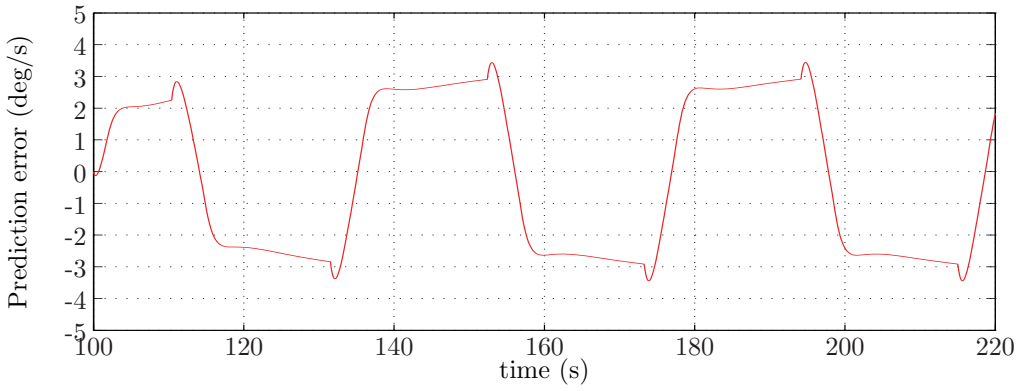

Figure 4.25: Prediction error for yaw rate.

Autopilot Model derived by Ross

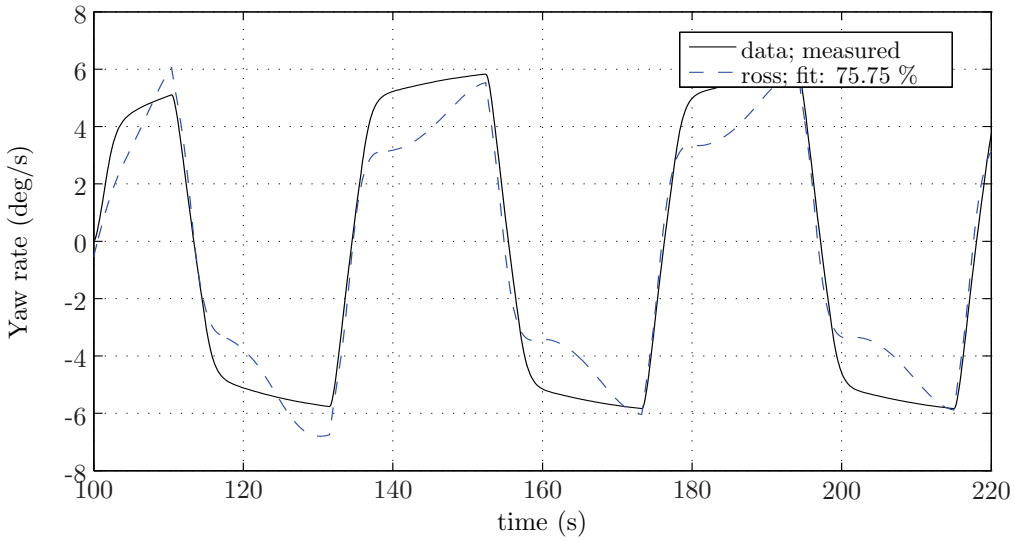

Figure 4.26: The estimated autopilot model of Ross compared to measured data from several zig-zag maneuvers.

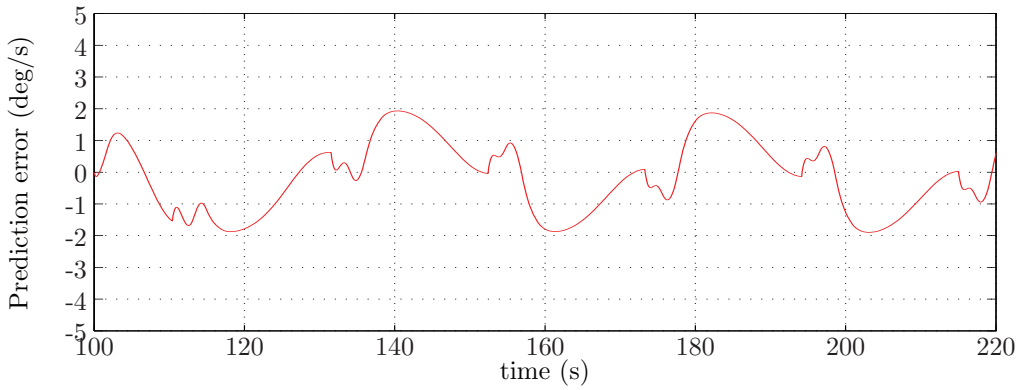

Figure 4.27: Prediction error for yaw rate.

Identification of the Nomoto model gave the loss function 1.72636 and the Akaike's FPE 1.72763. The estimated model of Ross yields the loss function 0.492535 and Akaike's FPE 0.49582. The estimated Nomoto model is clearly better compared to the estimates based on turning circles. For the autopilot model of Ross the estimated model is not quite capable of adapting the highly nonlinear yaw motion effect.

4.3.3 Data from the Suggested Maneuvers

Finally the merged experiments of the suggested maneuver are estimated. As in the previous cases only the measurements during the maneuver in 500 rpm are shown in Figure 4.28 and 4.30.

The Nomoto Model

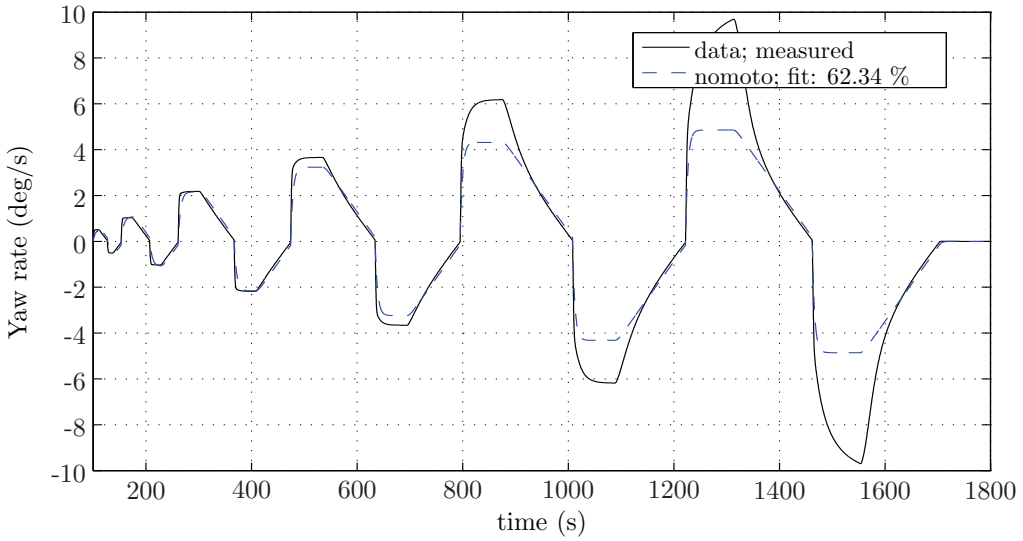

Figure 4.28: The estimated Nomoto model compared to measured data from two suggested maneuvers.

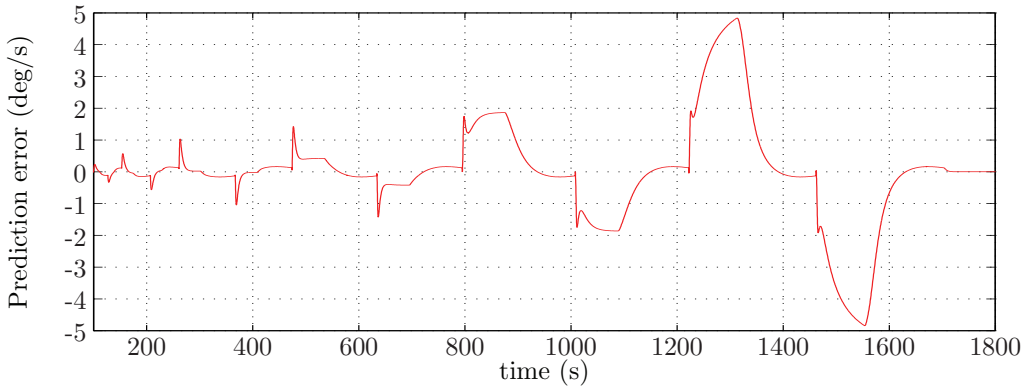

Figure 4.29: Prediction error for yaw rate.

Autopilot Model derived by Ross

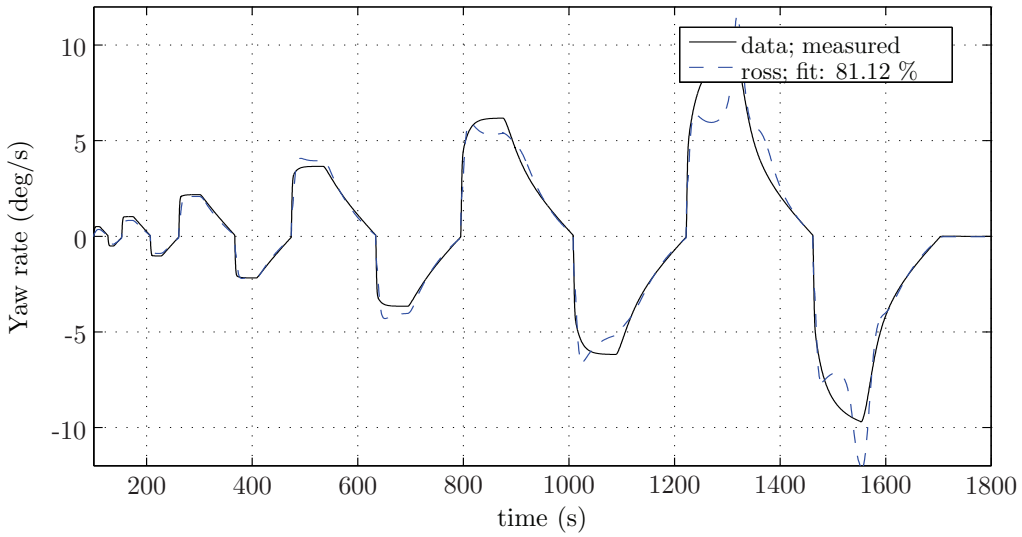

Figure 4.30: The estimated autopilot model of Ross compared to measured data from two suggested maneuvers.

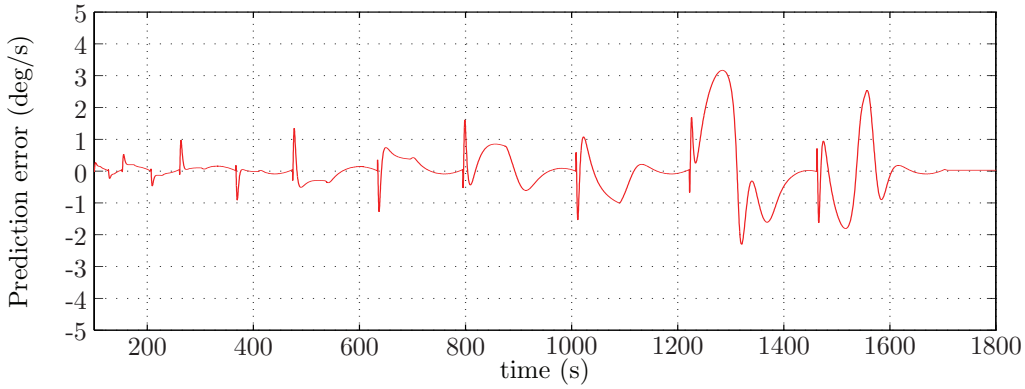

Figure 4.31: Prediction error for yaw rate.

The Nomoto model has a loss function of 2.5597 and Akaike's FPE of 2.56103. As already mentioned the model is not able to fit various velocities, but as seen on Figure 4.28 the results yields a fair average performance. On the other hand has the autopilot model of Ross a loss function of 1.07884 and Akaike's FPE of 1.08392. Compared to the single suggested experiment which fitted perfectly, the merged results indicates that the model suffer adapting the highly nonlinear force caused by the rudder deflection in various velocities. However, the model fits slightly better than the zig-zag estimated model.

Chapter 5

Autopilot Design

In this chapter the identified autopilot models will be implemented using a model-based autopilot controller. This is carried out to verify the models under other conditions than during the identification procedures. The ship will be simulated during both 300 and 400 rpm to check the models accuracy. In contrast, the model parameters are estimated during 500 and 200 rpm. Although advanced controllers can be derived, designing an autopilot system from a nonlinear dynamic model is rather comprehensive. Thus, in this thesis only the well known three term controller is considered, including a reference feed forward.

The first section presents a historical overview over the origin of the autopilot. In section two the model-based controller is derived based on both the Nomoto model and the autopilot model of Ross. Section three describes the simulation environment and the reference model, before the closed-loop results are presented in section four.

5.1 Historical Overview

The autopilot has its origin in the research followed by the invention of the electrically gyroscope. This invention took place by Hopkins as early as in 1890 and in 1908 Herman Anschütz patented the first north seeking gyrocompass. In 1911 Elmer Sperry constructed the first ship steering mechanism, referred to as the "Metal Mike", using feedback control and automatic gain adjustments [62]. Later, in 1922, Nicholas Minorsky came up with a position feedback control system using a three term control law, which is referred to nowadays as Proportional Integral Derivative (PID) control [18].

The ship autopilot controller can further be defined as a linear quadratic optimization problem [54]. Several steering criterion are developed such as Koyama [32], Norrbin [52] and Van Amerongen and Nauta Lemke [72]. When assuming full state feedback several controllers can be derived by means of Lyapunov stability theory, which includes adaptive feedback linearization [43] and nonlinear backstepping. More theory on nonlinear control can for instance be found in [30].

Recently a number of other sophisticated controller techniques are developed,

such as adaptive techniques described in [46], [60], [71], [72] and [76], model-reference approaches presented in [4] and [33], fuzzy-logic methods introduced in [57] and [74] and other robust approaches. A comprehensive review of nonlinear ship control is given in [17]. Further theory on numerical optimization is thorough described in [47].

5.2 Model-based Autopilot Controller

The main subject in this thesis is identification of autopilot models. Thus, the autopilot design is limited to only consider the conventional PID-controller including a feed forward term. The controller can according to [18] be stated as:

$$\tau_N = \tau_{FF} - K_p\tilde{\psi} - K_d\tilde{r} - K_i \int \tilde{\psi}(\tau)d\tau, \tag{5.1}$$

where τ_{FF} is the reference feed forward term.

When only the linear Nomoto model is considered the feed forward term can be written:

$$\tau_{FF} = \frac{T\dot{r}_d + r_d}{K}. \tag{5.2}$$

A final implementation will also require a wave-filter, but that is not covered in this subject. The controller gain K_p, K_i and K_d can be calculated using a pole placement algorithm [18]. Choosing the bandwidth ω_b and the relative damping ratio ξ, the simplified controller gain can be calculated by the following equations:

$$K_p = m\omega_n^2 \tag{5.3}$$

$$K_i = \frac{\omega_n}{10}K_p \tag{5.4}$$

$$K_d = 2\xi\omega_n m, \tag{5.5}$$

where $\omega_n = \omega_b/\sqrt{1 - 2\xi^2 + \sqrt{4\xi^4 - 4\xi^2 + 2}}$ is the natural frequency and m is the vessels mass. The conventional PID-controller with the Nomoto model in reference feed forward is implemented in Simulink straight forward from a predefined toolbox in [19].

The implementation of the autopilot model of Ross is carried out in the same manner, only extending the feed forward term τ_{FF} to include the model introduced in (3.7) using the model parameters estimated in section 4.3. Thus, the feed forward term is given by:

$$\begin{aligned}\tau_{FF} \;=\; & (I_z - N_{\dot{r}})\dot{r} - N^L_{uv\phi\phi}uv\phi^2 - N^L_{uv}uv - N^L_{uuv}u^2v - N^L_{vvv}v^3 \\ & -N^L_{rrv}r^2v - N_{|v|v}|v|v - N_{|r|v}|r|v - N^L_{ur}ur - N^L_{uur}u^2r \\ & -N^L_{rrr}r^3 - N^L_{vvr}v^2r - N_{|v|r}\,|v|r - N_{|r|r}|r|r + (X^0_{\dot{u}} - Y^0_{\dot{v}})uv \\ & -\frac{1}{2}(N^0_{\dot{v}} + Y^0_{\dot{r}})ru - \frac{1}{2}(Y^0_{\dot{p}} + K^0_{\dot{v}})p.\end{aligned} \tag{5.6}$$

5.3 Reference Model and Simulation Environment

To obtain smooth and bounded yaw rate and acceleration for steps in the desired heading, a third order reference model is implemented according to [18]:

$$\frac{\psi_d}{\psi_r}(s) = \frac{\omega_n^3}{(s+\omega_n)(s^2+2\xi\omega_n s+\omega_n^2)}, \tag{5.7}$$

where the reference ψ_r is the operator input, ψ_d is the desired heading, ξ is the relative damping ratio and ω_n is the natural frequency. The parameters in Table 5.1 is selected to generate a quick change of course to excite the vessels nonlinearities.

Heading step (deg)	45 deg
Step time (s)	100 s
Relative damping (ξ)	1.0
Natural frequency (ω_n)	0.2

Table 5.1: Reference model parameters.

5.4 Closed-loop Simulation Results

In this section the closed-loop results are reviewed. Based on the merged identification results the ship is simulated during a turn described in section 5.3. To obtain a comparable quantity the sum of residuals is calculated according to (3.19). Although the sum of residuals is not sufficient to conclude which maneuver gives the best estimates, it provides an indication of the quality.

5.4.1 Nomoto Model Reference Feed Forward

Since to different autopilot models are considered in this thesis the results are separated into two subsections. First, the Nomoto model reference feed forward is reviewed by means of estimates from each of the three experimental designs: turning circle, zig-zag maneuver and the suggested maneuver. Secondly, the autopilot model of Ross is employed as reference feed forward by means of the three different estimates. Although only the plots created during 300 rpm are presented in this chapter, both the residuals are available in the following tables. The other plots are available in Appendix B.

Parameters Identified from The Turning Circle

Simulating the Nomoto model in feed forward using the estimates from the turning circles gave surprisingly good results. In fact, for the simulations in 300 rpm the results are better than for both the zig-zag maneuver and the suggested maneuver. One of the reasons is that the turning circle excite the nonlinearities the least and thus generating a good linear approximation.

Simulation in 300 rpm	80.4113
Simulation in 400 rpm	44.7822

Table 5.2: Closed-loop residuals using the Nomoto model identified by measurements from the turning circles.

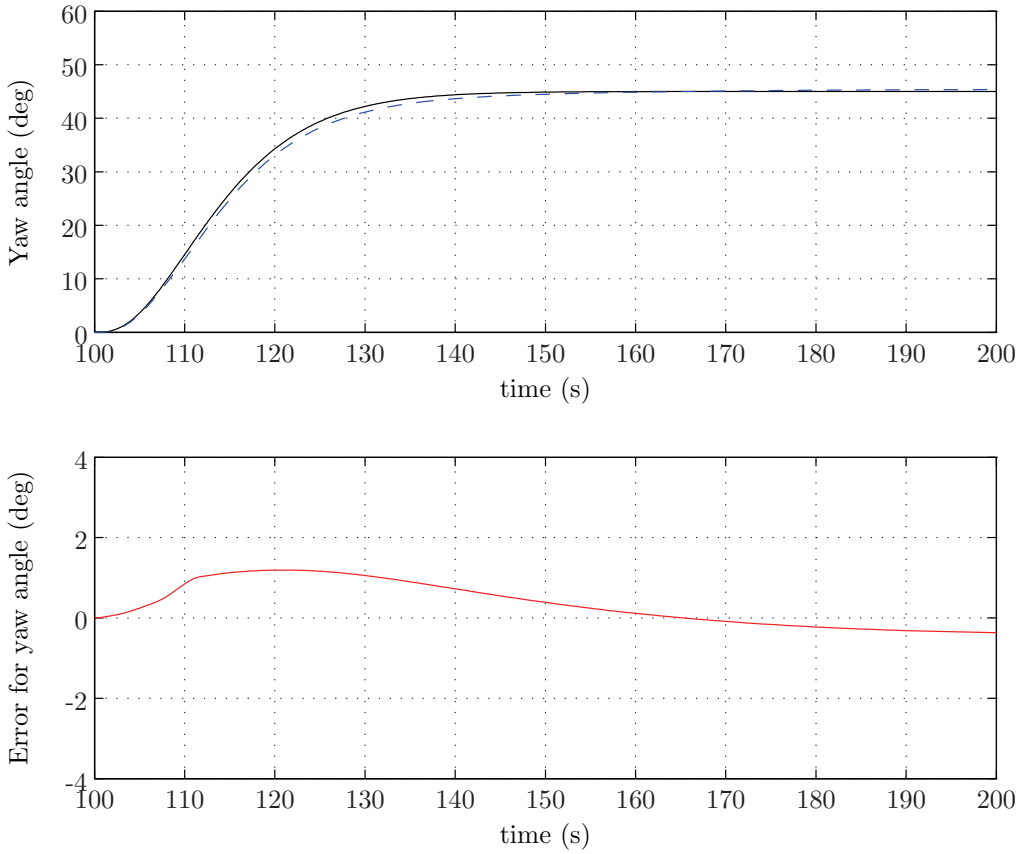

Figure 5.1: The Nomoto model in closed-loop (300 rpm).

Parameters Identified from The Zig-zag Maneuver

Further is the zig-zag estimate utilized in the feed forward loop. The results are presented in Table 5.2 and Figure 5.1. This substantiate that the response of the Nomoto model is extremely coupled with the velocity.

Simulation in 300 rpm	108.0843
Simulation in 400 rpm	17.3626

Table 5.3: Closed-loop residuals using the Nomoto model identified by measurements from the zig-zag maneuvers.

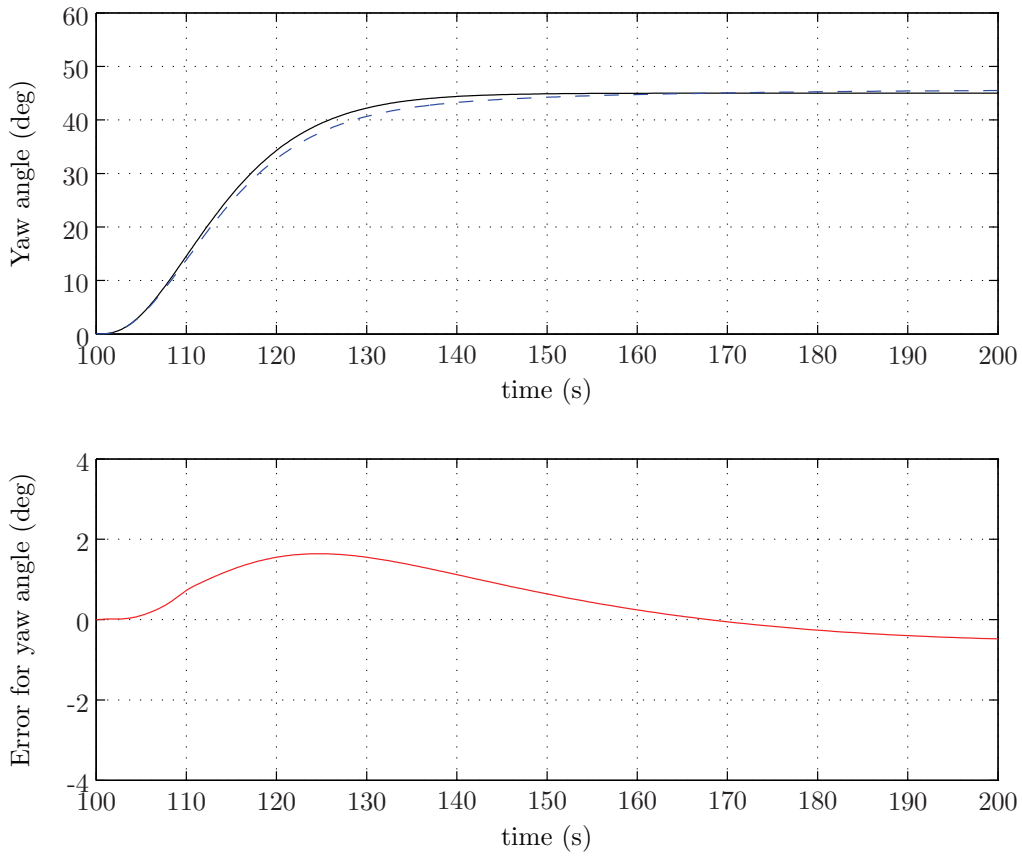

Figure 5.2: The Nomoto model in closed-loop (300 rpm).

Parameters Identified from The Suggested Maneuver

Finally the Nomoto estimate from the suggested maneuver is carried out in the feed forward loop. As seen in Figure 5.3 the results are not as good as for the turning circles. By evaluating the identification results in section 4.3, it is observed that the turning circle is generating a substantial smaller response, which fit this test better.

Simulation in 300 rpm	179.6080
Simulation in 400 rpm	69.0153

Table 5.4: Closed-loop residuals using the Nomoto model identified by measurements from the suggested maneuvers.

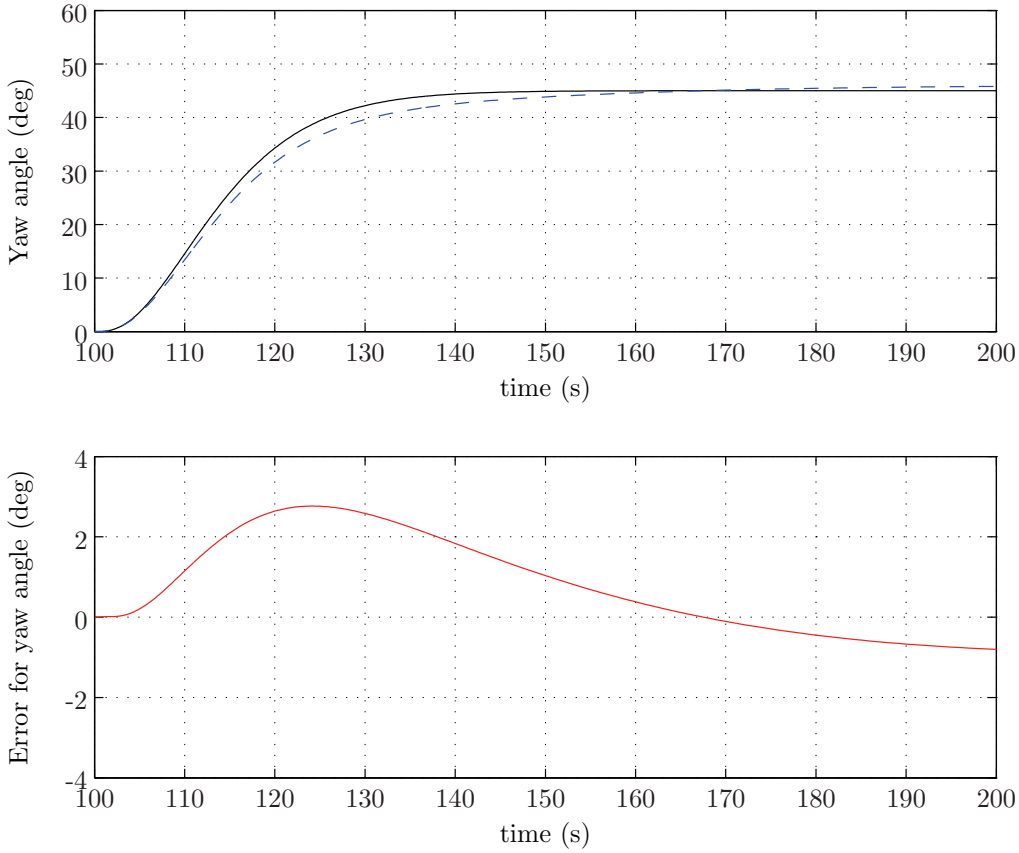

Figure 5.3: The Nomoto model in closed-loop (300 rpm).

5.4.2 Ross Autopilot Model Reference Feed Forward

In this subsection the autopilot model of Ross is applied as reference feed forward. This model is nonlinear and is able to adapt the maneuvering characteristics in various deflections and velocities. However, only a simple step in the heading reference is applied with two initial velocities. Thus, the best results in this subsection are only slightly better compared to the Nomoto model.

Parameters Identified from The Turning Circle

Using the estimates from the turning circles provide various results as seen in Table 5.5. The identification result in subsection 4.3.1 gave rather poor results during high velocities and the closed-loop simulation also suffer because of this.

Simulation in 300 rpm	110.0642
Simulation in 400 rpm	185.0572

Table 5.5: Closed-loop residuals using the autopilot model by Ross identified by measurements from the turning circles.

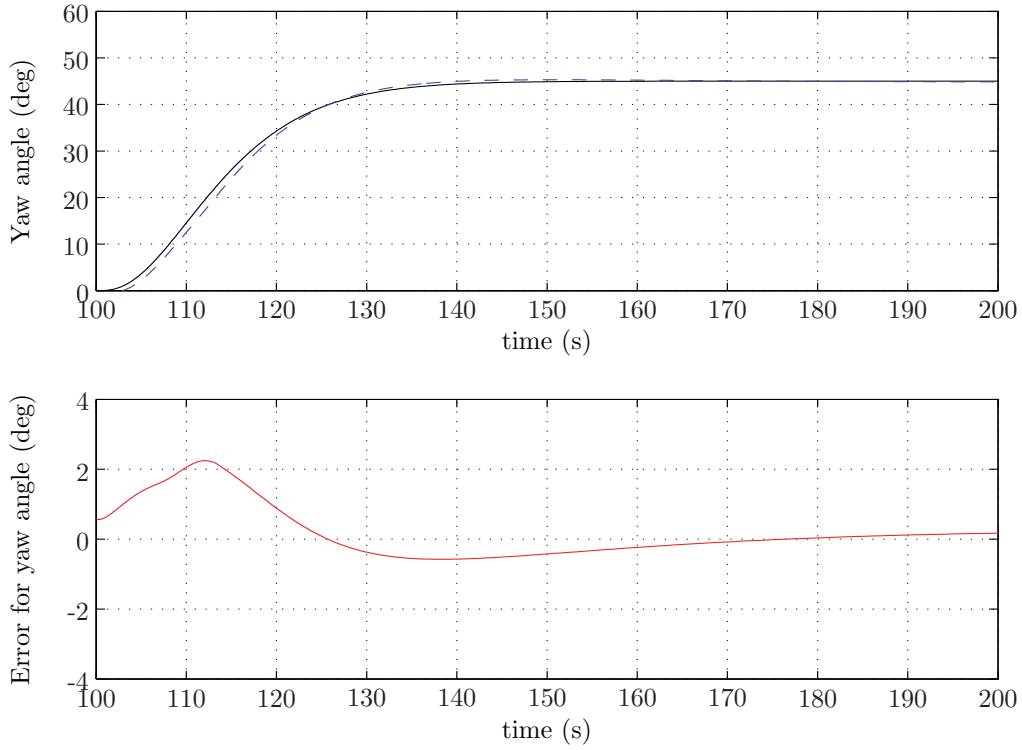

Figure 5.4: The autopilot model of Ross in closed-loop (300 rpm).

Parameters Identified from The Zig-zag Maneuver

In Figure 5.5 the closed-loop simulation during 300 rpm is shown. The estimated parameters clearly suffer from a slightly slow, but too large response.

Simulation in 300 rpm	125.1633
Simulation in 400 rpm	145.2591

Table 5.6: Closed-loop residuals using the autopilot model by Ross identified by measurements from the zig-zag maneuvers.

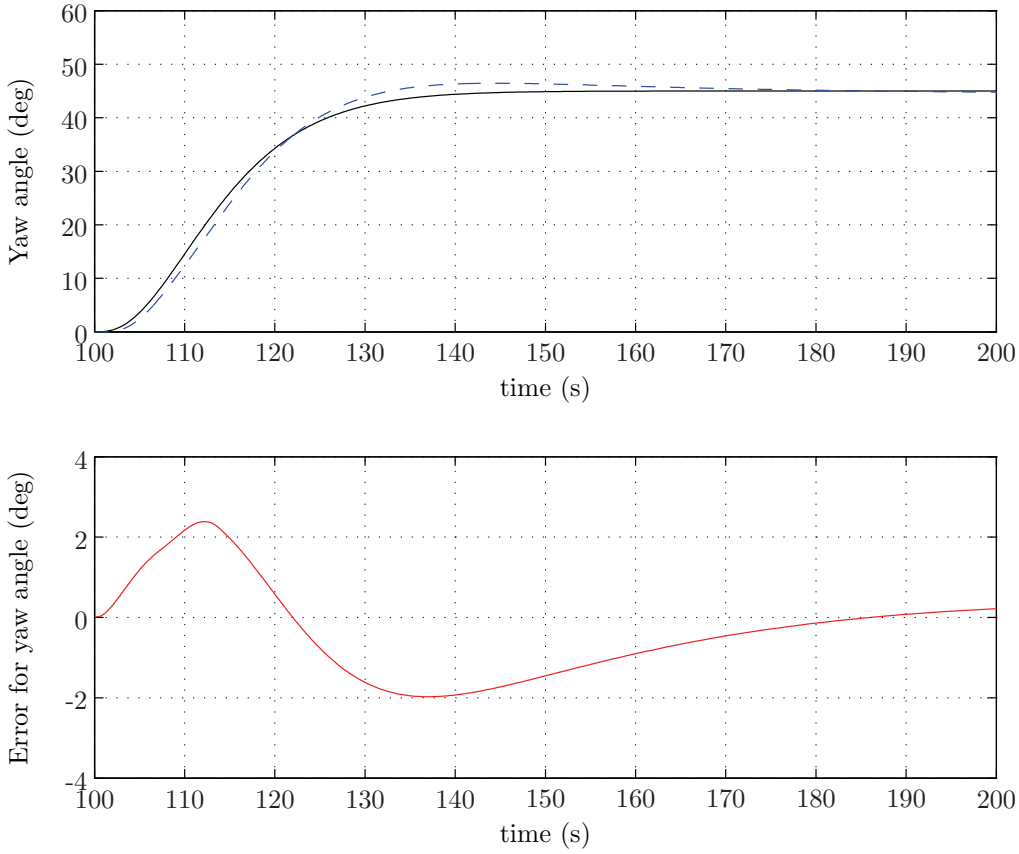

Figure 5.5: The autopilot model of Ross in closed-loop (300 rpm).

Parameters Identified from The Suggested Maneuver

At last the estimated model of Ross is simulated using the parameters from the suggested maneuvers. As seen in subsection 4.3.3 the autopilot model was not able to adapt the most extreme conditions, but the suggested maneuver excited the system well. Although the results are not excellent, the results from the suggested maneuver provide the best average performance.

Simulation in 300 rpm	78.7259
Simulation in 400 rpm	31.0921

Table 5.7: Closed-loop residuals using the autopilot model by Ross identified by measurements from the suggested maneuvers.

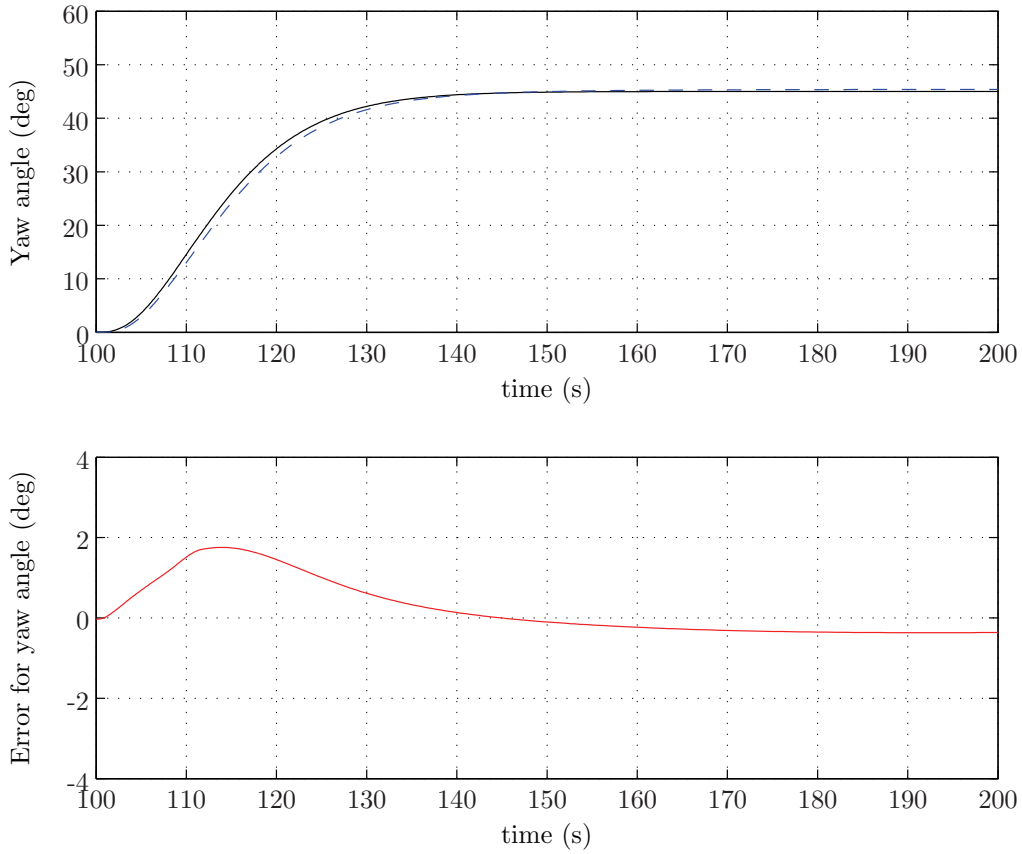

Figure 5.6: The autopilot model of Ross in closed-loop (300 rpm).

Chapter 6

Discussion

Through this thesis two autopilot models have been identified during several predefined ship maneuvers. The field of system identification has been reviewed and a prediction error method was chosen to estimate the model parameters. At last the autopilot models are simulated in closed loop by means of a model-based autopilot controller. In this chapter the different choices and results will be discussed.

6.1 Autopilot Models

Although several autopilot models exists, this thesis has considered the linear Nomoto model and a nonlinear autopilot model derived by Ross.

The Nomoto model shows good accuracy in a strictly bounded operation point as for the single experiments and is able to give a good approximation to both the turning circle and the zig-zag maneuver. Particularly the turning circle provide good estimates for the Nomoto model, and for slow-moving vessels like tankers the Nomoto model would give a fair approximation.

However, for faster ships a more sophisticated model is necessary. The nonlinear autopilot model of Ross clearly deliver far better results fitting the various maneuvers. During the single experiments the model fits exceedingly well. But as seen in section 4.3 also the nonlinear model suffer when pushing the vessel at its extremities. It should be mentioned that driving the yaw rate to ten radians per second is rather extreme, which is done during the tests. In addition should a model of the highly nonlinear rudder effect be included in the autopilot system, which probably would give better results in sense of parameter convergence.

6.2 Ship Maneuvers

In this thesis three experiment designs are implemented, namely the turning circle, zig-zag maneuver and the new suggested maneuver described in subsection 3.3.2. The main goal for the maneuvers is to produce maximum informative signals. Although the considered models performance not were excellent, the identification

results and closed-loop simulations gives an indication of the maneuver's performance.

Although the turning circle is not optimally in an identification point of view, satisfactory results were obtained for the linear Nomoto model. The widely used zig-zag maneuver performs fairly well using estimates generated from several experiments with various deflections. In the sense of informative signals white noise is an optimal solution. However, the relative slow steering dynamics involve performing predefined maneuvers. Although the performance of the suggested maneuver is not proven during this thesis, the results indicates better performance than both the turning circle and the zig-zag maneuvers for the nonlinear model.

6.3 Identification Methods

A review on identification methods has been presented. Based on the literary study an iterative prediction error method was chosen to estimate the model parameters. The method minimize the loss function and provide an unbiased estimate with excellent asymptotic properties. It is nevertheless difficult to characterize the quality of the estimates, as they are dependent of the data during the experiment design. However when the number of data tends to infinity, the asymptotic properties can be stated. In general the convergence property result in:

$$\hat{\theta}_N \rightarrow \theta^* \text{ as } N \rightarrow \text{inf}, \tag{6.1}$$

where

$$\theta^* = \arg\min_{\theta} E\ell(\epsilon(t,\theta)). \tag{6.2}$$

This means that as more and more data become available, the estimate converge to the value θ^* that minimize the expected value of the norm of the prediction errors. Which in a sense is the best possible approximation of the true system available within the model structure.

6.4 Model-based Autopilot Controller

Only one controller is considered, namely the conventional PID-controller including a model feed forward term. The controller was tuned to obtain a rather slow but critical damped system without considering the feed forward term. Although a number of real systems still are using simple PID-controllers, it is obviously not an optimal choice. Better results would probably be obtained when introducing saturation control, integrator-windup protection and model prediction control.

Chapter 7

Conclusion

This thesis has focused on identification of ship autopilot models. The main goal was to suggest a new ship maneuver suitable for identification of the steering characteristics. Secondly, a literary study on system identification was carried out and a suitable identification method was chosen to verify the suggested maneuver's convergence properties. To verify the identified autopilot models, the ship was simulated in closed-loop with a model-based autopilot controller.

Based on the theory of informative signals a new ship maneuver has been developed. The identification results and the closed-loop simulations indicates better convergence properties than the turning circle and zig-zag maneuver for the nonlinear autopilot model. However, identification of different nonlinear autopilot models and full-scale experiments have to be carried out to state a final conclusion.

To identify two different autopilot models an iterative prediction error method was chosen. This identification method provided great results, although it suffered because of the autopilot models. Finally a conventional PID-controller was implemented with a model reference feed forward term to verify the identification results.

Chapter 8

Further Research

Different Models

Based on the results in this report several improvements can be done. Further simulation with different ships can be performed. The identification results also clearly showed that even more complex autopilot models should be applied for highly nonlinear vessels performing very fast turns.

Optimization of The Suggested Maneuver

Although the suggested maneuver provides good results during the simulation in this thesis, further improvements can probably be done in sense of efficiency and parameter convergence.

Experimental Data

Further should the simulation environment be extended to contain both waves, current and measurement noise according to [15] and [38]. More experimental data will also substantiate the convergence properties of the suggested maneuver.

Model-based Controller

Better overall performance could also be reached by implementing a more sophisticated autopilot controller.

Bibliography

[1] M. A. Abkowitz. Lectures on ship hydrodynamics - steering and manoeuvrability. Technical report, Hydro- og Aerodynamisk Laboratorium, Report No. Hy-6, 1964.

[2] M. A. Abkowitz. Measurement of hydrodynamic characteristics from ship maneuvering trials by system identification. *SNAME, No. 10*, 1980.

[3] H. Akaike. Fitting autoregressive models for prediction. *Annals of the Institute of Statistical Mathematics, Vol. 21, pp. 243-247*, 1969.

[4] J. Van Amerongen. Adaptive steering of ships - a model reference approach. *Automatica, Vol. 20, No. 1, pp. 3-14*, 1984.

[5] J. G. Balchen, N. A. Jenssen, and S. Sælid. Dynamic positioning of floating vessels based on kalman filtering and optimal control. *Proceedings of the 19th IEEE Conference on Decision and Control, New York, pp. 852-864*, 1980.

[6] J. S. Bendat, P. A. Palo, and R. N. Coppolino. A general identification technique for nonlinear differential equations of motion. *Probabilistic Engineering Mechanics 7, 43-61*, 1992.

[7] S. K. Bhattacharyya and M. R. Haddara. Parametric identification for nonlinear ship maneuvering. *Journal of Ship Research, Vol. 50, No. 3, pp. 197-207*, 2006.

[8] S. K. Bhattacharyya and R. P. Selvam. Parameter identification of a large floating body in random ocean waves by reverse miso method. *Journal of Offshore Mechanics and Arctic Engineering*, 2002.

[9] H. L. Brinati. *System Identification Applied to Maneuvering Trials*. PhD thesis, Massachusetts Institute of Technology, 1973.

[10] R. G. Brown and P. Y. C. Hwang. *Introduction to Random Signals and Applied Kalman Filtering*. John Wiley and Sons, Third Edition, 1997.

[11] M. H. Casado, R. Ferreiro, and F. J. Velasco. Identification of nonlinear ship model parameters based on the turning circle test. *Journal of Ship Research, Vol. 51, No. 2, June 2007, pp. 174-181*, 2007.

[12] M. S. Chislett and J. Strøm-Tejsen. Planar motion mechanism tests and full-scale steering and manoeuvring predictions for a mariner class vessel. Technical report, Hydro- og Aerodynamisk Laboratorium, Report No. Hy-6, 1965.

[13] K. S. M. Davidson and L. I. Schiff. Turning and course keeping qualities. *Transactions of SNAME, Vol. 54*, 1946.

[14] P. Eykhoff. *System Identification : parameter and state estimation*. John Wiley and Sons Ltd., 1974.

[15] J. A. Farrel and M. Barth. *The Global Positioning System and Inertial Navigation*. McGraw-Hill, 1998.

[16] T. I. Fossen. *Nonlinear Modeling and Control of Underwater Vehicles*. PhD thesis, Norwegian University of Science and Technology, 1991.

[17] T. I. Fossen. A survey on nonlinear ship control: From theory to practice. *Proc. 5th IFAC Conference on Manoeuvering and Control of Marine Craft, Aalborg, Denmark*, 2000.

[18] T. I. Fossen. *Marine Control Systems - Guidance, Navigation and Control of Ships, Rigs and Underwater Vehicles*. Marine Cybernetics, 3rd edition, 2002.

[19] T. I. Fossen and T. Perez. *Marine Systems Simulator (MSS) and (GNC) Toolbox*. http://www.marinecontrol.org. Accessed 2 February, 2009.

[20] T. I. Fossen, S. I. Sagatun, and A. J. Sørensen. Identification of dynamically positioned ships. *Journal of Control Engineering Practice*, 1996.

[21] J. Goclowski. Dynamics of an automatic ship steering system. *IEEE Transactions on Control, Vol. AC-11, No. 3*, 1966.

[22] P. G. Guest. *Numerical Methods of Curve Fitting*. Cambridge, 1961.

[23] I. Gustavsson, L. Ljung, and T. Söderström. Survey paper, identification of processes in closed loop. *Automatica, Vol. 13. pp. 59-75*, 1977.

[24] M. N. Hayes. *Parametric Identification of Nonlinear Stochastic Systems Applied to Ocean Vehicle Dynamics*. PhD thesis, Massachusetts Institute of Technology, 1971.

[25] W. Hwang. *Application of System Identification to Ship Maneuvering*. PhD thesis, Massachusetts Institute of Technology, 1980.

[26] ITTC. Full scale manoeuvring trials procedure. *ITTC - Recommended Procedures and Guidelines, 7.5-04-02-01*, 2002.

[27] J.M.J. Journée. A simple method for determining the manoeuvring indices k and t from zigzag trial data. Technical report, Delft University of Technology, 1970.

[28] T. Katayama. *Subspace Methods for System Identification*. Springer, 2005.

[29] G. Kempf. Measurements of the propulsive and structural characteristic of ships. *Transactions of SNAME, vol. 40. pp. 42-57*, 1932.

[30] H. K. Khalil. *Nonlinear Systems*. Prentice Hall, Third Edition, 2002.

[31] C. G. Källström and K. J. Åström. Experiences of system identification applied to ship steering. *Automatica, Vol. 17, No. 1, pp 187-198*, 1981.

[32] T. Koyama. On the optimum automatic steering systems of ships as sea. *J.S.N.A., Vol. 122*, 1967.

[33] T. Laudal and T. I. Fossen. A globally stable adaptive ship autopilot with wave filter using only yaw angle measurements. Technical report, Norwegian University of Science and Technology, 1995.

[34] M. Le and S. Nguyen. Online estimation of ship steering dynamics and its applications in designing an optimal autopilot. *International Symposium on Communications and Information Technologies, Sapporo, Japan, October 26-29*, 2004.

[35] L. Ljung. *System Identification, Theory for the User*. Prentice Hall PTR, Second Edition, 1999.

[36] L. Ljung. Prediction error estimation methods. *Circuits, Systems, and Signal Processing. Vol. 21, Nr. 1, pp. 11-21*, 2002.

[37] L. Ljung and T. Sõderstrõm. Theory and practice of recursive identification. *The MIT Press series in signal processing, optimization, and control 4*, 1983.

[38] O. Lundbäck. A test procedure and evaluation method for seakeeping trials with address to broaching-to. *Naval Architecture, KTH, S-100 44, Stockholm, Sweden*, 2001.

[39] J. G. Lundblad. *Application of the Extended Kalman Filtering Technique to Ship Maneuvering Analysis*. PhD thesis, Massachusetts Institute of Technology, 1975.

[40] Matlab. Optimization toolbox user's guide. *The MathWorks, Inc. Version 4.2 (Release 2009a)*, 2009.

[41] Matlab. System identification toolbox user's guide. *The MathWorks, Inc. Version 7.3 (Release 2009a)*, 2009.

[42] T. L. Moran, A. B. Wemple, and W. E. Smith. Mariner surface ship system identification. *Proc. 7th Ship Control Systems Symposium, Bath, 24 - 27 Sept. 1984. Vol. 3, p. 217*, 1984.

[43] L. Moreira, T. I. Fossen, and C. G. Soares. Path following control system for a tanker ship model. *Ocean Engineering 34, 2074-2085*, 2007.

[44] J. Nagumo. A learning method for system identification. *IEEE Transaction on Automatic Control, Vol. AC-12, No. 3*, 1967.

[45] H. D. Nguyen. Recursive identification of ship manoeuvring dynamics and hydrodunamics. *Anziam J. 49 (EMAC2007) pp.C717-C732, 2008*, 2008.

[46] T-H Nguyen, T-T Ha, H-S Pham, T-H Hoang, V-D Giap, and T-V Le. Study on an effective adaptive ship autopilot. *SICE Annual Conference in Sapporo, August 4-6*, 2004.

[47] J. Nocedal and S. J. Wright. *Numerical Optimization*. Springer Series in Operation Research and Financial Engineering, 2006.

[48] K. Nomoto. Analysis of kempf's standard maneuver test and proposed steering indices. *Proceedings of 1st Symposium on Ship Maneuverability*, 1960.

[49] K. Nomoto, T. Taguchi, K. Honda, and S. Hirano. On the steering qualities of ships. *International Shipbuilding Progress, Vol. 4, No. 35*, 1957.

[50] N. H. Norrbin. On the design and analyses of the zig-zag test on base of quasi-linear frequency response. Technical report, Technical Report B 104-3, Gothenburg, Sweden, 1963.

[51] N. H. Norrbin. Theory and observations on the use of a mathematical model for ship manoeuvring in deep and confined waters. *Extended Symposium on Naval Hydrodynamics, Pasadena, Cal. 1970*, 1971.

[52] N. H. Norrbin. On the added resistance due to steering on a straight course. *Proceedings of the 13th ITTC. Berlin, Hamburg, Germany*, 1972.

[53] SNAME (The Society of Naval Architects and Marine Engineers). Nomenclature for treating the motion of a submerged body through a fluid. *Technical and Research Bulletin No. 1-5*, 1950.

[54] G. J. Olsder. On the time optimal course changing of ships. *Journal of Engineering Mathematics, Vol. 3, No. 2, April 1969*, 1969.

[55] G. Rajesh and S. K. Bhattacharyya. System identification for nonlinear maneuvering of large tankers using artificial neural network. *Applied Ocean Research, Indian Institute of Technology Madras, India*, 2008.

[56] H. J. Rice and J. A. Fitzpatrick. A procedure for the identification of linear and non-linear multi-degree-of-freedom systems. *Journal of Sound and Vibration, 149, 397-411*, 1991.

[57] G. N. Roberts, R. Sutton, A. Zirilli, and A. Tiano. Intelligent ship autopilots - a historical perspective. *Mechatronics 13, 1091-1103*, 2003.

[58] A. Ross. *Nonlinear Manoeuvring Models for Ships: a Lagrangian Approach*. PhD thesis, Norwegian University of Science and Technology, 2008.

[59] R. P. Selvam, S. K. Bhattacharyya, and M. Haddara. A frequency domain system identification method for linear ship maneuvering. *Int. Shipbuild. Progr., 52, no. 1 (2005) pp. 5-27*, 2003.

[60] R. Skjetne, Ø. Smogeli, and T. I. Fossen. Modeling, identification, and adaptive maneuvering of cybership ii: A complete design with experiments. *Proc. of the IFAC CAMS'04, Ancona, Italy*, 2004.

[61] D. A. Smallwood. Adaptive identification of dynamically positioned underwater robotic vehicles. *IEEE Transaction on Control Systems Technology, Vol. 11, No. 4*, 2003.

[62] J.P. Strand and A.J. Sørensen. *The Ocean Engineering Handbook*, chapter 3.1 Marine Positioning Systems, pages 163–176. CRC Press, 2001.

[63] K. Åström, C. G. Källström, N. H. Norrbin, and L. Byström. The identification of linear ship steering dynamuics using maximum likelihood parameter estimation. *Göteborg, Publications of the Swedish Shipbuilding Experimental Tank*, 1975.

[64] K. J. Åström and P. Eykhoff. System identification - a survey. *Automatica, Vol. 7, pp. 123-162*, 1971.

[65] K. J. Åström and C. G. Källström. Identification and modelling of ship dynamics. *Report 7202 Mars 1972, Lund Institute of Technology, Division of Automatic Control*, 1972.

[66] K. J. Åström and C. G. Källström. Identification of ship steering dynamics. *Automatica, Vol. 12. pp. 9-22*, 1976.

[67] J. Strøm-Tejsen and M. S. Chislett. A model testing technique and method of analysis for the prediction of steering and manoeuvring qualities of surface vessels. *Presented at the Sixth Symposium on Naval Hydrodynamics, Washington D.C.*, 1966.

[68] World Geodetic System. Its definition and relationships with local geodetic systems. *Technical and Research Bulletin No. 1-5*, 1950.

[69] FORCE Technology. *US Navy Combatant, DTMB 5415 Geometry and Conditions, SIMMAN 2008*. http://www.simman2008.dk. Accessed 16 February, 2009.

[70] A. Tiano. Comparasion of non linear identification methods for underwater vehicles. *University of Pavia, Department of Informatics and Systems, Italy*, 2004.

[71] V. Tran, H. Nguyen, T. Hoang, T. Nguyen, X. Cu, and V. Nguyen. An optimal autopilot for ships using a regressive exogenous model. *International Symposium on Communications and Information Technologies, Sapporo, Japan, October 26-29*, 2004.

[72] J. van Amerongen and H.R. van Nauta Lemke. Criteria for otimum steering of ships. *Symposium on Ship Steering Automatic Control, 25-27 June, Genova, Italy*, 1980.

[73] G. van Leeuwen and J.M.J. Journée. Prediction of ship manoeuvrability. Technical report, Delft University of Technology, Report No. 1585, 1972.

[74] J. Velagic, Z. Vukic, and E. Omerdic. Adaptive fuzzy ship autopilot for track-keeping. *Control Engineering Practice 11, 433-443*, 2003.

[75] É. Walter and L. Pronzato. *Identification of Parametric Models*. Springer, 1997.

[76] X. Wang and H. Xu. Robust autopilot with wave filter for ship steering. *Journal of Marine Science and Application, Vol. 5, No. 2, pp. 24-29*, 2006.

[77] H. K. Yoon and K. P. Rhee. Identification of hydrodynamic coefficients in ship maneuvering equations of motion by estimation-before-modeling technique. *Department of Naval Architecture and Ocean Engineering, Seoul National University, South Korea*, 2003.

[78] L. A. Zadeh. From circuit theory to system theory. *Proceedings of the IRE, Vol. 50, pp. 856-865*, 1962.

[79] W.-W. Zhou. *Identification of Nonlinear Marine Systems*. Servolaboratoriet, Denmark, 1987.

Appendix A

Further Simulation Results

In this chapter all of the experiments utilized during the merged identification process are presented. First the different turning circles are shown, followed by the zig-zag maneuvers. The suggested maneuver during 200 rpm are subsequently displayed. At last the closed-loop identification results during 400 rpm are presented.

A.1 Turning Circle

20 degree step with 500 rpm

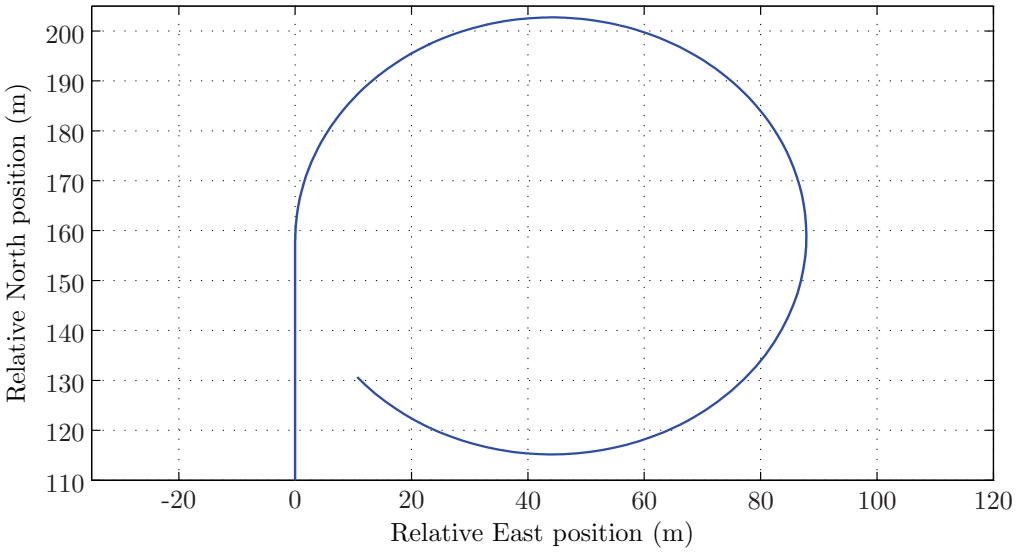

Figure A.1: North-East plot of the 20 degree turning circle (500 rpm).

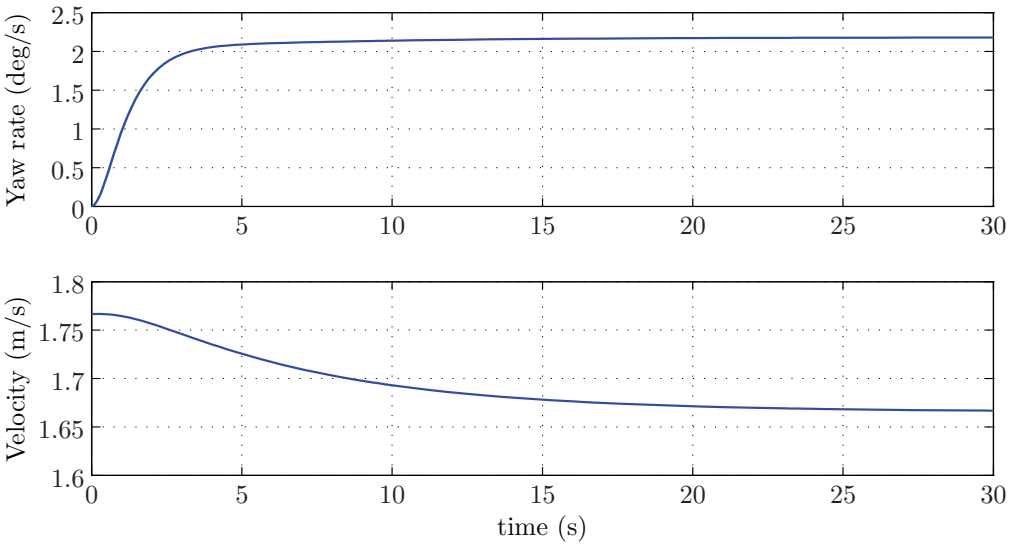

Figure A.2: Yaw rate and velocity during the 20 degree turning circle (500 rpm).

10 degree step with 500 rpm

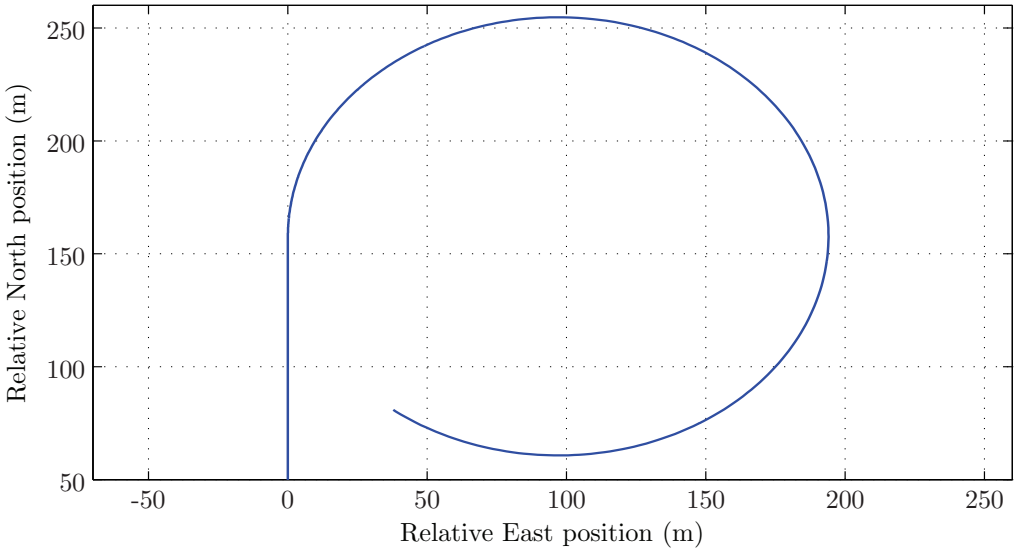

Figure A.3: North-East plot of the 10 degree turning circle (500 rpm).

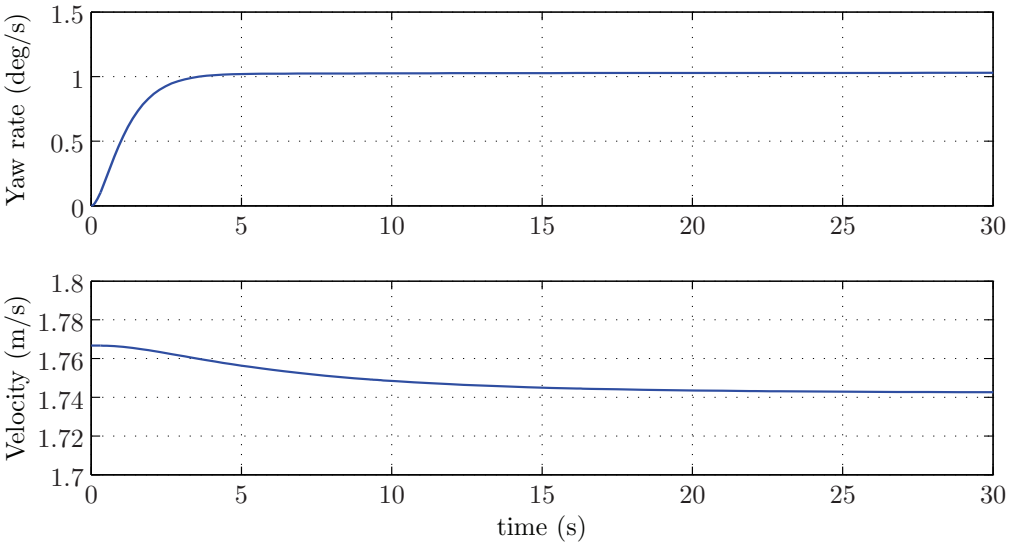

Figure A.4: Yaw rate and velocity during the 10 degree turning circle (500 rpm).

40 degree step with 200 rpm

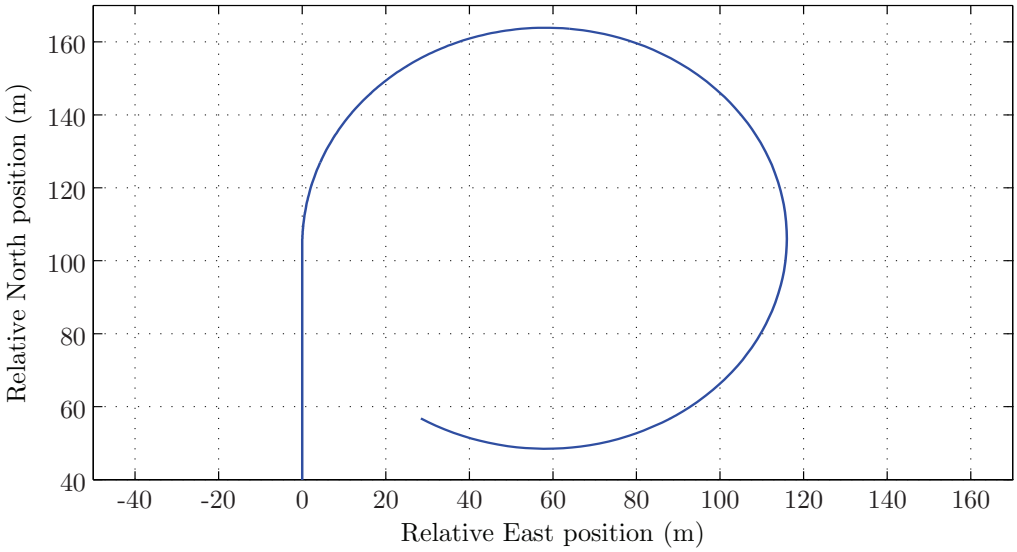

Figure A.5: North-East plot of the 40 degree turning circle (200 rpm).

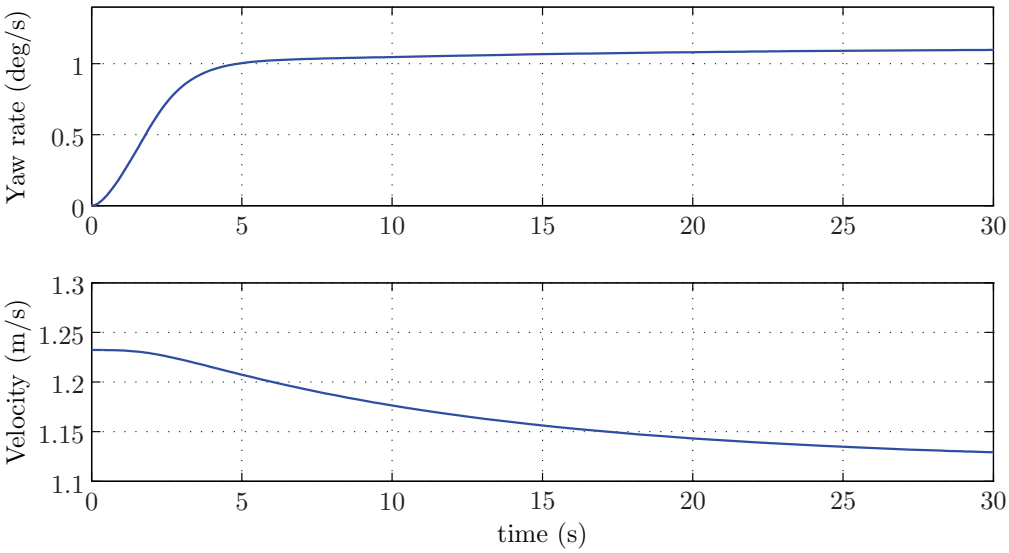

Figure A.6: Yaw rate and velocity during the 40 degree turning circle (200 rpm).

20 degree step with 200 rpm

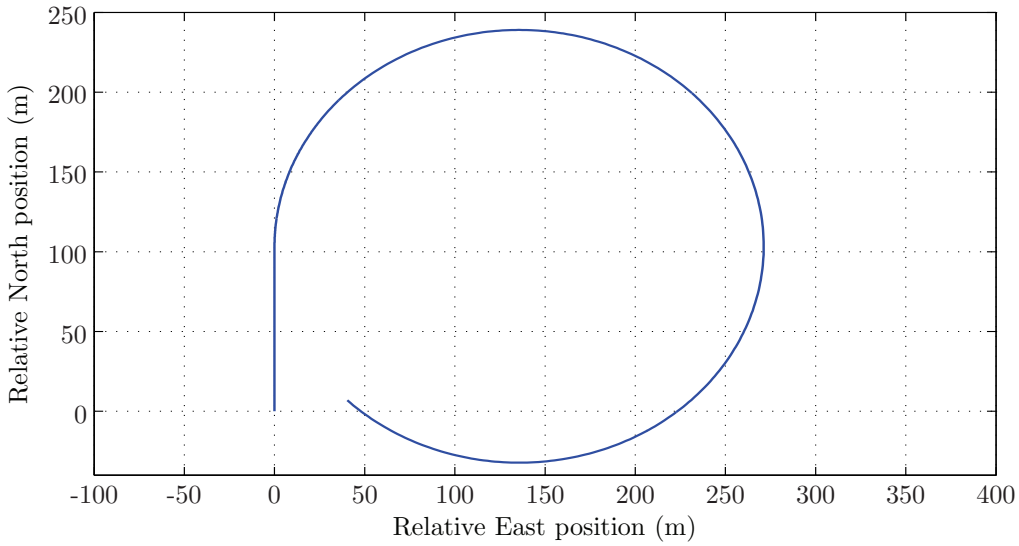

Figure A.7: North-East plot of the 20 degree turning circle (200 rpm).

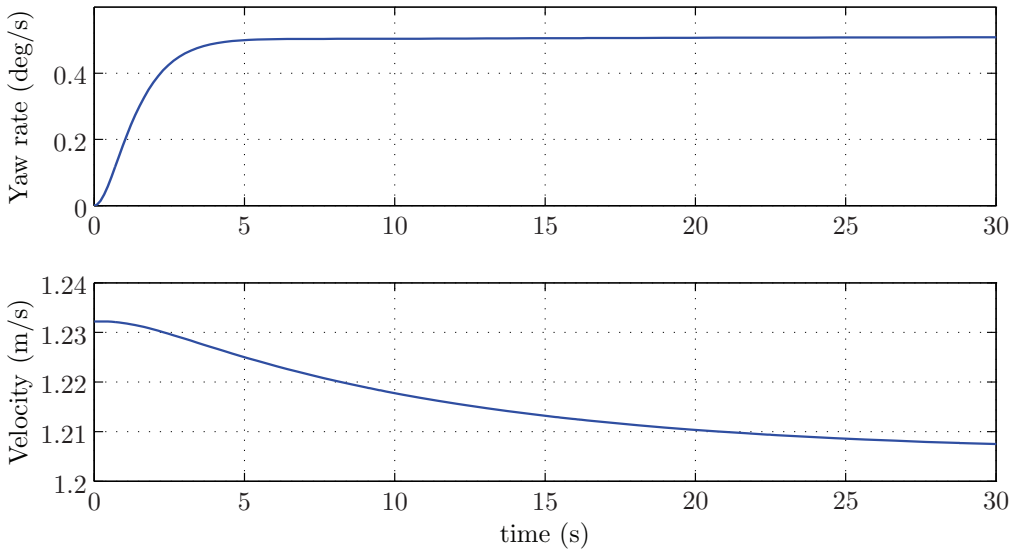

Figure A.8: Yaw rate and velocity during the 20 degree turning circle (200 rpm).

10 degree step with 200 rpm

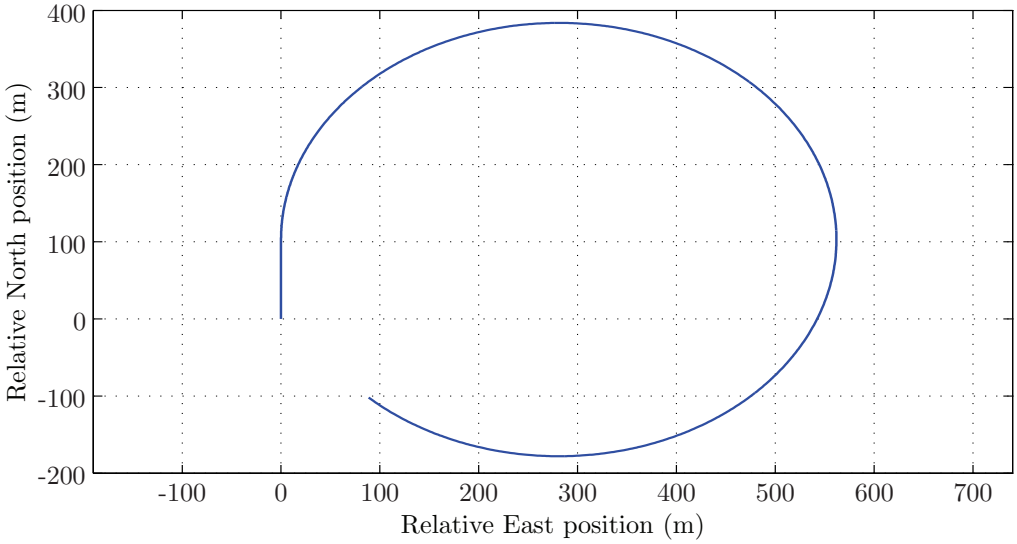

Figure A.9: North-East plot of the 10 degree turning circle (200 rpm).

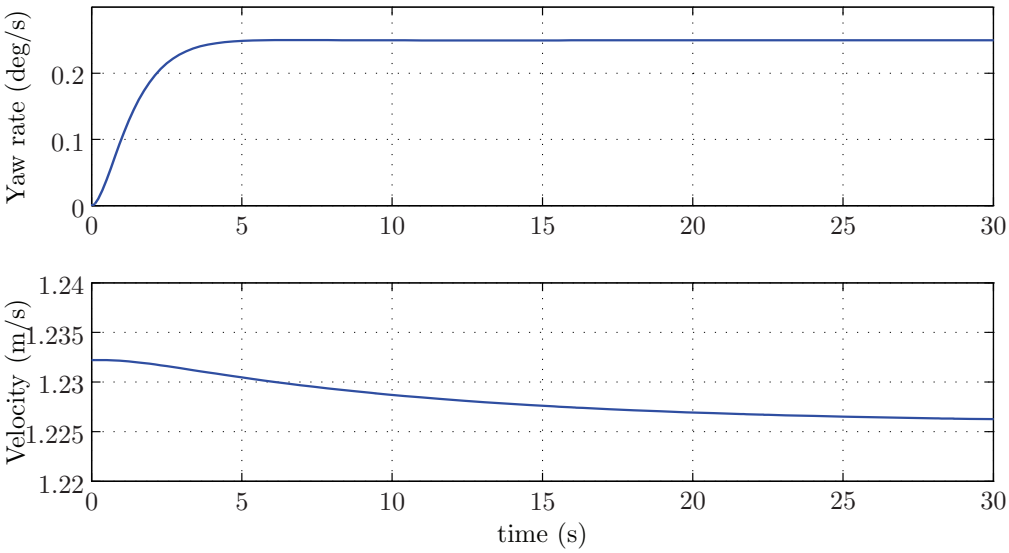

Figure A.10: Yaw rate and velocity during the 10 degree turning circle (200 rpm).

A.2 Zig-zag Maneuver

20-20 zig-zag maneuver with 500 rpm

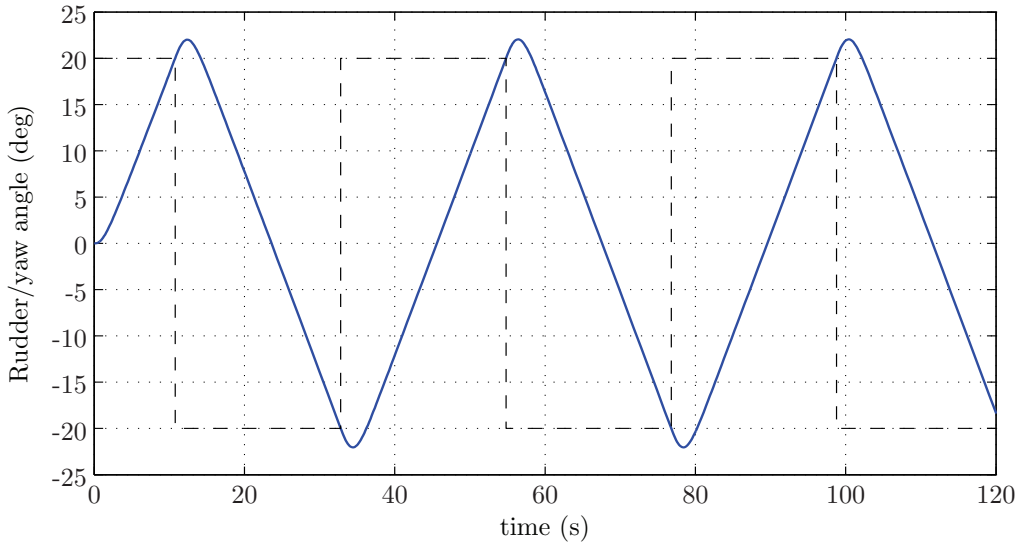

Figure A.11: Rudder/yaw plot of the 20-20 zig-zag maneuver (500 rpm).

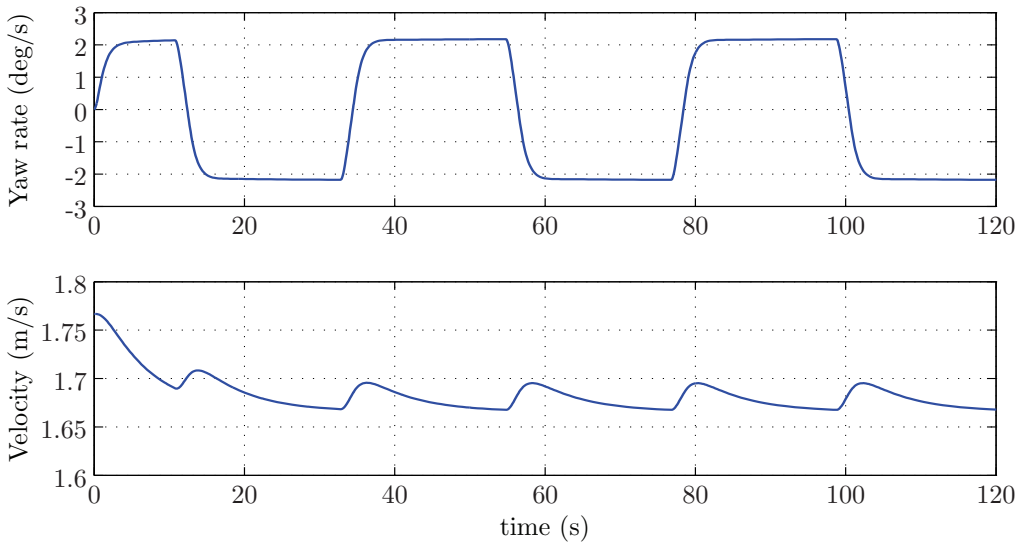

Figure A.12: Yaw rate and velocity during the 20-20 zig-zag maneuver (500 rpm).

10-10 zig-zag maneuver with 500 rpm

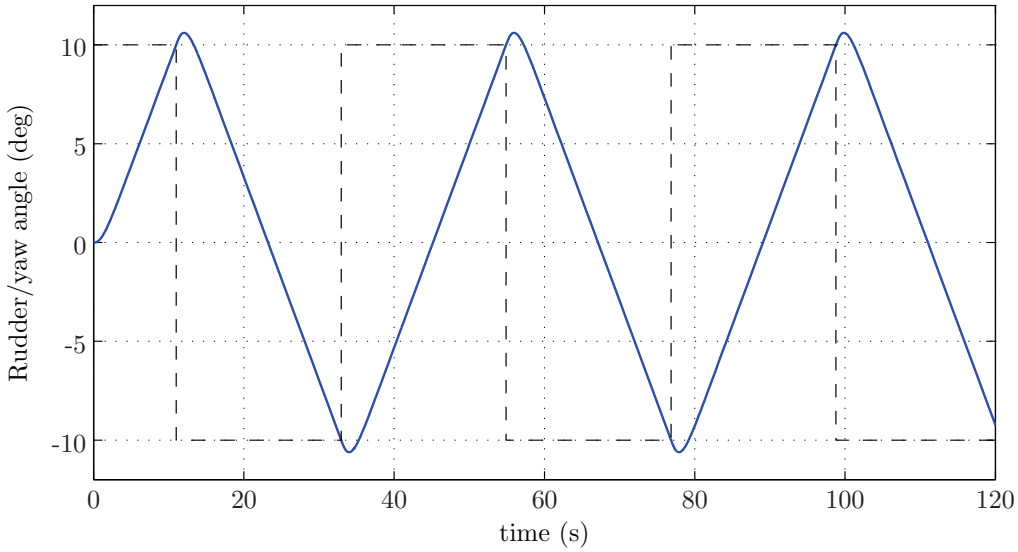

Figure A.13: Rudder/yaw plot of the 10-10 zig-zag maneuver (500 rpm).

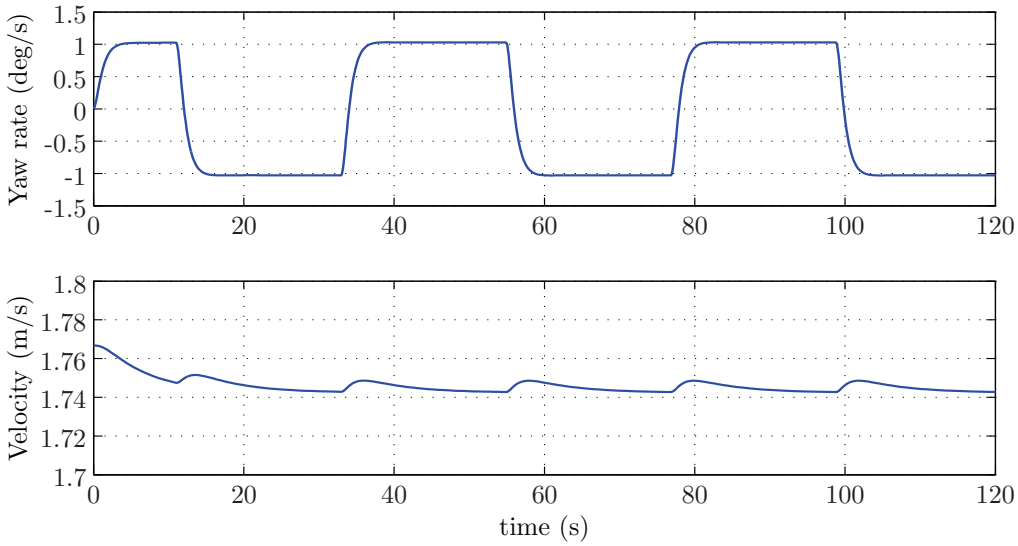

Figure A.14: Yaw rate and velocity during the 10-10 zig-zag maneuver (500 rpm).

40-40 zig-zag maneuver with 200 rpm

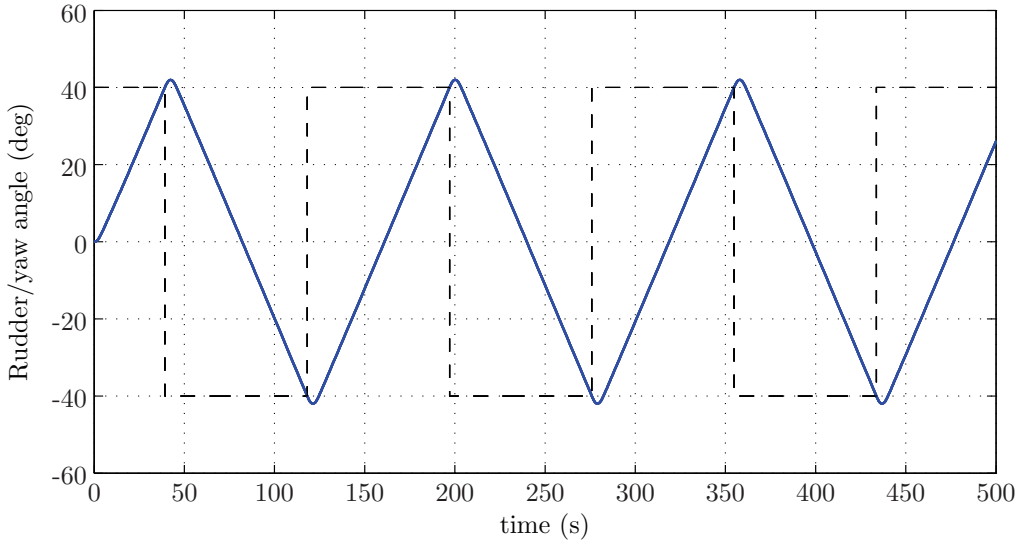

Figure A.15: Rudder/yaw plot of the 40-40 zig-zag maneuver (200 rpm).

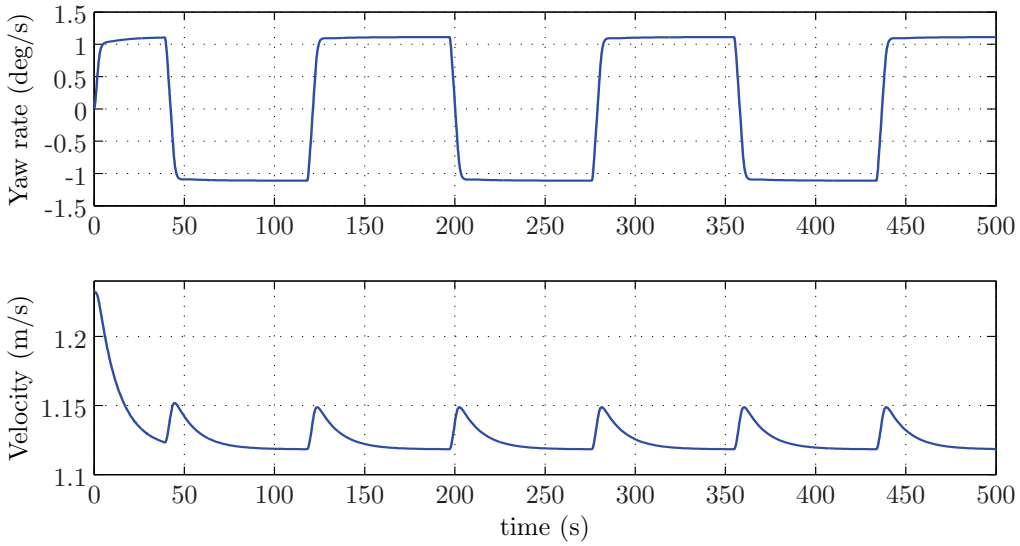

Figure A.16: Yaw rate and velocity during the 40-40 zig-zag maneuver (200 rpm).

20-20 zig-zag maneuver with 200 rpm

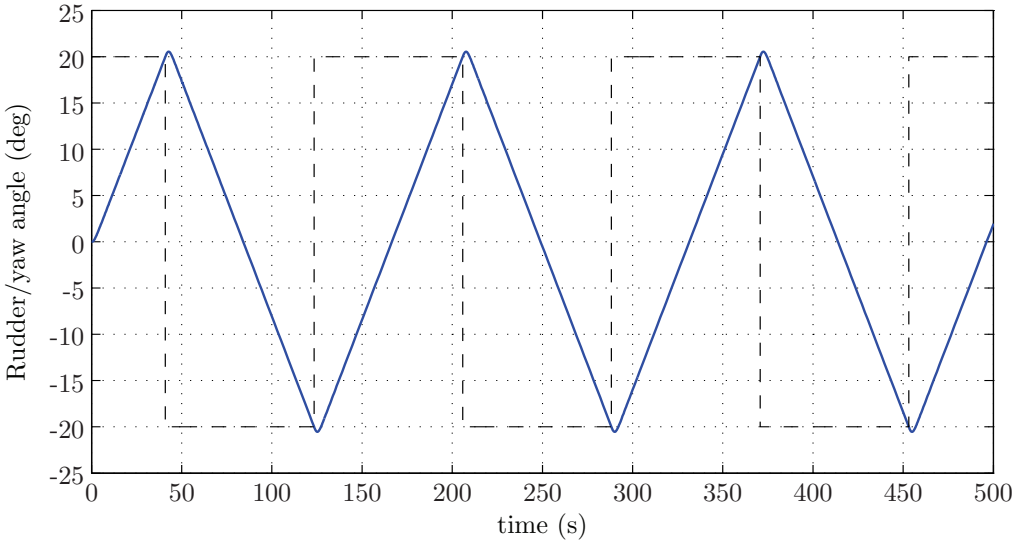

Figure A.17: Rudder/yaw plot of the 20-20 zig-zag maneuver (200 rpm).

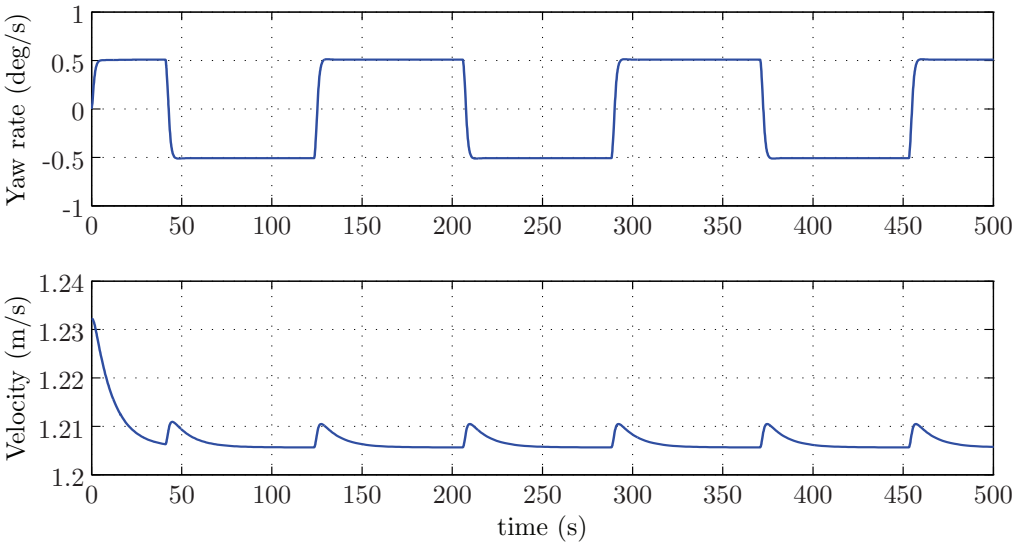

Figure A.18: Yaw rate and velocity during the 20-20 zig-zag maneuver (200 rpm).

10-10 zig-zag maneuver with 200 rpm

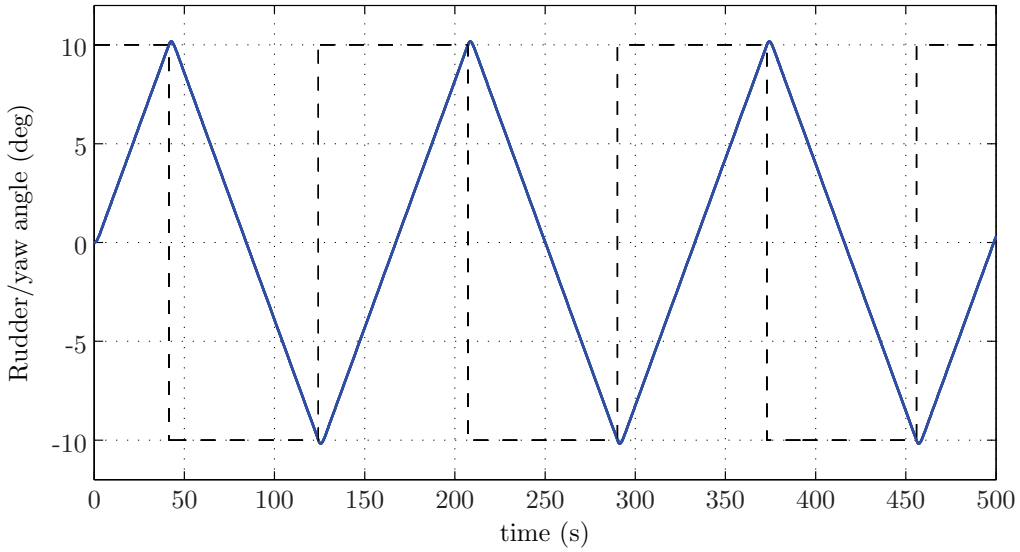

Figure A.19: Rudder/yaw plot of the 10-10 zig-zag maneuver (200 rpm).

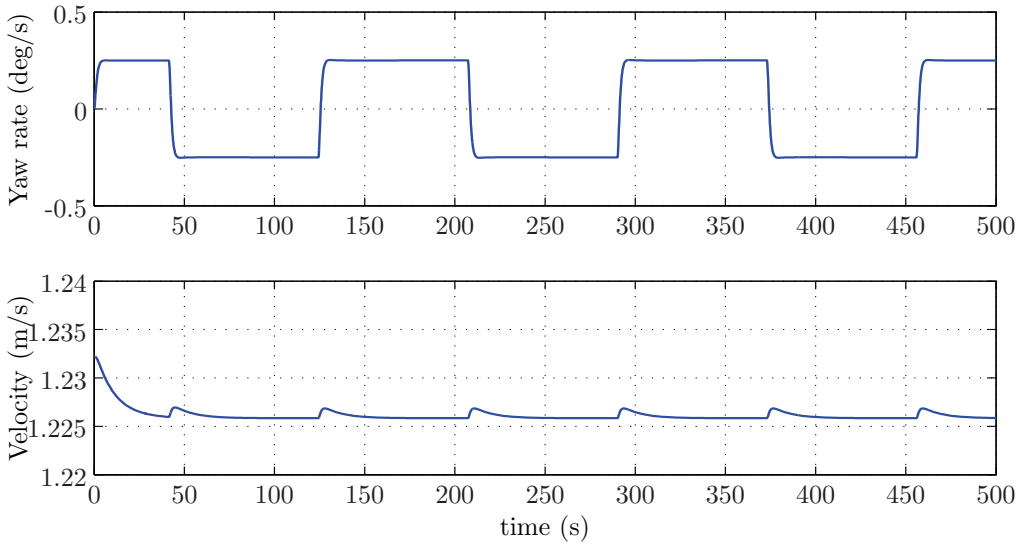

Figure A.20: Yaw rate and velocity during the 10-10 zig-zag maneuver (200 rpm).

A.3 Suggested Maneuver

The suggested maneuver with 200 rpm

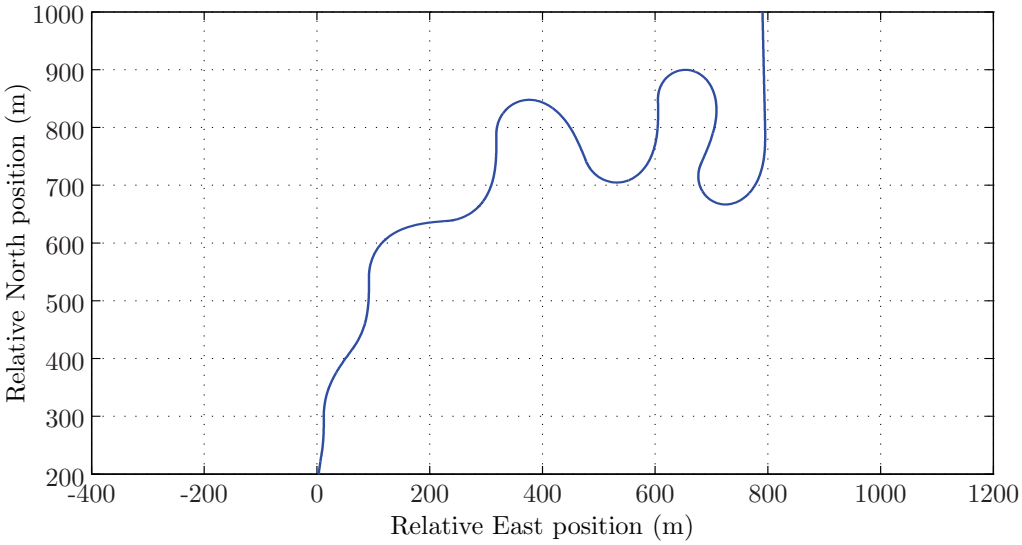

Figure A.21: North-East plot of the suggested maneuver (200 rpm).

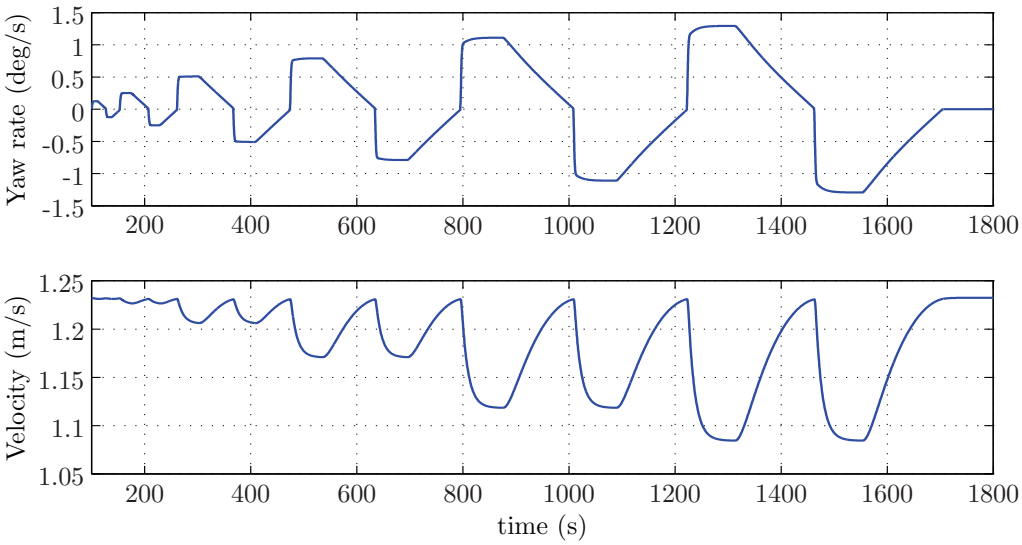

Figure A.22: Yaw rate and velocity during the suggested maneuver (200 rpm).

A.4 Closed-loop Simulation Results

In this section the closed-loop simulations in 400 rpm are presented. The results are discussed in section 5.4.

Nomoto Model Reference Feed Forward

Parameters Identified from The Turning Circle

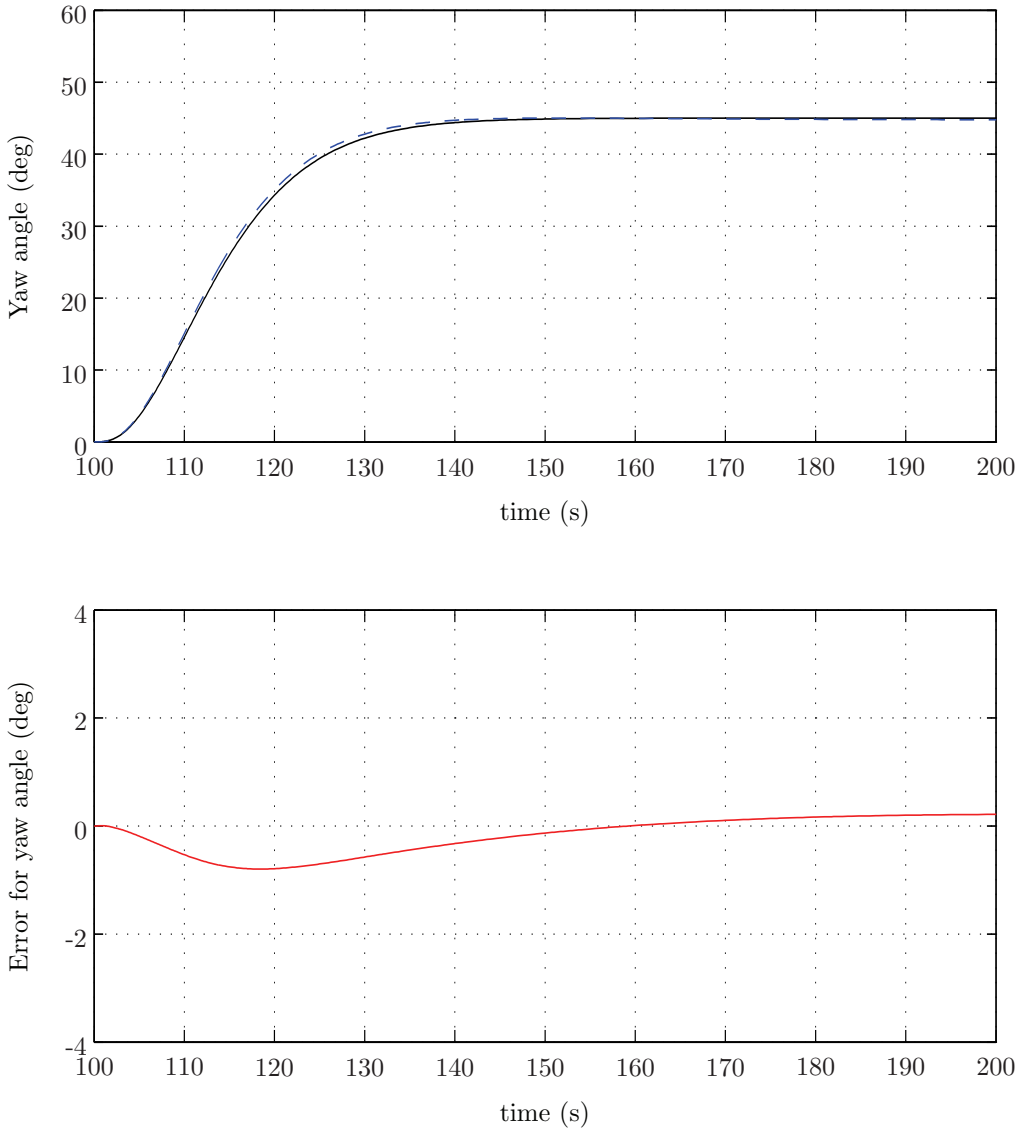

Figure A.23: The Nomoto model in closed-loop (400 rpm).

Parameters Identified from The Zig-zag Maneuver

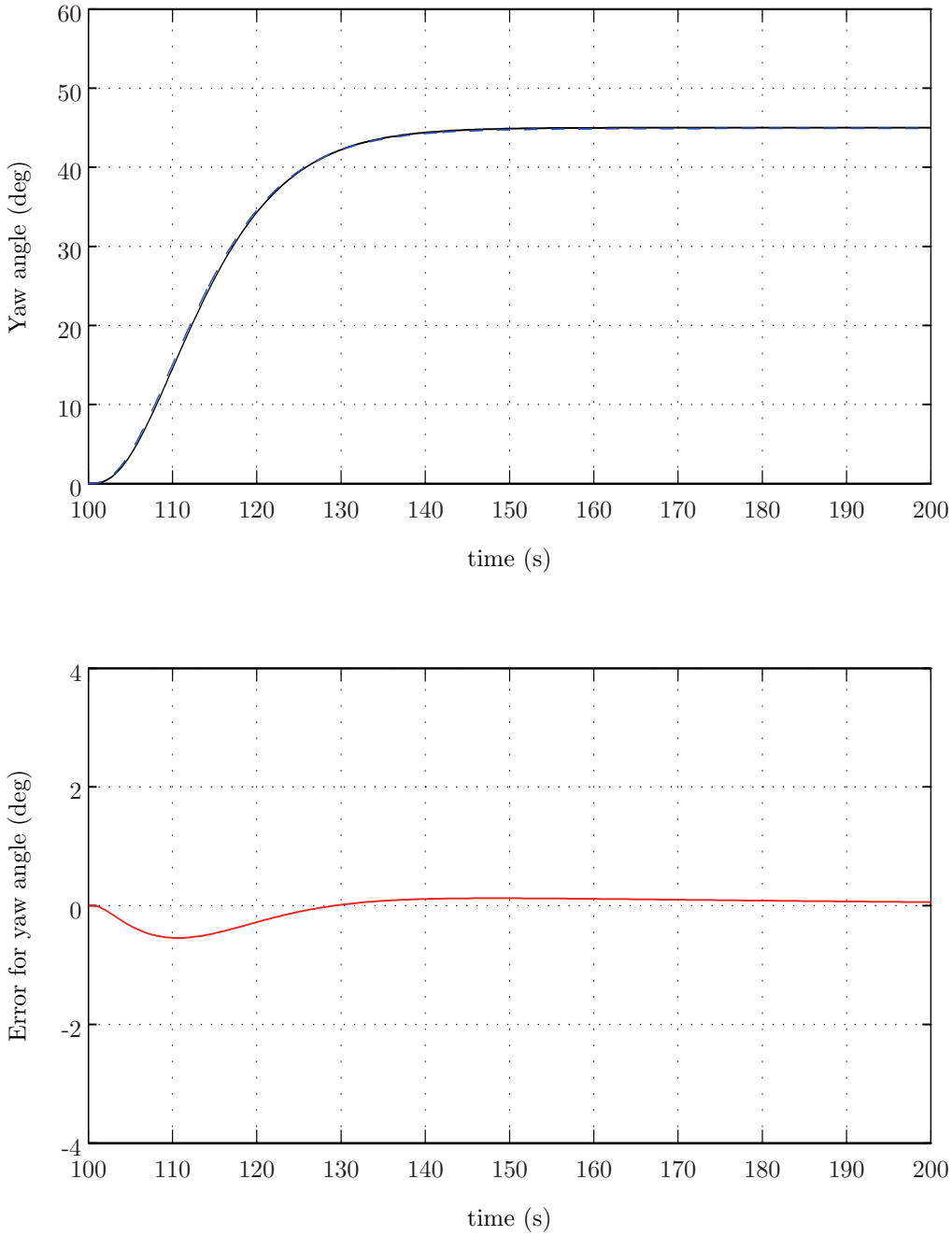

Figure A.24: The Nomoto model in closed-loop (400 rpm).

Parameters Identified from The Suggested Maneuver

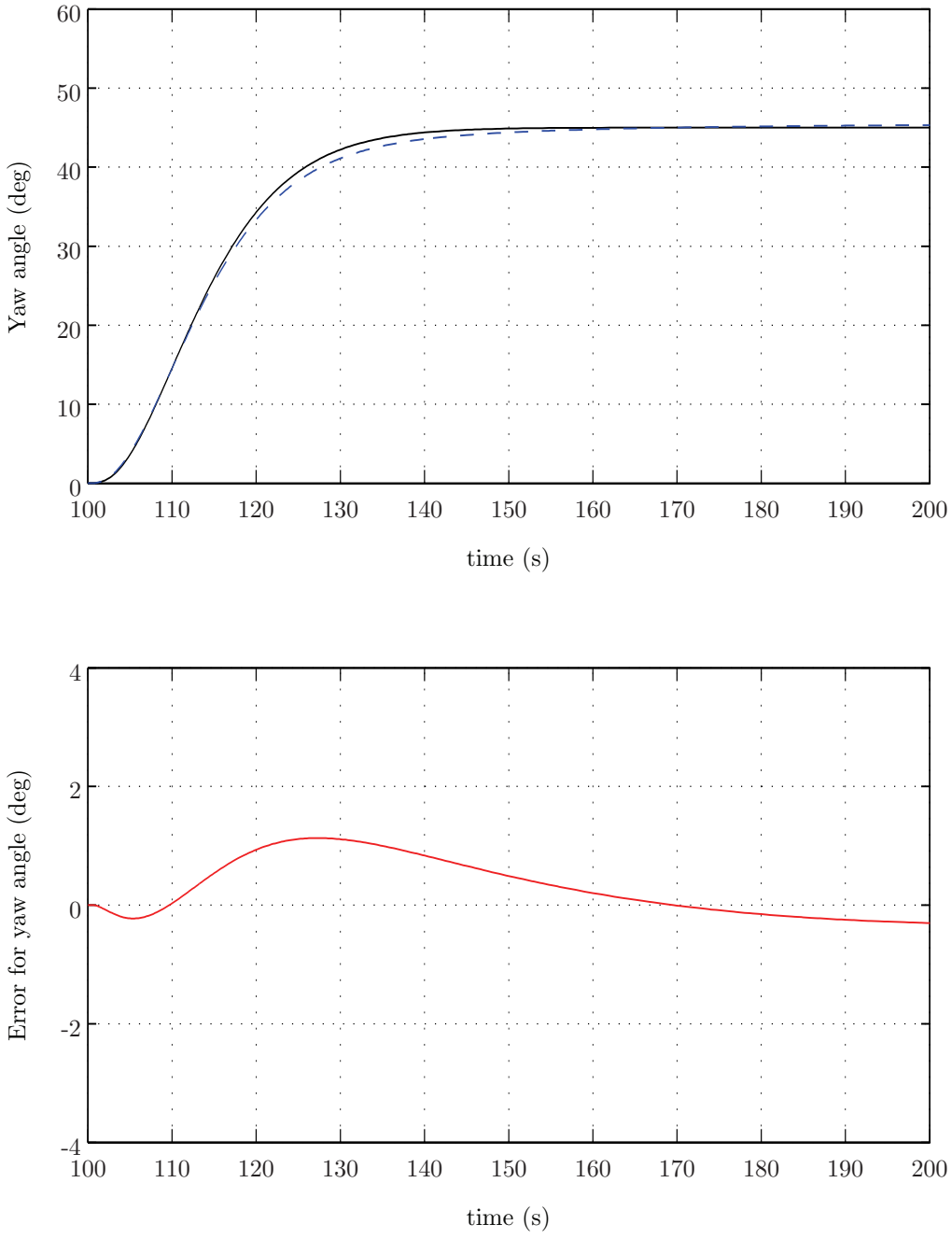

Figure A.25: The Nomoto model in closed-loop (400 rpm).

Ross Autopilot Model Reference Feed Forward

Parameters Identified from The Turning Circle

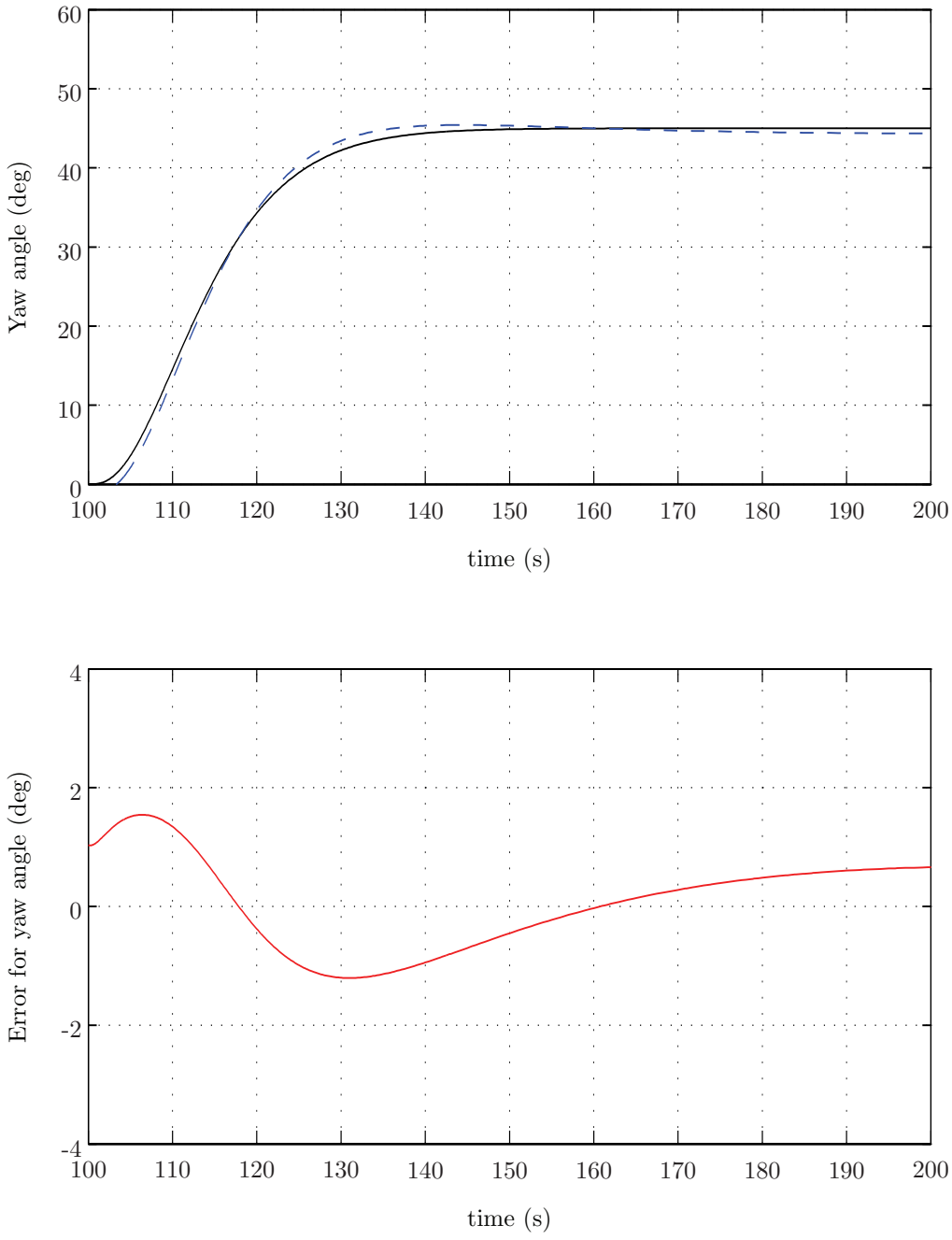

Figure A.26: The autopilot model of Ross in closed-loop (400 rpm).

Parameters Identified from The Zig-zag Maneuver

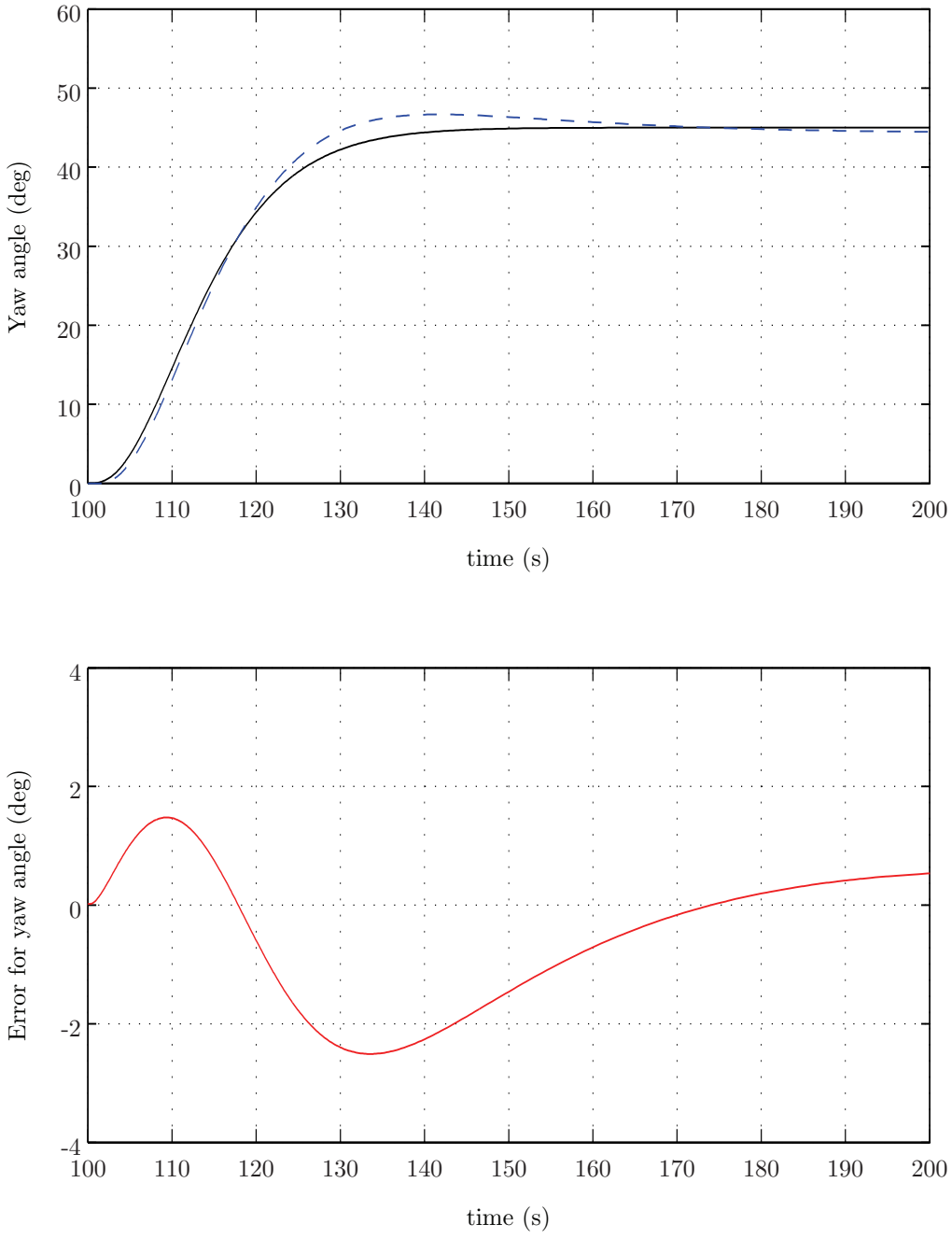

Figure A.27: The autopilot model of Ross in closed-loop (400 rpm).

Parameters Identified from The Suggested Maneuver

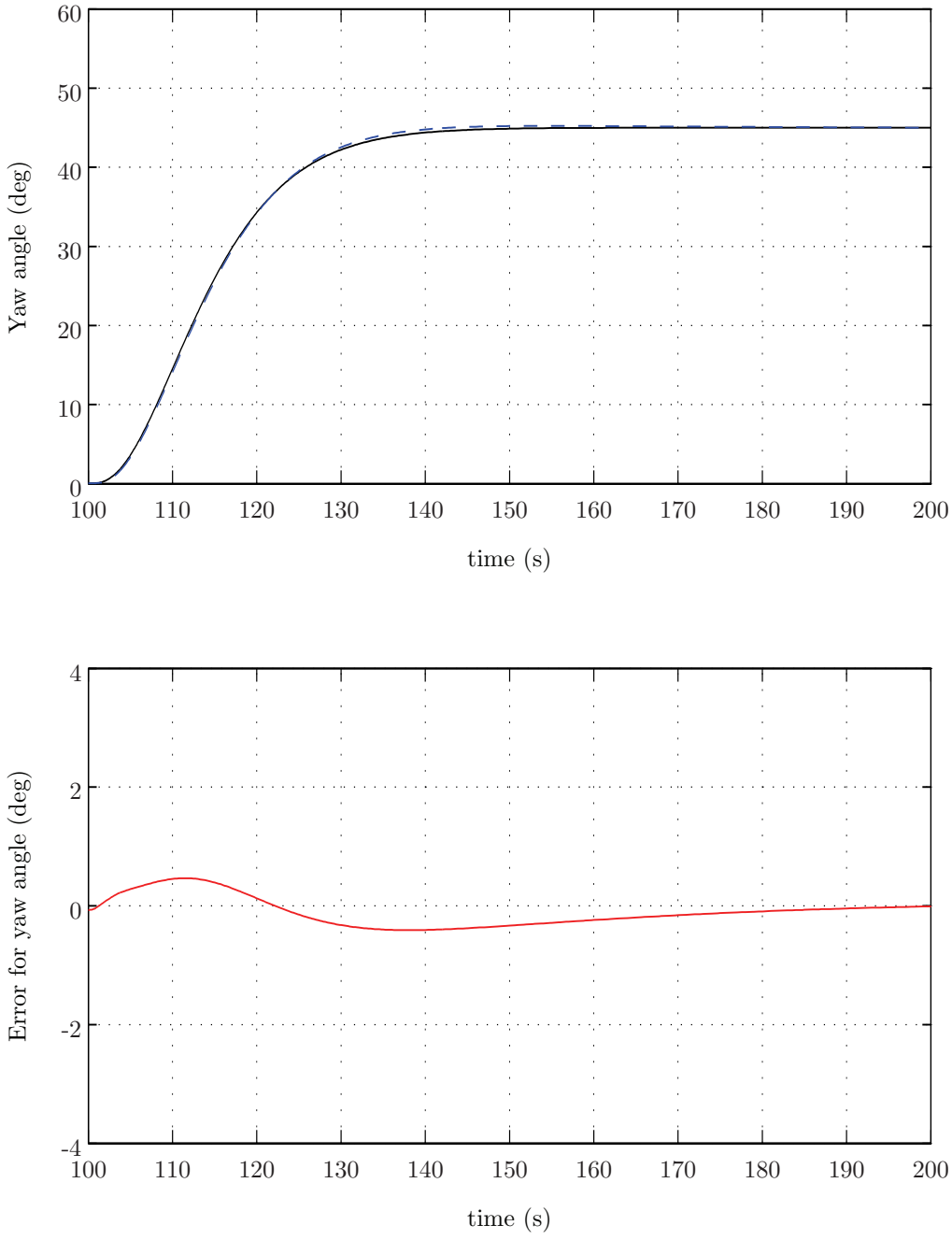

Figure A.28: The autopilot model of Ross in closed-loop (400 rpm).

Appendix B

MATLAB Models

This chapter presents the Simulink diagrams and Matlab code used in this thesis. A digital version of the diagrams and code is also available in Appendix C.

Simulink Diagrams

Project/Vessel

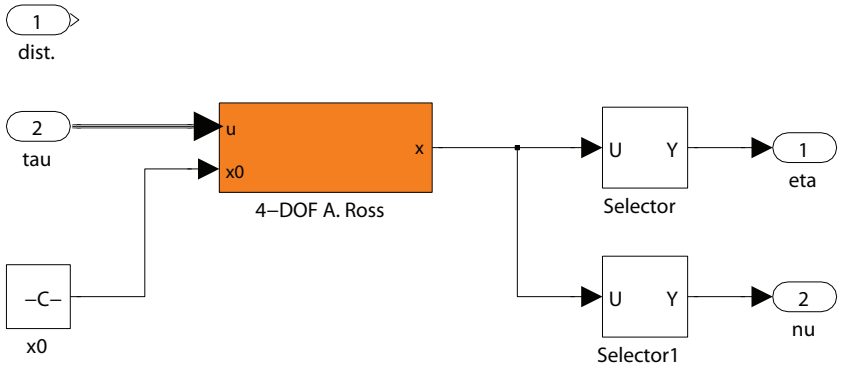

Figure B.1: Project/Vessel

Project/Vessel/4-DOF

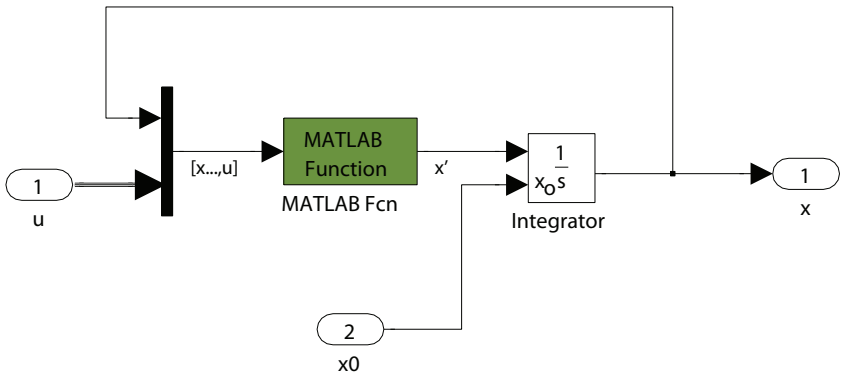

Figure B.2: Project/Vessel/4-DOF.

Project/Turning Circle

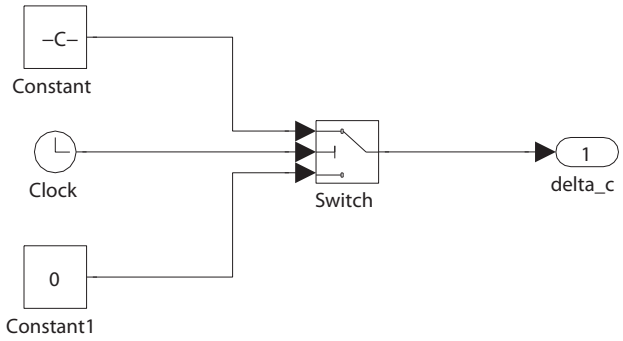

Figure B.3: Project/Turning Circle.

Project/Zig-zag Maneuver

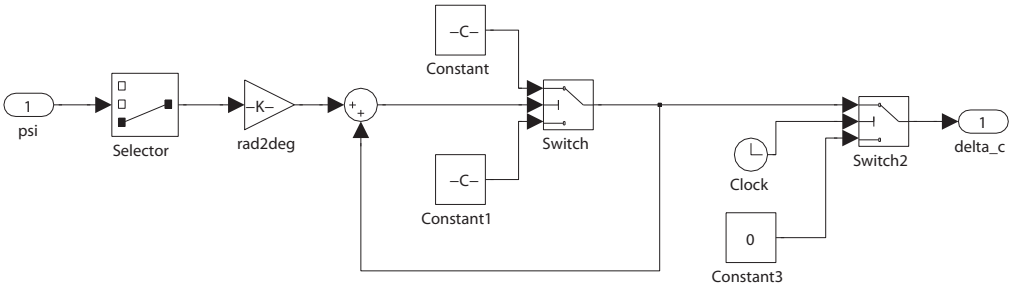

Figure B.4: Project/Zig-zag Maneuver.

Project/Suggested Maneuver

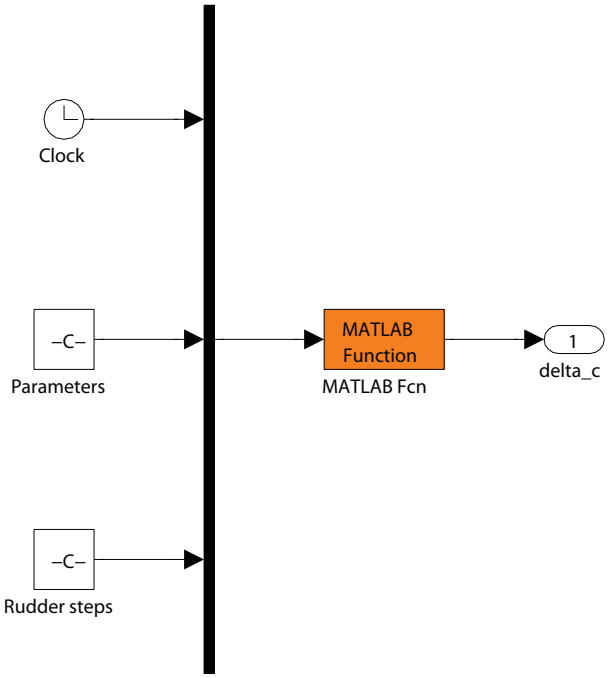

Figure B.5: Project/Suggested Maneuver.

Project/Model-based Autopilots

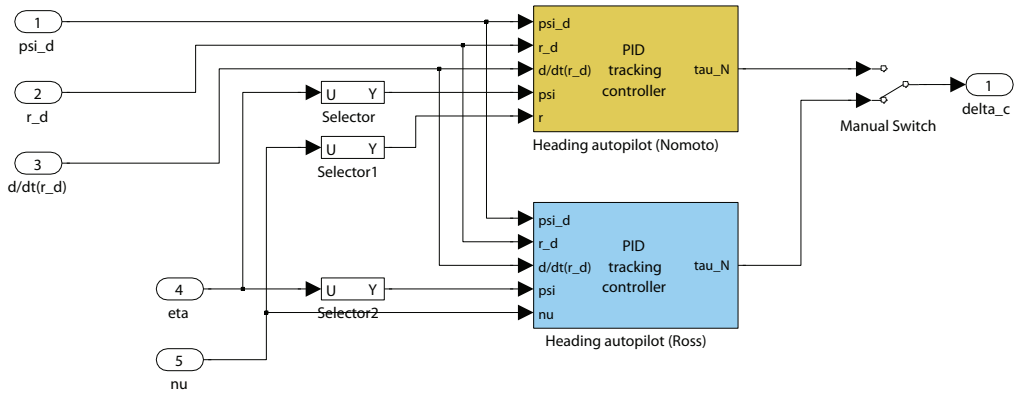

Figure B.6: Project/Model-based Autopilots.

Project/Model-based Autopilots/Heading autopilot (Nomoto)

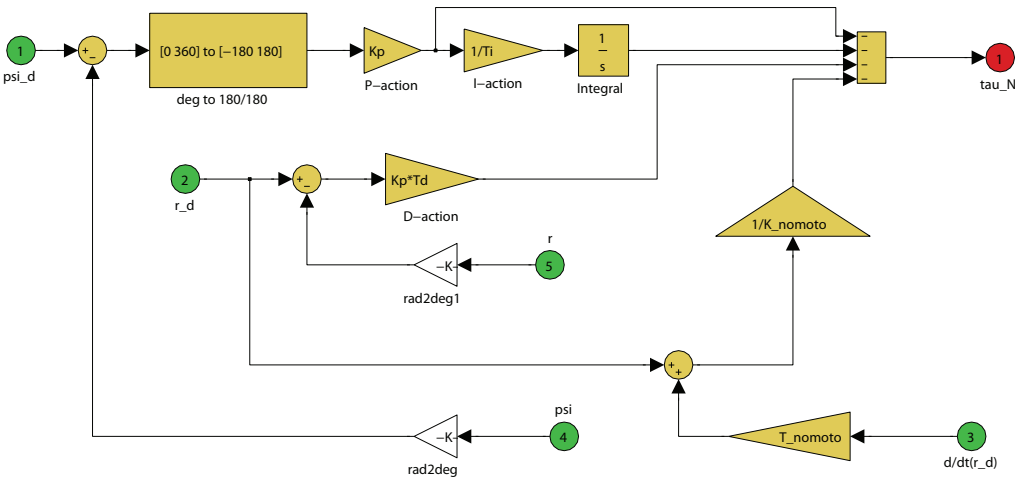

Figure B.7: Project/Model-based Autopilots/Heading autopilot (Nomoto).

Project/Model-based Autopilots/Heading autopilot (Ross)

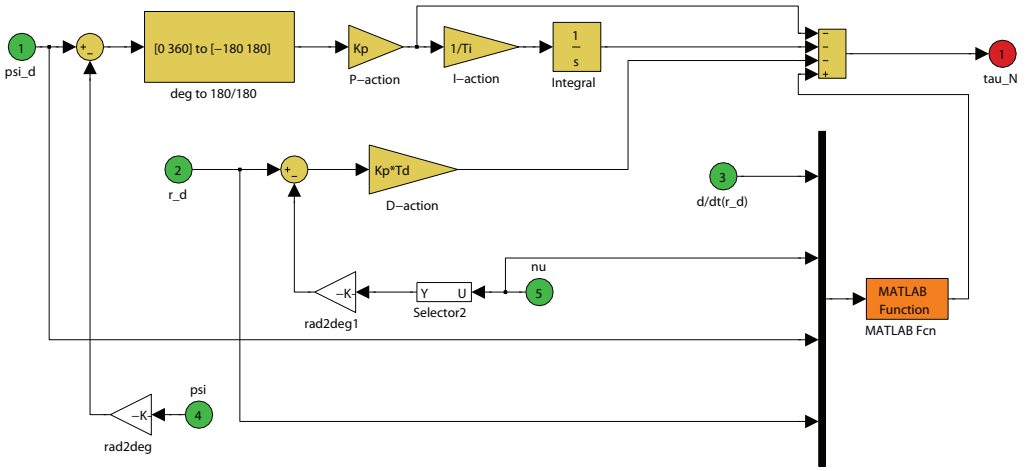

Figure B.8: Project/Model-based Autopilots/Heading autopilot (Ross).

Project/Reference model

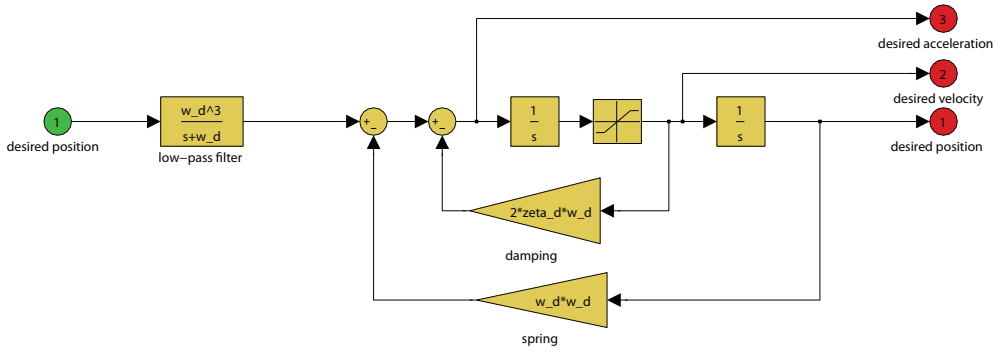

Figure B.9: Project/Reference model.

Project/Reference

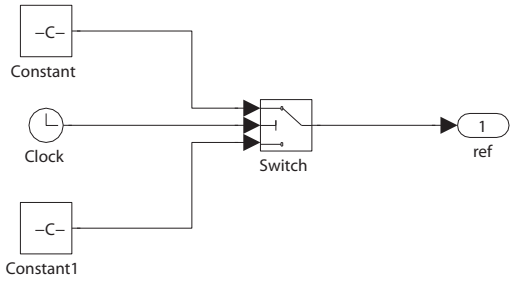

Figure B.10: Project/Reference.

Project/Thrust

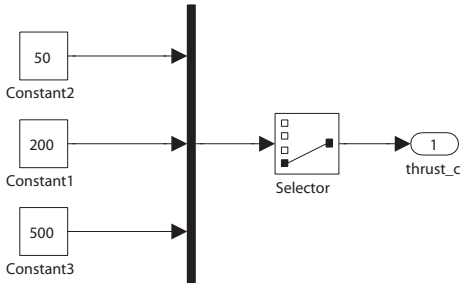

Figure B.11: Project/Thrust.

Project/Control Input

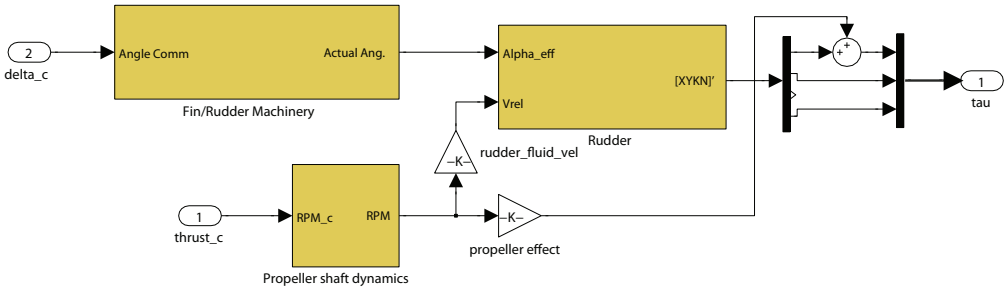

Figure B.12: Project/Control Input.

Project/Control Input/Rudder Machinery

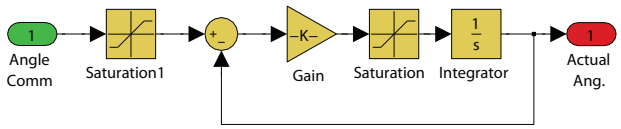

Figure B.13: Project/Control Input/Rudder Machinery.

Project/Control Input/Shaft dynamics

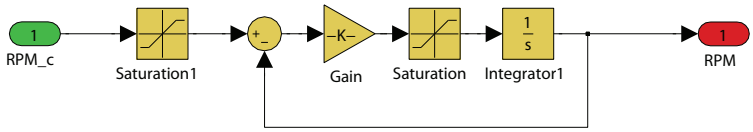

Figure B.14: Project/Control Input/Shaft dynamics.

Project/Control Input/Rudder

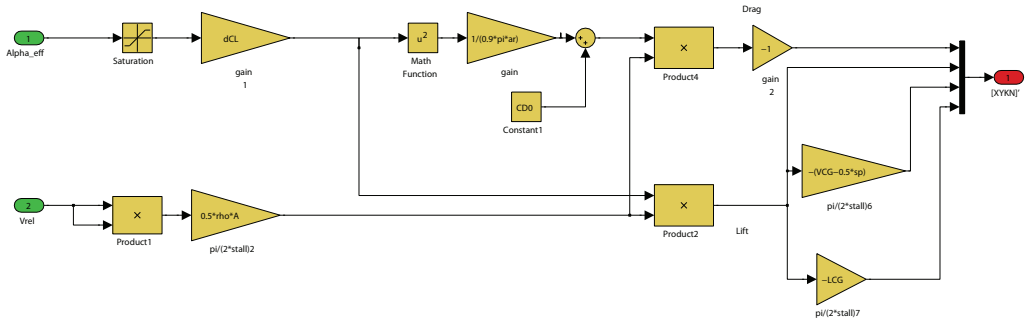

Figure B.15: Project/Control Input/Rudder.

M-files

main_init.m

```
% ------------------------------------------------------------------------
% > Main initialization
% ------------------------------------------------------------------------

clc
clear all

vessel.n0 = 0; %init pos [m]
vessel.e0 = 0; %init pos [m]
vessel.phi0 = 0; %init roll ang [rad]
vessel.psi0 = 0; %init yaw ang [rad]

vessel.u0 = 0;%1.56; %init surge vel [m/s]
vessel.v0 = 0; %init sway vel [m/s]
vessel.p0 = 0; %init roll rate [rad/s]
vessel.r0 = 0; %init yaw rate [rad/s]

vessel.eta0 = [vessel.n0 vessel.e0 vessel.psi0]';
vessel.nu0 = [vessel.u0 vessel.v0 vessel.r0]';
vessel.init = [vessel.eta0; vessel.nu0];


%% Rudder
rudder.max = 45; %60; %max rudder [deg]
rudder.rate = 15.0; %max rudder rate [deg/s]
rudder.ts = 1; %time constant [s]
rudder.surge = 0.7; %0.3; %rudder effect on surge
rudder.sway = 4.0;%1.5%2.5; %rudder effect on sway
rudder.roll = 0.6; %rudder effect on roll
rudder.yaw = -2.3; %6.3 %-3.3%-5.3; %rudder effect on yaw

%% Thrust
thrust.max = 500; %max RPM
thrust.rate = 100; %max RPM Rate
thrust.ts = 1; %time constant [s]
thrust.rudder_fluid_vel = 1/200; %generated fluid velocity
thrust.effect = 0.05; %thrust effect on surge

%% Turning Circle
maneuver.circle = 45; %turning circle rudder deflection [deg]
maneuver.circle_threshold = 100; %threshold time [s]

%% Zig-zag Maneuver
maneuver.zigzag = 20; %zig-zag test [deg]
maneuver.zigzag_threshold = 100; %threshold time [s]

%% The suggested Variable Step Maneuver
maneuver.new_step = [0 5 10 20 30 40 45 0 0]; %rudder steps [deg]
maneuver.new_param = [100 2 0.3]; %threshold,switch,ramp

%% Autopilot
%Controller
autopilot.wb = 0.05; %bandwidh
autopilot.xi = 1.5; %relative damping ratio
autopilot.wn = (1/(sqrt(1-2*autopilot.xi^2+sqrt(4*autopilot.xi^4 ...
                -4*autopilot.xi^2+2))))*autopilot.wb; %natural frequency

%Calculate controller gain
autopilot.Kp = (190*autopilot.wn^2)
```

```
autopilot.Kd = (2*autopilot.xi*autopilot.wn*190)
autopilot.Ki = ((autopilot.wn/10)*autopilot.Kp)

%Nomoto model reference forward
autopilot.ffK = 0.107937
autopilot.ffT = 4.467136

%% Reference model
refmod.xi = 1; %relative damping ratio
refmod.wn = 0.2; %natural frequency
refmod.max_velocity = 10; %saturate r_ref [deg/s]

%% Reference step
reference.steptime = 100;
reference.init = 0;
reference.step = 45;

display Initialization_completed
```

vesselmodel.m

```
%% See Appendix C
```

suggested_maneuver.m

```
function [output] = suggested_maneuver(input)
% ------------------------------------------------------------------------
% > Suggested ship maneuver
% ------------------------------------------------------------------------
% > Input vector: [clock,param,step]
% > Output vector: [rudder]
% ------------------------------------------------------------------------

% Rename input vector
clock = input(1);
threshold_start = input(2);
threshold_switch = input(3);
ramp = input(4);
rudder_step = input(5:13);

persistent stepNumber; %define persistent counter
persistent threshold_temp; %define persistent threshold
persistent stepNow; %define persistent psi
persistent stepPhase; %define persistent step phase
persistent out; %define persistent output

if isempty(out)
    out = 0;
end

if isempty(stepPhase)
    stepPhase = 0;
end

if isempty(stepNow)
    stepNow = 0;
end

if isempty(stepNumber)
    stepNumber = 1;
```

```
end

if isempty(threshold_temp)
    threshold_temp = 0;
end

if(clock > threshold_start)
    if(stepNumber == 1)
        stepNumber = 2;
        stepPhase = 1;
        threshold_temp = clock;
        out = -rudder_step(stepNumber);
    end
end

threshold_switch = threshold_switch*rudder_step(stepNumber);

if(stepNumber > 1 && stepNumber < 9)
    if(stepPhase == 1 && ((threshold_temp + threshold_switch) < clock))
        out = -rudder_step(stepNumber) +(clock - threshold_temp - ...
              threshold_switch)*ramp;
        if(out > 0)
            stepPhase = 2;
        end
    elseif(stepPhase == 2 && ((threshold_temp + threshold_switch) ...
           < clock))
        stepPhase = 3;
        threshold_temp = clock;
        out = rudder_step(stepNumber);
    elseif(stepPhase == 3 && ((threshold_temp + threshold_switch) < clock))
        out = rudder_step(stepNumber) -(clock - threshold_temp - ...
              threshold_switch)*ramp;
        if(out < 0)
            stepPhase = 4;
        end
    elseif(stepPhase == 4 && ((threshold_temp + threshold_switch) ...
           < clock))
        stepNumber = stepNumber + 1;
        stepPhase = 1;
        threshold_temp = clock;
        out = -rudder_step(stepNumber);
    end
end

if(stepNumber > 8)
    out = 0;
end

output=[out];
```

identification.m

```
% ------------------------------------------------------------------------
% > Identification
% ------------------------------------------------------------------------
% > Iterative Prediction-Error Minimization
% > lsqnonlin | Trust-Region Reflective Newton Search
% ------------------------------------------------------------------------

%% Estimating Nonlinear Grey-Box Models
display Identification_started
nomoto = pem(data, nom.nlgr, 'Display', 'Full') %parameter estimation
```

```
%ross = pem(data, ros.nlgr, 'Display', 'Full') %parameter estimation
display Identification_completed
```

model_nomoto.m

```
function [dx, y] = model_nomoto(t, x, u_, K, T, varargin)
% ------------------------------------------------------------------------
% > IDNLGREY Model File
% ------------------------------------------------------------------------
% > The autopilot model of Nomoto
% ------------------------------------------------------------------------

N = u_(1); %rudder input

y = x(1); %output

dx = [(K/T)*N-(1/T)*x(1)]; %state equation
```

model_ross.m

```
function [dx, y] = model_ross(t,x,u_, Ndr, NuvppL, NuvL, NuuvL, NvvvL, ...
                              NrrvL, Nvv, Nrv, NurL, NuurL, NrrrL, ...
                              NvvrL, Nvr, Nrr, Xdu0, Ydv0, Ndv0, Ydr0, ...
                              varargin)
% ------------------------------------------------------------------------
% > IDNLGREY Model File
% ------------------------------------------------------------------------
% > Autopilot model derived by Ross
% ------------------------------------------------------------------------

N = u_(1); %rudder input
u = u_(2); %sway velocity
v = u_(3); %surge velocity
r = u_(4); %yaw rate
p = u_(5); %yaw

r = x(1);
y = r; %output

dx = [(1/(-Ndr))*(N+NuvppL*u*v*p^2+NuvL*u*v+NuuvL*u^2*v+NvvvL*u^3 ...
      +NrrvL*r^2*v+Nvv*abs(v)*v+Nrv*abs(r)*v+NurL*u*r+NuurL*u^2*r ...
      +NrrrL*r^3+NvvrL*v^2*r+Nvr*abs(v)*r+Nrr*abs(r)*r-(Xdu0-Ydv0)*u*v ...
      +(1/2)*(Ndv0+Ydr0))]; %state equation
```

data_structure.m

```
% ------------------------------------------------------------------------
% > Data Structure
% ------------------------------------------------------------------------
% > Representing Time-Domain Data as IDDATA Objects
% > Constructing IDNLGREY Object of the models
% ------------------------------------------------------------------------

%load Simulation/circle_40deg_500
%load Simulation/zigzag_40deg_500
load Simulation/suggested_500
id.startsim = 95; %start simdata
id.endsim = length(simout_time); %end simdata
```

```
id.minx = 100; %plot minx
id.maxx = 200; %plot maxx

%% Time-Domain Data as IDDATA Objects
id.u = [simout_rudder_c.signals.values(id.startsim:id.endsim) ...
        simout_u.signals.values(id.startsim:id.endsim) ...
        simout_v.signals.values(id.startsim:id.endsim) ...
        simout_r.signals.values(id.startsim:id.endsim) ...
        simout_psi.signals.values(id.startsim:id.endsim)]; %input
id.y = [simout_r.signals.values(id.startsim:id.endsim)]; %output
id.Ts = 0; %nonuniformly sampled data
id.TimeVector = simout_time(id.startsim:id.endsim); %time
data = iddata(id.y,id.u,id.Ts,'SamplingInstants',id.TimeVector); %iddata

%% IDNLGREY Object | Nomoto autopilot model
nom.FileName = 'model_nomoto'; %file describing the model structure
nom.Order = [1 5 1]; %model orders [ny nu nx]
nom.Parameters = [-0.15; 3]; %initial parameters
nom.InitialStates = [0]; %initial initial states
nom.Ts = 0; %time-continuous system
nom.nlgr = idnlgrey(nom.FileName, nom.Order, nom.Parameters, ...
                    nom.InitialStates, nom.Ts, 'Name', 'Nomoto Model');

%% IDNLGREY Object | Ross autopilot model
ros.FileName = 'model_ross'; %file describing the model structure
ros.Order = [1 5 1]; %model orders [ny nu nx]
ros.Parameters = [15; 0; 200; -400; 0.01; -2; 70; -8; 11; -2.5; 0.05; ...
                  100; -10; -1; -200; 200; -0.05; -0.05; ]; %init param.
ros.InitialStates = [0]; %initial initial states
ros.Ts = 0; %time-continuous system
ros.nlgr = idnlgrey(ros.FileName, ros.Order, ros.Parameters, ...
                    ros.InitialStates, ros.Ts, 'Name', 'Ross Model');

display Data_Structure_Created
```

autopilotmodel.m

```
function [output] = autopilotmodel(input)
% ------------------------------------------------------------------------
% > Autopilot model
% ------------------------------------------------------------------------
% > Input vector: [d/dt(r_d),r_d,eta,psi_d,nu]
% > Output vector: [N]
% ------------------------------------------------------------------------

% Rename input vector
dr  = input(1);
r   = input(2);
u   = input(3);
v   = input(4);
p   = input(6);

% Insert identified parameter vector
param = []

% Rename parameter vector
Ndr = param(1);
NuvppL = param(2);
NuvL = param(3);
NuuvL = param(4);
NvvvL = param(5);
NrrvL = param(6);
```

```
Nvv = param(7);
Nrv = param(8);
NurL = param(9);
NuurL = param(10);
NrrrL = param(11);
NvvrL = param(12);
Nvr = param(13);
Nrr = param(14);
Xdu0 = param(15);
Ydv0 = param(16);
Ndv0 = param(17);
Ydr0 = param(18);

% Calculate new states
N = (Ndr*dr-NuvppL*u*v*p^2-NuvL*u*v-NuuvL*u^2*v-NvvvL*u^3 ...
     -NrrvL*r^2*v-Nvv*abs(v)*v-Nrv*abs(r)*v-NurL*u*r-NuurL*u^2*r ...
     -NrrrL*r^3-NvvrL*v^2*r-Nvr*abs(v)*r-Nrr*abs(r)*r+(Xdu0-Ydv0)*u*v ...
     -(1/2)*(Ndv0+Ydr0));

output=[N];
```

Appendix C

CD

Master thesis

In this folder a digital version of the thesis is available in PDF and PS format.

Matlab Scripts and Diagrams

In this folder all the Matlab scripts and diagrams are available.

References

In this folder the digital references used in the thesis are available.